Inaugural dissertation
for
obtaining the doctoral degree
of the
Combined Faculty of Mathematics, Engineering and Natural Sciences
of the
Ruprecht - Karls - University
Heidelberg

Presented by
M. Sc. Emilio Ulises Isaías Camacho
born in: Tlalnepantla de Baz, México
Oral examination: 02.10.2025

WHISKER SOMATOSENSATION IN THE MOUSE SUPERIOR COLLICULUS: PATHWAYS AND BEHAVIOUR

A ground study on whisker-relevant collicular function

Referees: Prof. Dr. Alexander Groh
Prof. Dr. Simon Wiegert

Emilio Ulises Isaías Camacho: *Whisker somatosensation in the mouse superior colliculus: pathways and behaviour,* A ground study on whisker-relevant collicular function, © June 2025

To my loved ones and all those mice sacrificed in the name of science.

ABSTRACT

Animals can react quickly to stimuli in their environment, e. g. orienting towards a stimulus or escaping a threat. The superior colliculus (SC) is a phylogenetically old midbrain brain structure producing swift orientation and defence movements to enhance the individual's survival. However, these movements could be wasteful without adaptation or even modulation. Mice rely on their whiskers to perceive and interact with their environment. The whisker-related connectivity to SC, involving the layer 5 (L5) of motor cortex (MC) and barrel field cortex (BC), and the brainstem (Bs), as well as from collicular recipient neurons (RNs) was described by different viral strategies, including an intersectional viral approach, revealing novel long-range projections from SC. I developed a behavioural paradigm to quantify mice's SC-dependent evoked behaviour upon an unpredictable whisker puff. Pharmacologically blocking the SC reduced the puff evoked behaviour and showed that SC is an important node in the orientation circuit of the brain. Building on the collicular whisker network, the cortical influence to modulate and adapt SC-mediated orientation behaviours was tested by *a*. optogenetically manipulating cortical axons in SC, and *b*. optogenetically manipulating RNs directly. Modelling of the sensorimotor transformation showed that the SC performs part of the computation for orientation movements and that activation of a specific RNs population is a likely candidate for modulating and even adapting SC-dependent behaviour. My results reveal that top-down modulation of SC-dependent behaviour is achieved through specific neural populations in SC, controlled by L5-MC inputs and reflects the high level of natural alertness mice need to escape predators and feed.

ZUSAMMENFASSUNG

Tiere können schnell auf Reize in ihrer Umgebung reagieren, z. B. indem sie sich einem Reiz zuwenden oder vor einer Bedrohung fliehen. Das Tectum (superior colliculus, SC) ist eine phylogenetisch alte Mittelhirnstruktur, die schnelle Orientierungs- und Abwehrbewegungen erzeugt, um das überleben des Individuums zu sichern. Ohne Anpassung oder Modulation könnten diese Bewegungen jedoch ineffizient oder sogar kontraproduktiv sein. Die taktile Wahrnehmung über die Vibrissen ist für Mäuse essenziell, um ihre Umwelt zu erfassen und mit ihr zu interagieren. Die vibrissenbezogene Konnektivität zum SC, unter Einbezug der Schicht 5 (L5) des motorischen Kortex (MC), des Barrelkortex (BC) und des Hirnstamms (Bs), sowie der colliculären

Projektionsneurone (RNs), wurde mithilfe verschiedener viraler Strategien beschrieben – darunter auch ein kombinatorischer viraler Ansatz, der neuartige weitreichende Projektionen vom SC offenbarte. Ich entwickelte ein Verhaltensparadigma, um SC-abhängiges Verhalten von Mäusen nach einem unvorhersehbaren Luftstoß auf die Vibrissen zu quantifizieren. Die pharmakologische Blockade des SC reduzierte das durch den Luftstoß ausgelöste Verhalten und zeigte, dass der SC ein wichtiges Zentrum in der Orientierungsverschaltung des Gehirns ist. Aufbauend auf dem colliculären Vibrissennetzwerk wurde der kortikale Einfluss auf die Modulation und Anpassung SC-vermittelter Orientierungsreaktionen durch *a*. optogenetische Manipulation kortikaler Axone im SC, und *b*. direkte optogenetische Manipulation der RNs getestet. Die Modellierung der sensomotorischen Transformation zeigte, dass der SC einen Teil der Berechnung für Orientierungsbewegungen übernimmt und dass die Aktivierung einer spezifischen RN-Population ein wahrscheinlicher Kandidat für die Modulation und sogar Anpassung SC-abhängigen Verhaltens ist. Meine Ergebnisse zeigen, dass die top-down Modulation SC-abhängigen Verhaltens durch spezifische neuronale Populationen im SC erfolgt, die von L5-MC-Eingängen gesteuert werden – ein Mechanismus, der das hohe Maß an natürlicher Wachsamkeit widerspiegelt, das Mäuse benötigen, um Raubtieren zu entkommen und Nahrung zu finden.[1]

1 Thanks to Katharina Ziegler for helping me proofread the German version of my abstract!

PUBLICATIONS

I collaborated with **Martín-Cortecero et al., 2023** during the first stage of my Ph. D. work. In addition, my colleagues and I are preparing a second manuscript with the results of the second stage (**Isaías-Camacho et al., 2025**).

Isaías-Camacho, Emilio U.*, Jesús M. Martín-Cortecero*, James A. Auwn, Katharina Ziegler, Ann-Kristin Kenkel and Alexander Groh (2025). 'A motor cortico-collicular pathway shapes superior colliculus generated tactile orienting behaviour'. Manuscript in preparation.

Martín-Cortecero*, Jesús M., **Emilio U. Isaías-Camacho***, Berin E. Boztepe*, Katharina Ziegler, Rebecca A. Mease and Alexander Groh (2023). 'Monosynaptic trans-collicular pathways link mouse whisker circuits to integrate somatosensory and motor cortical signals'. In: *PLoS Biology* 21 (5). ISSN: 15457885. DOI: 10.1371/journal.pbio.3002126.

In addition, I participated in the following projects in parallel. My contribution to **Ziegler et al., 2023** was a triggered analysis pipeline of the spike-sorted activity in primary somatosensory cortex and ventral posterior lateral nucleus (VPL) of the thalamus upon a combination of optogenetic and mechanical stimulation of L5 or layer 6 (L6) of primary somatosensory cortex (S1) and the hind paw, respectively. The main findings of this work are: *a*. L6 stimulation decreases pain thresholds and increases spontaneous nocifensive behaviour, increases thalamic somatosensory activity recorded in VPL, and suppresses L5; and *b*. L5 activation increases pain threshold and decreases nocifensive behaviour, whereas suppressing L5 mimics pain enhancements as with L6 stimulation.

I collaborated with **Sumser et al., 2025** in a whisker kinematic study in the ventral posterior medial nucleus (VPM) and posteriomedial complex (POm) of the thalamus. My contribution was based on the main finding of the study which is that VPM relays whisker touch regardless if the mouse actively touches something or something touched the mouse's whiskers without its intent. On the other hand, POm only relays unintended touches, meaning that only unexpected touches elicit a neural response. I classified recorded cells peri-stimulus time histograms (PSTHs) according to their response to passive whisker puffs and active whisking touches. Due to the clear differential activity of these nuclei upon passive whisker deflection

* authors contributed equally.

or active touch of a pole, the classifier accuracy was up to 100 % after 15-fold cross-validation.

Sumser, Anton, **Emilio Ulises Isaías-Camacho**, Rebecca Audrey Mease and Alexander Groh (Apr. 2025). 'Active and passive touch are differentially represented in the mouse somatosensory thalamus'. In: *PLOS Biology* 23 (4). Ed. by Alberto Bacci, e3003108. ISSN: 1545-7885. DOI: 10.1371/journal.pbio.3003108. URL: https://dx.plos.org/10.1371/journal.pbio.3003108.

Ziegler, Katharina et al. (2023). 'Primary somatosensory cortex bidirectionally modulates sensory gain and nociceptive behavior in a layer-specific manner'. In: *Nature Communications* 14 (1). ISSN: 20411723. DOI: 10.1038/s41467-023-38798-7.

I am grateful for the people that pushed me forward,
and for the challenges that have shaped me.

ACKNOWLEDGMENTS

I want to thank Prof. Dr. Alexander Groh, Alex, for considering my application to the Ph. D. project. Thank you for showing me among many cool things, juxtacellular recordings in what was probably VPM in an anaesthetised mouse. I was mesmerised with the spiking activity of the neuron we were recording. Thank you for all the personal support when I was moving into Heidelberg, and later when Monika and I were moving to Weststadt. I learned loads. Both technical and personal. Thanks for this great opportunity!

I would like to extend my thanks to Dr. Rebecca Mease who looked over my shoulder for the first two years of my journey. Many analysis ideas and know-hows came from your suggestions, constructing the building blocks for the pipelines used in the published papers and in this thesis. Thank you for the boot camp!

Thanks to my thesis advisory committee who gave me invaluable inputs in and out of the meetings! Prof. Dr. Valery Grinevich, Dr. Kevin Allen: thanks for your insightful questions and suggested directives! You helped me shape the project. Thanks to Prof. Dr. J. Simon Wiegert and Dr. Claudio Acuña Goycolea for accepting my invitation to be part of my examination committee!

Learning from Dr. Sailaja Antharvedi Goda while she prepared and performed her anaesthetised experiments for the pain project was the way I witnessed for the first time routine procedures for electrophysiology experiments. Thank you, Sailaja.

As Dr. Jesús M. Martín-Cortecero, "El profesoraco", applied for a postdoctoral position in the lab, Alex asked me in a very solemn voice: "Hey, Emilio: Would you like to meet Jesus?". I continue to tell this little pun to this day. After Jesús was interviewed and hired, we became close while discussing about silly things and neuroscience. We became even closer while finding single whisker responding neurons in VPM in two out of ten experiments, sharing frustration. Muchas gracias, Jesús. Por tu pasión y amistad. Sin ti, este proyecto no hubiera sido el mismo. Todas las pláticas y discusiones que tuvimos a los largo de estos años han sido muy productivas; personal y profesionalmente. Muchas tormentas de ideas rindieron muy pocos frutos, otras tantas dieron fruto de simple curiosidad y ahora están publicadas, nuestas pláticas siempre fueron bastante amenas. Espero que haya dejado una huella en ti como tú la dejaste en mí. ¡Quiérete, porque muchos te queremos! Y una vez más: ¡Muchas gracias, profesoraco!

James A. Auwn, Señor Jaime, thanks a lot for bringing your unbeatable enthusiasm and passion for the project and science in general! I'm glad we met, even if it was at the end of this journey.

Berin E. Boztepe, Berinoide, you slowly became the target of my bullying and a dear friend from a colleague with whom I rarely interacted. Some days I had near-zero motivation to go into the lab, but then I considered that being able to bully you was enough for me to make it. Be sure that when you need someone to make you feel bad about yourself, you can always count on me. Like when you started your Ph. D. in your current lab and wrote me that you were bored and needed some verbal abuse. I interrupted my MC→iRN experiments to talk to you. Thanks a lot for that and many other things, Berinoide!

Katharina Ziegler, Frau Katha Strophe little penguin, there is no way that the project and my own mind would have endured this journey without your unstoppable push and support, technical and personal. All our nonsense talks, weird noises, laughter, few photoshoot sessions, translation sessions, and a couple of drunken hours together made my time in the lab unforgettable. I couldn't ask for a better office partner. Thanks for helping me review this thesis and translate my abstract, Kathita!

Ross Folkard (now Dr. Folkard), yo! I think my Ph. D. would have been negatively impacted without all those hours and hours discussing ideas of how the brain might work. Most of those discussions turned into cool ideas in both of our projects. I bet you can trace our mutual influence in each of our projects. Some other discussions await your testing, buddy! We had each other backs in many aspects, personally, scientifically, professionally... one of the best partners for improvisation jokes. Thanks for everything, Ross!

Everyone past and present in the Groh Lab: Lennart, Nadin, Filippo, Josephine (Delfina and her squad), Ann-Kristin (Anki), Tim, Melina, Jan, and Antonio. You definitely enriched my experience in the lab. Thanks a lot! A big thanks to the Draguhn and T. Kuner labs that allowed us to settle in Heidelberg and in the University. Special mention to Dr. Martin Both, Märt (now Dr. Rannap), Dimitri, Mathias, Katia, Nadine, Elke, Paul, Drs. Hannah and Ivo Sonntag, Livia, and Ursel for their friendliness and for making me feel welcome. Dr. Isabella Boccuni and Dr. Janina Kupke shared with me their great theses so I could have a blueprint on how to best structure mine. Thanks for that grand gesture! The lunch train of late with Groh and Breckwoldt labs: Ralph, Marta, Jonas, Julius, and Johannes. Thanks for making lunch time a fun time!

Muchísimas gracias a mis papás y a mi hermano, Silvia, Jorge, y Jorge O., que siempre me han apoyado en mis travesías. Miles de consejos, palabras de aliento cuando no veía la luz al final del túnel, visitas para levantarme los ánimos, etc. ¡Gracias por todo! Sin ustedes, sus enseñanzas y su amor incondicional, nunca habría podido llegar

hasta donde estoy. Desde las regañizas y las palas de cocina rotas, hasta los apapachos y momentos que guardo muy profundo en mi corazón: !Les debo todo!

También a Luis Pacheco y Hideki Hata que les encantaba preguntarme que cómo iba con la tesis cada quince días. Aquí la tienen. Lista para que finalmente les pueda contestar: "¡Ya! Finalmente está terminada." Estuvo chingón cuando nos visitaste, Hideki. Se suponía que Luis nos visitaría aquí en Heidelberg, pero nada más lo vi media hora en Frankfurt antes de que se fuera a Madrid.

To the marvellous woman who was my girlfriend when this journey started and transformed into my wife only two years ago: All those days that I came home late from an experiment, fixing a problem in my code, or coming up with a "quick and dirty" solution for a long-standing problem in data collection, analysis or visualisation, Monika was there to receive me with such warmth and love. All my problems melted instantly. Ďakujém moja žena! Želám si byť pre tvoj svet takým silným atlasom, akým si bol ty pre môj!

My thesis work was supported by the Heidelberg Graduate Academy completion grant through the Landesgraduiertenförderung programme with funds allocated by the German Ministry of Science, Research and Arts LGFG 2022-89, and by the German Research Foundation DFG Grants GR3757/3-1, and GR3757/4-1.

CONTENTS

LIST OF FIGURES

LIST OF TABLES

ACRONYMS

SC	superior colliculus	vii
OT	optic tectum	6
SCs	superficial layers of SC	6
SCi	intermediate layers of SC	7
SCd	deep layers of SC	36
VPM	ventral posterior medial nucleus	ix
VPL	ventral posterior lateral nucleus	ix
TRN	thalamic reticular nucleus	51
Sp5	spinal trigeminal nucleus	14
POm	posterio-medial complex	ix
MC	motor cortex	vii
L5	layer 5	vii
L6	layer 6	ix
S1	primary somatosensory cortex	ix
Bf	barrel field	4
BC	barrel field cortex	vii
Bs	brainstem	vii
VC	visual cortex	8
AC	auditory cortex	8
ZI	zona incerta	25
TRN	reticular nucleus of the thalamus	51
7N	facial nucleus	52
PAG	periacueductal grey	53

RTf	brainstem reticular formation	53
OB	orienting behaviour	57
$FeCl_3$	ferric chloride	71
ChR2	channelrhodopsin-2	8
PFA	paraformaldehyde	72
PBS	phosphate buffered saline	
DV	dorso-ventral	5
AP	antero-posterior	5
ML	medio-lateral	5
ip	intraperitoneal	67
sc	subcutaneous	64
ap	action potential	16
GAD	glutamic acid decarboxylase	20
FPS	frames per second	72
GPU	graphics-processing unit	73
MUA	multi-unit activity	73
PSTH	peri-stimulus time histogram	ix
IQR	interquartile range	30
3-D	three-dimensional	7
DLC	DeepLabCut	27
PCA	principal component analysis	40
PC	principal component	40
Gaussian GLM	Gaussian generalised linear model	37
ChR2	channel-rhodopsine	8
iRN	inhibitory recipient neuron	18
eRN	excitatory recipient neuron	35
RN	recipient neuron	vii
CSV	comma-separated value	72
LFP	local-field potential	68
ISI	inter-spike interval	73
DAC	digital-to-analogue converter	69
iN	inhibitory neuron	18
SEM	standard error of the mean	30
R^2	goodness-of-fit	29
GAD	glutamic acid decarboxylase	20

Part I

INTRODUCTION

1

INTRODUCTION

From an evolutionary point of view, the cerebral neocortex or cortex is the latest brain region to evolve. Mammals are the only animals that evolved a neocortex and are, to our understanding and measurement capabilities, the most cognitively capable animals on the planet.

Recent evidence points to some birds – crows and parrots, specifically – that perform cognitive tasks comparable to a young child (six-seven years old) or great apes [27].

The macro and micro anatomy and functions of the cortex have been widely studied to understand the advantages it brings to species that evolved a neocortex compared to species that lack it. Furthermore, species with neocortex differ in the proportion it occupies within their brain. Primates and cetaceans have the highest neocortex proportion among mammals, while rodents have the smallest. Nevertheless, cognitive tests have demonstrated that rats can solve certain puzzles and live in organised societies with implicit rules.

When the cortex expands in species with a high cortex-to-brain proportion, folds, called gyri, maximise its volume in an animal's skull. Increasing the volume and, therefore, capacity of the brain has important trade-offs such as a high metabolic cost, a long developmental stage (foetal and infancy, the longest in humans) and, with these, a dramatic increase in the likelihood of maternal and infant mortality. Despite these high costs, having a cortex increases the individual's survival chances, e. g. mammals normally live in organised societies that would protect each member from external threats, especially pregnant or lactating females. Some clear advantages of the cortex are associative learning, working memory, and behavioural adaptability to the environment.

Animal cognition is an advancing field that has uncovered surprising abilities in a wide variety of animals in a broad range of brain:body and encephalisation index; from insect to bird cognition.

Comparing between different species with and without cortex, mammals that adapt their behaviour to the environment are animals that do not hibernate during winter and accumulate resources to survive scarce food and shelter, e. g. squirrels, arctic foxes, and polar weasels. Unlike species that do not have a cortex, such as fish, amphibians, or reptiles, mammals learn seasonal periodicity and plan their stash, anticipating predictable adversity. Amphibians that endure stark seasonal changes undergo hibernation through their cells' ability to freeze without damage, rather than through learning environmental predictability to devise a strategy. On the other hand, some mammals belonging to the Ursus family hibernate throughout winter. However, they follow a similar strategy to other mammals and stash resources to survive months without food (with a reduced metabolic rate as well), only to emerge once spring has sprung.

One way to study cortical influence in the mammalian brain is to chemically, genetically, or physically remove the whole or a spe-

cific area of the cortex and test for effects against individuals with a sham or control intervention. My colleagues, Heimburg et al. [28], are preparing a manuscript in which mice learn a whisker-dependent discrimination task using classic punishment/reward associative learning in an automated freely-moving setup. They observed that removal of barrel field (Bf) in S1, either prior to or following the learning phase, resulted in mice requiring approximately four times the number of trials to achieve statistically significant performance in comparison to the untouched-brain control group. Furthermore, once the performance of experimental mice for learning was barely crossed after an extended learning phase, Bf-less mice could not sustain significant performance, occasionally dropping to a subthreshold performance. Removing a region of the cortex has acute behavioural and cognitive effects on an individual. These results add to the wealth of literature on ischaemic and haemorrhagic stroke in humans and other animal models in which an individual's cognitive, sensory, or motor capabilities are impaired when the cortex is lesioned. Although through rehabilitation therapy and an unbendable will, many suffering brain damage aftermath show signs of recovery, most likely due to high cortical plasticity[1].

Damage to any brain region that affects enough neural population could lead to severe cognitive, and sensorimotor impairments.

In summary, even if people reading this introduction need no convincing that the cortex is a crucial element in the mammalian brain, I believe that a fundamental function of the cortex is to accelerate, refine, and modulate behaviours. In species that lack a cortex, behaviours that are classified as instinctive are governed by evolutionarily older brain structures. Although instinctive behaviour in mammals remains, cortex functions and interaction with subcortical brain regions increase the environmental adaptability of a species beyond mere likelihood of survival. Investigating cortico-subcortical interactions could reveal valuable insights into the cortical contribution to flexible behaviour through learning and inference.

1.1 INTEREST AND MOTIVATION

My main interest is the ability of the cortex to provide behavioural adaptability to the individual according to the environment. To study this phenomenon, I focused on a cortico-subcortical interaction that has been shown to have a direct and measurable behavioural impact. A well-established structure that receives input from the cortex and is responsible for reflex-like orientation behaviours is the SC.

My motivation for studying the whisker-related SC is that the majority of SC research has been centred on the visual and auditory systems, leaving an important gap in the somatosensory system [1]. Perhaps one reason why visual and auditory studies are more common is

1 Plasticity in this context meaning that other regions of the cortex take over some functions of the lost tissue.

that humans who are lucky to have all their senses functional, mainly explore the environment using sight; we are visual creatures. Other mammals, such as dolphins or bats, star-nosed moles or mice, possess the ability to explore and orient themselves using sound (echolocation) or touch (somatosensation) in addition to sight, respectively; abilities that most of us do not have or have not developed. Therefore, understanding a system that we share with other mammals might be more organic than echolocation in dolphins and bats, electric field detection in sharks, or magnetic field detection in migrating birds.

Some people lacking sight or hearing, sharpen their remaining senses and are able develop extraordinary abilities.

I took the less studied somatosensory SC as an opportunity to investigate the anatomical organisation and behavioural relevance of whisker-related pathways to SC in my ultimate interest of investigating the impact of cortex on 'less evolved' brain regions. Together with Prof. Dr. Groh's expertise in the whisker system within the Bf in S1: BC $\leftrightarrow$ thalamus loop [24–26, 53, 54, 68], the whisker-related SC seemed like an open highway to describe and characterise.

1.2 THE SUPERIOR COLLICULUS

1.2.1 *SC/OT across vertebrates*

SC is a highly conserved structure in vertebrates. From the simplest vertebrate to mammals with laminar compartmentalisation and direct sensory input, SC has similar organisation and connectivity across a wide range of species. SC presence across species point to a phylogenetically ancient brain network that likely evolved following vision (beyond mere photoreception), allowing predation and escape behaviours to develop during the highly competitive "Cambrian explosion" approximately 560 to 540 million years ago [9, 23, 59]. The conservation of structures between species highlights their critical roles for survival [74]. In mammalian brains, the cortex heavily innervates SC, which raises the question of how cortical innervation influences SC-associated or even SC-dependent behaviours; or to what extent does the SC retains its primitive functions among more evolved regions.

Although 'optic tectum' is the correct term for non-mammalian vertebrate species, I use SC to refer to both homologous structures.

1.2.2 *Anatomy*

The SC is a layered structure in the midbrain that integrates upcoming visual, auditory, and somatosensory information to generate fast and coordinated motor commands critical for orientation and survival [3, 13, 74]. The mouse SC extends roughly 2 mm in the antero-posterior (AP) axis, 2 mm in the medio-lateral (ML) axis, and is 1 mm thick[2]. Relative to the rodent brain (AP: 5 to 6 mm, ML: 4 to 5 mm from the midline laterally to the edge of one hemisphere, and dorso-ventral (DV): 5 to 6 mm) the SC is a large structure.

2 Because SC is curved, its depth does not mean thickness

The SC divides into three layers on the DV axis: superficial, intermediate, and deep. The superficial layer subdivides into stratum griseum superficiale (SGS) and stratum opticum (SO). The superficial layers of SC (SCs) receives inputs from the retina, the visual thalamus, and the visual cortex. Due to its connectivity and responsiveness, SCs is referred to as "visuosensory". The intermediate and deep layers of SC (SCi and SCd, respectively) subdivide into grey and white layers each, i. e. stratum griseum intermediale, stratum griseum profundum, stratum album intermediale, and stratum album profundum (SGI, SGP, SAI, SAP). Together, SCi and SCd are referred to as "motor layers" since neurons in this region exhibit stereotypical activity prior to a quick movement of the eyes toward a specific target (saccades) [3, 19, 42, 52].

Main inputs to and outputs from SC include the entire cortex, ascending sensory organs (retinas, cochleae, mechanoreceptors in the skin and vibrissae), thalamic and hypothalamic nuclei, cerebellum, brainstem, and medulla [4]. Most of these connections are bidirectional, except those with the cortex. SC communicates with the cortex through several structures, including thalamus and hypothalamus [21], basal ganglia [63], and periaqueductal grey [61].

1.2.3 *Innate behaviours*

Gandhi and Katnani [17], and Hoy and Farrow [30], in their recent review, point to the importance of SC as a centre for sensorimotor transformation, and more specifically for animal orientation. The Encyclopaedia of Neuroscience defines orientation behaviour as the "ability to move in space with respect to an external reference system or by actively generating spatial information (like in echo location)" [35]. Most of the SC-associated behaviours listed in [30] could be clustered as approach/exploration or escape/avoidance. For example, gaze shift, arm reach, pursuit and hunting are behaviours that require the sensory organs to be (re)directed toward the stimulus source to explore/interact with or eat it. On the other hand, freezing and escape are behaviours whose intentions are to increase the distance between the individual and the stimulus source, passively or actively. A special note goes to species-specific and developmental behaviours such as collicular orientation of human babies to "face-like shapes" or virgin female mice caring for other mice's pups [30].

To study the bat SC would be very interesting since their navigation relies as much on audition as humans on vision.

Moreover, Allen et al. enlisted several studies in which researchers stimulated SC and observed saccades, head, pinnae and vibrissae movements, and even vocalisations [70] in mammalian species, and locomotion and prey-catching behaviour in lamprey[3] and toads, respectively [1]. Isa et al. proposed that SC is nature's solution to provide

3 Perhaps the simplest vertebrate with an optic tectum (OT) closely resembling the anatomy and function of the mammalian SC [1].

animals with perception of their own body and environment or, as in their own words: "to register events in the surrounding space" [32].

SCs receives inputs from the retina and the lateral posterior and pulvinar nuclei in the thalamus. These visual inputs are organised retinotopically to keep the neural representation of objects and their movements as close as possible to the real world. Half a century ago, two independent studies by Stein, Magalhães-Castro and Kruger, and by Dräger and Hubel showed that somatosensory inputs to the intermediate layers of SC (SCi) are organised according to the way the animal sees its own body and that single collicular neurons are multimodal; single neurons receive a combination of visual, auditory, or somatosensory inputs. Specifically, they showed somatotopographic organisation in mice SCi, which corresponds to the retinotopic map in SCs, which results in their bodies proportionally represented according to the perspective self-projection into their retinas. Whiskers, face, and forelimbs have a larger SC representation than the tail and hindlimbs [15, 66].

Genetic tools have opened a broad new path in neuroscience research. Evidence for this is the series of studies from the Tripodi lab [22, 50, 75] in which excitatory neurons expressing the genetic marker Pitx2 in SCi produce three-dimensional (3-D) head-orienting movements in SCi. Pitx2 neurons were systematically stimulated using optogenetic tools, resulting in different head movements depending on where in the SCi the light was delivered. These results validated a motor map for head movements already suggested by Wilson et al. [75]. In addition, head-movement amplitudes varied as a function of stimulation duration and frequency [50]. González-Rueda et al. proposed a hypothesis for visuomotor transformation, in which visual information reaches motor neurons in SCi to produce movement vectors to lock in a target [22]. These reviews and studies presented here have shown that SC is an orientation centre.

Paired-like Homeodomain Transcription Factor 2 (Pitx2) is crucial during embryonic development; specifically, for subthalamic and midbrain nuceli [47].

Recent evidence [14, 37, 45, 72] puts SC forth as part of the attention network.

1.2.4 *Cortico-collicular pathways in the literature*

As Hoy and Farrow wrote in their review: "... there is a strong interplay between the cortex and colliculus both for performing sensory detection tasks, as well as for executing the motor consequences of decisions..." [30]. The interaction between cortex and SC could result in a more efficient use of resources. For example, by refining and reducing defence behaviours in a context-specific manner, or delegating sensorimotor transformations that do not require cortical computations to be performed.

The systematic labelling of pathways from the entire cortex to SC presented by Benavidez et al. [4] verified and extended on a variety of cortico-collicular pathways that earlier studies have discovered and described. Since Benavidez et al. showed that the entire cortex

projects to SC, a feature that, to my knowledge, is unique to SC, I took a deeper interest in cortico-collicular pathways. In addition, a myriad of subcortical inputs and outputs have been reported, which almost include the entire subcortical brain [4]. Efforts to address cortico-collicular pathways in the literature include whisker-dependent pathways. Mederos et al. [55] is an example of cortex suppressing "fast instinctive" responses through cortico-subcortical plasticity. Mederos and colleagues showed that posterolateral higher visual areas (plHVAs) are necessary for the learning process about a non-harmful sudden stimulus. After learning, the newly acquired behaviour is controlled by the ventrolateral geniculate nucleus (vLGN), which underwent plastic changes and is now able to inhibit excessive defence behaviour.

Castro-Alamancos and Favero described whisker-related cortico- and trigemino-collicular pathways by injecting chemical tracers in BC and the trigeminal nucleus of the Bs. Electrophysiology experiments revealed that neurons in the region where BC and Bs axons reached SC had one of three possible combinations of early and late responses to a whisker deflection stimulation, suggesting functional convergence of BC and Bs axons in a single collicular neuron [10].

Liang et al. investigated the visual cortico-collicular pathway by evoking a light-induced SC-dependent "freezing" behaviour in mice. The main observation of this study was that visual cortex (VC)→SC pathway is responsible for freezing behaviour since silencing or exciting VC neurons projecting to SC had consistent results in behaviour, i. e. reduction and evoking freezing, respectively [41]. In a similar line, Zingg et al. [78] expressed channel-rhodopsine (ChR2) in auditory cortex (AC)→ and VC→SC with the trans-synaptic anterograde virus strategy and reported that optostimulation of either VC or AC RNs in SC (VC→ and AC→RNs, respectively) or the axons from RNs in their targets elicited freezing behaviour in freely moving mice. Zingg et al. discussed that using a transgenic mouse line, specific cell types could be labelled.

The intersectional viral strategy was based on the work of Zingg et al. [78] and Fenno et al. [16].

With these genetic and viral toolsets, my colleagues and I were one step away from applying (and refining) these techniques to study the whisker-relevant collicular pathways.

1.3 PH. D. STAGES

My colleagues and I have focused on studying cortex innervation and influence on SC and SC-associated behaviours. My Ph. D. project was divided into two stages. In the first stage, my colleagues and I expanded the current anatomical and physiological knowledge of whisker-related cortico- and trigemino-collicular pathways. In the second stage, I pinpoint the behavioural relevance of specific components of the motor cortico-collicular pathway (MC→SC).

1.3.1 "Monosynaptic trans-collicular pathways link mouse whisker circuits to integrate somatosensory and motor cortical signals"

The first stage consisted of a series of injections to label and reveal the now published [48] cortico- and trigemino-collicular pathways, and their cell-type-specific targets, organisation and trans-collicular connectivity. A state-of-the-art viral approach was implemented to highlight the intersection of two sets of neural circuits to achieve anatomical identification by coupling a recombinase toolkit [16] with the anterograde trans-synaptic infection of downstream neurons [78]. Injection surgeries were performed by Berin E. Boztepe during her master's thesis under the supervision of Dr. Martín-Cortecero, and by Katharina Ziegler. For physiological identification, I conducted anaesthetised experiments in transgenic mice expressing Cre in cortical L5 (Rbp4-Cre). By injecting AAV DIO-ChR2 in whisker-related MC and BC, I independently opto-stimulated MC- and BC-L5, and deflected a subset of whiskers using a mesh attached to a piezo. Finally, I validated the somatosensory representation in SC of the whiskers in awake, head-fixed mice by delivering an air puff to the whisker set contralateral to the neural recording site. I extend these results in chapter 2 and point to my contributions.

During my experimentation with anaesthetised mice, Dr. Martín-Cortecero and I discussed conceptual ideas and how to implement them, enriching physiological and anatomical experiments.

1.3.2 *Behavioural relevance of cortico- and trigemino-collicular pathways*

The second stage consists of the behavioural relevance of cortico-collicular pathways, aiming to uncover the role of the cortex in adapting reflexive orienting behaviour. To achieve this goal, I built a low-friction roller set-up in which I could elicit and measure SC-associated behaviours of awake, head-fixed mice. I used several viral techniques to manipulate specific components of cortico-collicular pathways, including the new mosquito-derived opsine eOPN3 [46] and the same intersectional approach from the anatomical study, but in this case to express ChR2 in a specific collicular population. Moreover, I used a pharmacological approach to dissect the contribution of cortico-collicular pathways to reflexive behavioural adaptation. In this stage, I performed several surgeries and most experiments, but still shared the workload with Dr. Martín-Cortecero, Katharina Ziegler, James A. Auwn, and Ann-Kristin Kenkel. Moreover, my colleagues and I are preparing a manuscript with the findings of the second stage. In chapter 3, I present these results and point to the contributions that my colleagues made along the way.

Part II

RESULTS

2

ANATOMICAL AND PHYSIOLOGICAL LINK OF CORTICAL AND SUBCORTICAL WHISKER CIRCUITS IN SUPERIOR COLLICULUS

Teamwork: dreamwork

— Dr. Jesús M. Martín-Cortecero

The reader can safely assume that all the material from this Chapter was taken and/or adapted from Martín-Cortecero et al. [48] unless otherwise stated.

In this chapter, I describe the results of the first stage of my Ph. D. project, which greatly overlaps with data and figures published by Martín-Cortecero et al. [48]. Surgeries and cell counting were performed by Berin E. Boztepe during her master's thesis under the supervision and collaboration of Dr. Martín-Cortecero, and Katharina Ziegler. Although I did not directly contribute to the anatomical experiments and analysis, Dr. Martín-Cortecero and I shared conceptual work. My primary contribution was performing awake and anaesthetised experiments aimed at recording neural activity in the whisker-sensitive region of SC to find post-synaptic neurons with inputs from MC, BC or both. I validated the anatomical finding after encountering single units responding to MC- and BC-L5 optogenetic activation in SC. In addition, I found very rare putative neurons with converging inputs from BC, MC, and Bs.

In Martín-Cortecero et al. [48] three main questions were established (Figure 2.1): 1) Do axons from RNs project to structures outside of SC or stay within SC? 2) As discussed by Zingg et al. [78], what is the functional nature, i. e. excitatory or inhibitory, of RNs? 3) Given the multimodal nature of SC, do projections to SC from cortex or Bs overlap in single RNs?

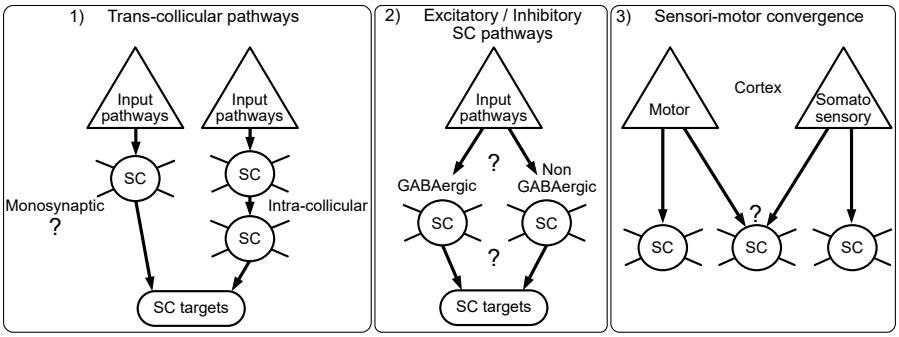

FIGURE 2.1 – Main questions resolved by anatomical and physiological experimentation.
Figure taken and adapted from Martín-Cortecero et al. [48].

2.1 WHISKER-SENSITIVE REGION IN SUPERIOR COLLICULUS

I targeted 64 channel silicone probes to the lateral SC of awake, head-fixed mice to record neural responses in the whisker-sensitive region [6, 10, 12, 48]. Mice's contralateral whiskers to the recording site were stimulated using an air puff to evoke a neural response (Figure 2.2A). I found approximately 30 % significantly modulated units in twelve recordings from eight mice. The estimated locations of the modulated units were determined using micro-manipulator coordinates along with dye trails from the probe in brain slices.

Figure 2.2B shows an example recording PSTH of single units (rows) ordered by descending first spike latency from top to bottom. The unit with the shortest latency is at the bottom, while the unit with the largest is at the top. Both single unit and population PSTHs showed a two-component puff response. The earlier component might be the product of the ascending input from Bs, while the latter, second component could be due to cortical inputs. Figure 2.2C shows the estimated locations of the modulated units; consistent with findings from prior research.

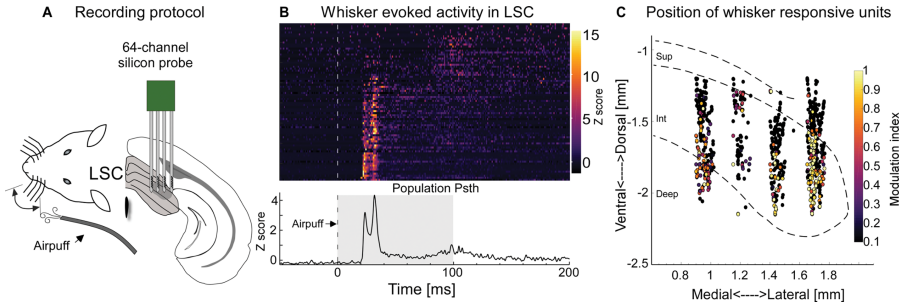

FIGURE 2.2 – **A.** Schematic showing the whisker stimulation using an air puff and the electrophysiology recording in SC. The stimulated whiskers were contralateral to the recording site. **B.** Example single unit and population PSTH aligned to the whisker puff. Units are ordered by first-spike latency from bottom to top and their firing rate is represented in z-score. **C.** Estimated positions for puff modulated units in SC. Awake electrophysiology experiments conducted and analysed by me.
Figure taken from Martín-Cortecero et al. [48].

2.2 WHISKER-RELATED COLLICULAR PROJECTING REGIONS

Once the physiological signature of the whisker-sensitive region in SC was identified, the whisker-related inputs to SC were labelled by injecting a retrograde virus (rAAV$_2$ tdTomato, Figure 2.3A). The brain was sliced and imaged, and found several regions in the ipsilateral cortex, such as MC, BC, auditory, insular and ectorhinal cortices as well as in the contralateral spinal trigeminal nucleus (Sp5) in Bs (Figure 2.3B & E).

MC: parts of primary and secondary motor cortex

Additionally, the cortical origin of the cortico-collicular pathway was verified by repeating the retrograde virus experiment in Ntsr1-Cre ×EYFP mice to differentiate corticofugal layers. Figure 2.3C shows the differential labelling of the mouse line L6 EYFP in green and the retrograde expression of tdTomato in L5. A colour histogram analysis demonstrated the separation of expression between tdTomato in L5 and EYFP in L6. These results pinpoint the origin of the cortico-collicular pathway as L5 and not L6, unlike AC→SC as shown by Zurita et al. [79] (Figure 2.3D).

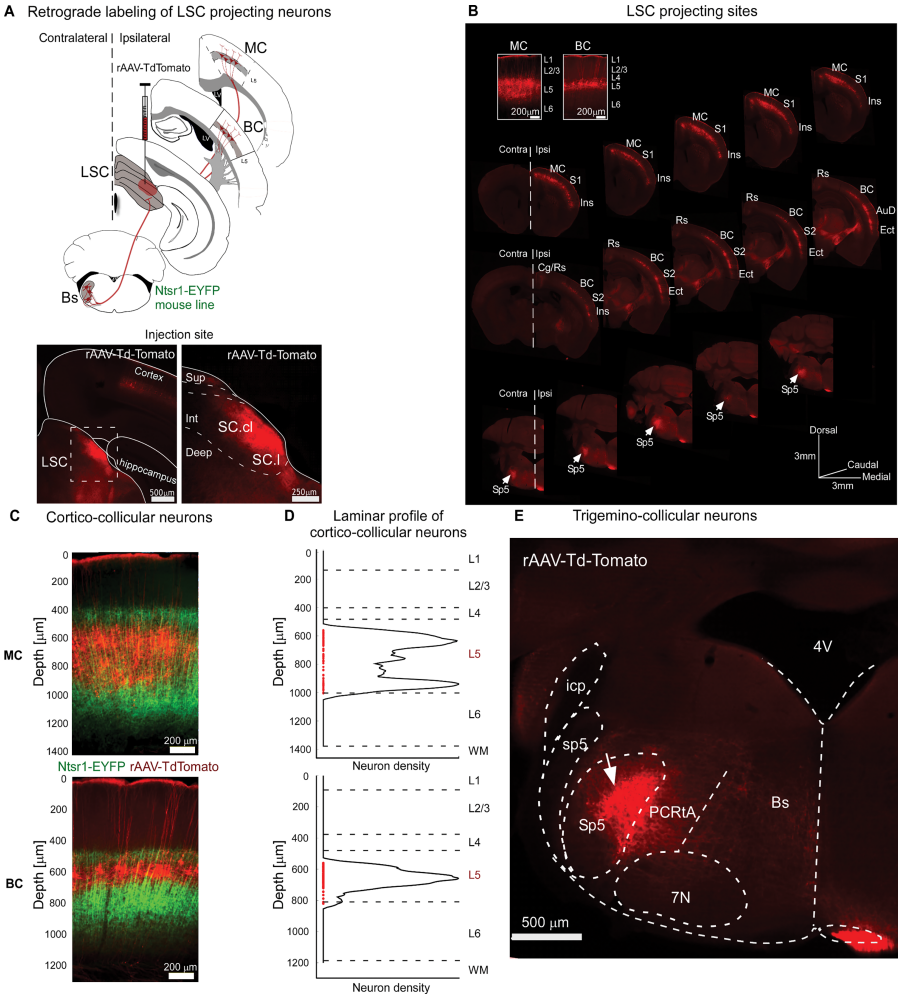

FIGURE 2.3 – **A.** Schematic showing the injection protocol to retrogradely label SC-projecting cells (top) and example of the injection site expressing tdTomato (bottom). **B.** Retrograde expression of $rAAV_2$ tdTomato in consecutive slices in SC-projecting regions: ipsilateral MC and BC, and contralateral Bs Sp5. **C.** Example slices from the Ntsr1×ChR2 mice experiments expressing EYFP (green) in L6 and tdTomato (red) in L5. **D.** Histogram analysis for cortical depth expression of EYFP and tdTomato (**B.**) showing exclusive labelling of L5 cells in MC and BC. **E.** Example slice showing SC-projecting cells from the contralateral Bs Sp5.
Figure taken from Martín-Cortecero et al. [48].

2.3 RECIPIENT NEURONS ORGANISATION IN WHISKER-RELATED SUPERIOR COLLICULUS

Question #1 from Figure 2.1 presents a way for whisker-relevant projecting regions to integrate their output with the collicular neural network and computations directly or indirectly. A direct pathway from whisker-relevant regions to collicular target regions could be advantageous for swift motor commands aided by processed whisker information. On the other hand, an indirect pathway could increase the computation capability at the expense of time-consuming polysynaptic intra-collicular networks before leaving SC.

The distribution of RNs in SC from MC, BC, and Bs was first revealed by employing the viral anterograde 'jumping' strategy. This viral strategy consisted on injecting a cocktail of AAV_1-Cre + AAV_2-DIO mCherry in MC, BC, and Bs to validate the injection site, and AAV_2-DIO EGFP in SC to reveal the post-synaptic neurons of each pathway (target coordinates in Table 5.1, Figure 2.4A & B).

MC- and BC-L5, and Bs neurons that project to SC infect their corresponding RNs to express Cre (Figure 2.4B) to study their distribution in SC. RNs from MC, BC, and Bs were counted and their location registered to construct an AP distribution as well as their position in SC with nuclei borders of the mouse brain atlas [60]. RNs from the whisker-related regions are clustered in the lateral portion of the SC (Figure 2.4C). RNs have a considerable overlap along the AP axis, although cortical RNs share a similar organisation with a slight distinction only on the ML axis (Figure 2.4D). MC→RNs were located most medially, while Bs→RNs are the most lateral and ventral of these three pathways, surrounding BC→RNs (Figure 2.4E). Bs→RNs differ significantly on every axis with respect to cortical RNs (Figure 2.4D-F).

Our cortical projection labelling in SC revealed with the transsynaptic viral strategy [78] is consistent with the projections reported by Benavidez et al. [4] (Figure 2.4E). Results from the retrograde (Figure 2.3) and anterograde (Figure 2.4) strategies suggest the existence of a "whisker SC" that integrates peripheral upstream and cortical downstream information [48]. With RNs labelled, collicular targets could be identified to answer question #1.

2.4 WHISKER-RELEVANT PROJECTING AREAS INNERVATE GABAERGIC CELLS IN SUPERIOR COLLICULUS

Question #2 from Figure 2.1 poses the possibility that whisker-relevant regions project to different cell types in SC. One way to control action potentials (aps) propagation within a neural network is via GABAergic neurons. An anatomical indication that a long-range projecting region is contributing to controlling a neural network is by asking RNs about their identity. So, do MC, BC, or Bs directly innervate GABAergic

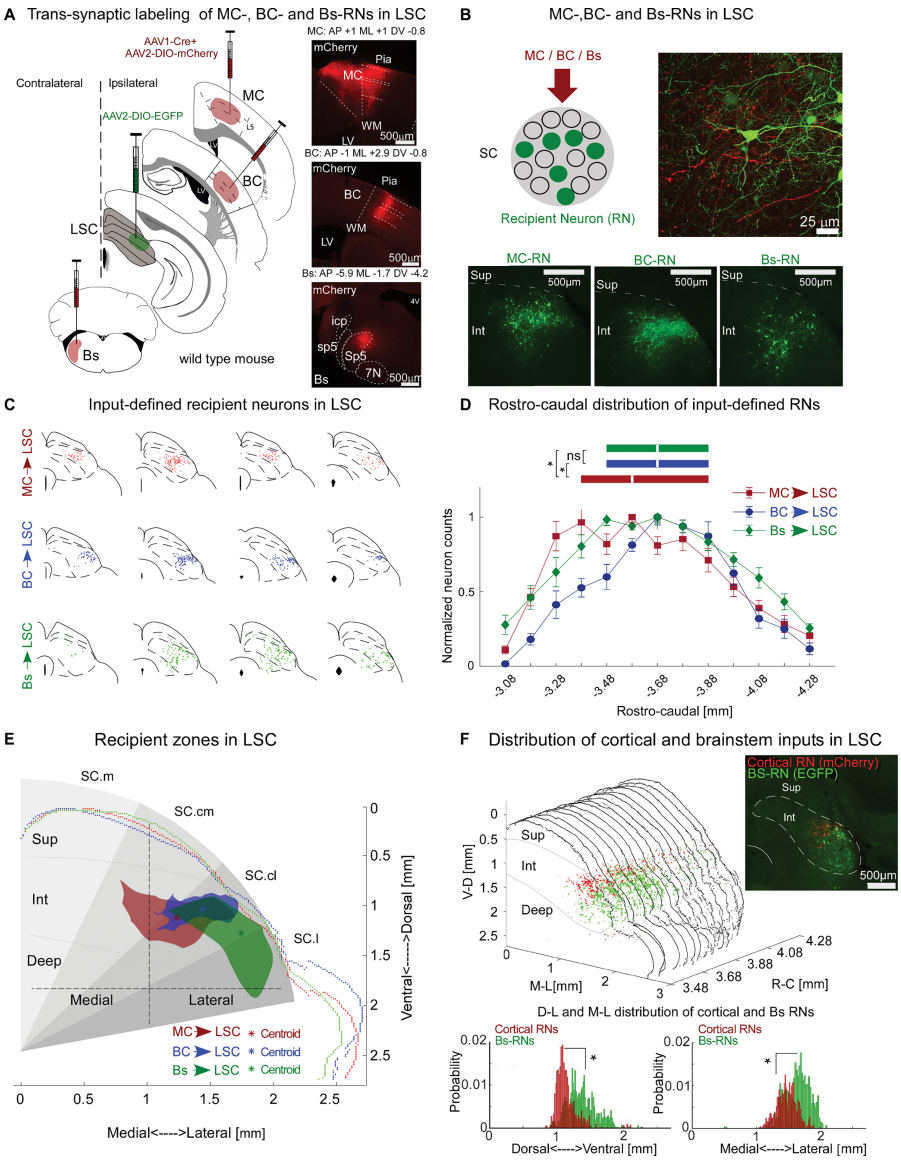

FIGURE 2.4 – **A.** Schematic showing the trans-synaptic viral approach using a cocktail of AAV_1-Cre + AAV_2-DIO mCherry in MC, BC, or Bs and AAV_2-DIO EGFP in SC to exclusively label RNs. Images to the right show examples of virus expression in projecting sites. **B.** (From top to bottom and left to right) Schematic exemplifying expression of EGFP for all three projecting sites. High magnification of a MC→RNs in the whisker-sensitive region of SC. Overview of MC→, BC→, and Bs→RNs. **C.** Schematic reconstruction of AP slices from the three labelled pathways. **D.** Normalised mean distributions along the AP axis in 100 µm steps for the three labelled pathways. **E.** Shadows of recipient areas for the three projecting regions and their polygon centroid showing certain spatial organisation of input-defined collicular neural populations in agreement with Benavidez et al. [4]. **F.** 3-D reconstruction of 15 consecutive slices of cortical (MC→ & BC→RNs, red) and Bs→RNs (green) showing a distinct distribution between these two pathway origins.
Figure taken from Martín-Cortecero et al. [48].

neurons in SC? Before looking at the proportion of non-GABAergic vs. GABAergic RNs, the collicular proportion of GABAergic (inhibitory neuron, iN) to non-GABAergic neurons was determined using GAD-GFP mice. Collicular slices were stained using a neural marker (NeuN-Alexa 647) to label all neurons. iNs were co-labelled from the mouse line GFP and from the neural staining with NeuN-Alexa 647, which looked yellow when creating a composite. The iNs proportion estimation was around 23 % in the lateral intermediate layers, where the whisker-sensitive region is located (Figure 2.5A). After measuring the proportion of collicular iNs, inhibitory recipient neuron (iRN) populations could be labelled and analysed.

Liu et al. [43] reported approximately 30 % of inhibitory neuron (iN) in the superficial layers of SC.

To achieve this purpose, an intersectional approach was used where an AAV_1-Flpo virus was injected in MC, BC, and Bs of GAD-Cre mice. Neurons expressing Cre from the mouse line and Flpo from the trans-synaptic virus would be labelled with the double condition reporter virus AAV_8-Con/Fon EYFP in SC [16]. An additional reporter virus (AAV_2-fDIO mCherry) labelled RNs to verify Flpo infection (Figure 2.5B). Similar to Fig. 2.5A, neurons expressing both EYFP and mCherry appear yellow (Figure 2.5C). EYFP emission spectrum peaks at around 530 nm wavelength, which is within the green domain (Wavelength approximate colour: ●).

iRN populations from all three pathways overlapped with their respective RNs, showing no special organisation in any axes. Example slices and reconstructed schematics from Figure 2.5D show non-iRNs and iRNs populations intermingled. However, the innervated proportion of iRNs to RNs was significantly higher than the proportion of collicular iNs to non-iNs. Each pathway targeted between 34 and 37 % of iRNs, whereas the proportion of iNs in SC ranges from 22 to 23 % (Figure 2.5E-G), which means that the three pathways projecting to SC target preferentially iNs. This could give the cortex a way to control or at least contribute to the control of collicular computations.

2.5 MOTOR AND SOMATOSENSORY CONVERGENCE IN SINGLE COLLICULAR NEURONS

Question #3 proposed that different projecting sites target the same neuron, integrating their outputs. Convergence of two (or more) projecting sites into single neurons would allow for high temporal precision, accelerating computations. In [48], my colleagues and I presented two key pieces of evidence showing that motor commands and processed somatosensory information from MC and BC converge into single collicular neurons.

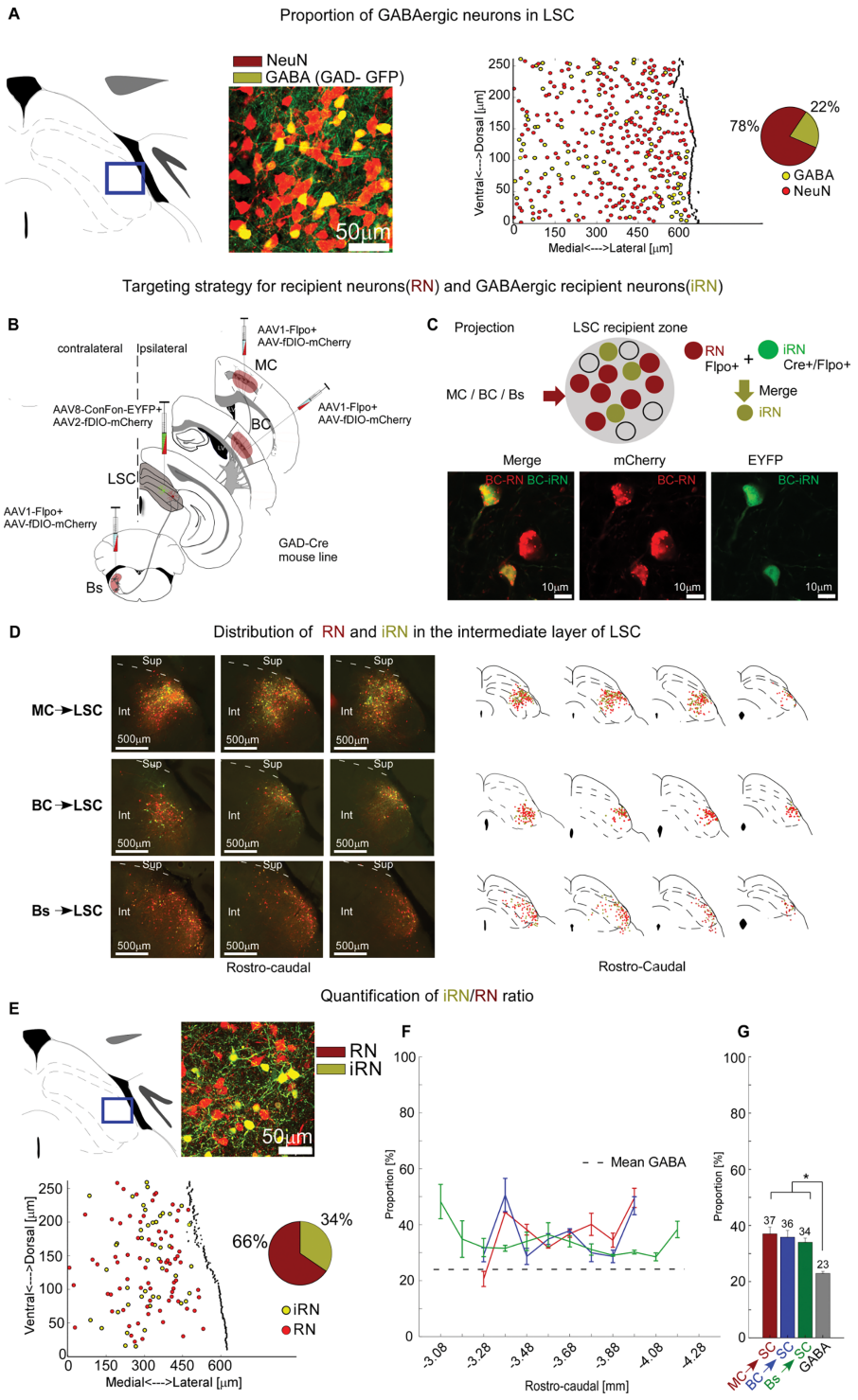

FIGURE 2.5 – *Caption on next page.*

2.5.1 *Anatomy experiments*

RNs distribution (shown in Figure 2.4) has considerable overlap, which suggests a likely convergence between, e. g. MC→ and BC→RNs. To test this hypothesis, the same intersectional strategy deployed to reveal

iRNs was used but in this case AAV_1-Cre was injected in e. g. MC, and AAV_1-Flpo in BC, such that a single collicular neuron receiving input from these two cortices would express Cre and Flpo. Therefore, an injection of AAV_8-Con/Fon EYFP in SC would reveal RNs with converging inputs. Figure 2.6A show the injection protocol to reveal "3 choose 2" combinations of MC, BC, and Bs with representative slices on the right. A schematic reconstruction of the label neurons along the AP axis is shown in Figure 2.6B. Convergent RNs distribution positions (medians) for the three combinations were significantly different in the AP axis. Cortico-cortical RNs were 2.33-fold more predominantly populating the tissue than cortico-trigeminal RNs (Figure 2.6C-E).

Single collicular neurons receive input from more than one projecting region.

Finally, a two-component Gaussian mixture model was fitted to the cells' (x, y) coordinates. The mean of the fitted two-component Gaussian distribution for MC and BC convergent RNs were the following: ML (x): 1492 µm, DV (y): 1126 µm, in the dorsal part of the lateral intermediate layer. These results suggest that single cells in SC could integrate motor commands and somatosensory feedback with high temporal precision.

2.5.2 *Physiological experiments*

To functionally test monosynaptic convergence in single cells, I performed anaesthetised experiments in Rbp4-Cre×EYFP-ChR2 mice, which expressed Cre-dependent ChR2 in cortical L5. I optostimulated MC- and BC-L5 sequentially with a blue laser (Figure 2.7A), and observed activation of single units with response latencies between 9 and 12 ms. The response latency suggests that units with laser-evoked activity are monosynaptically connected to MC and BC [54]. A total of 30 cells responded to either cortex, of which nine responded to both.

FIGURE 2.5 *(cont.)* – **A.** Schematic showing the lateral intermediate layers of SC in a blue rectangle where the GABAergic (inhibitory neuron, iN) were counted, and example picture with NeuN-Alexa 647 marking all neurons and EGFP from the mouse line labelling all iNs. iNs (22 to 23 %) were double labelled and therefore shown in yellow. **B.** Injection protocol schematic for the intersectional labelling approach in glutamic acid decarboxylase (GAD)-Cre mice, in which iNs express both Cre and Flpo. **C.** Example schematic explaining the result of the approach and an image of one iRNs (green, and yellow in merged image) and one non-inhibitory RN (red). **D.** Example of consecutive AP slices and schematic reconstruction of MC→, BC→, and Bs→iRNs (green) and RNs (red). **E.** High-magnification example image of MC→iRNs (green) and RNs (red) and a its proportion in a pie chart with 34 % of iRNs. **F.** Proportion of iRNs throughout the AP axis for the three pathways (MC→SC in red; BC→SC in blue; Bs→SC in green; and iNs as a dashed grey line). **G.** Significantly higher average iRNs proportions throughout the AP axis for the three pathways (colour-code as in **F**) vs. collicular iNs.
Figure taken from Martín-Cortecero et al. [48].

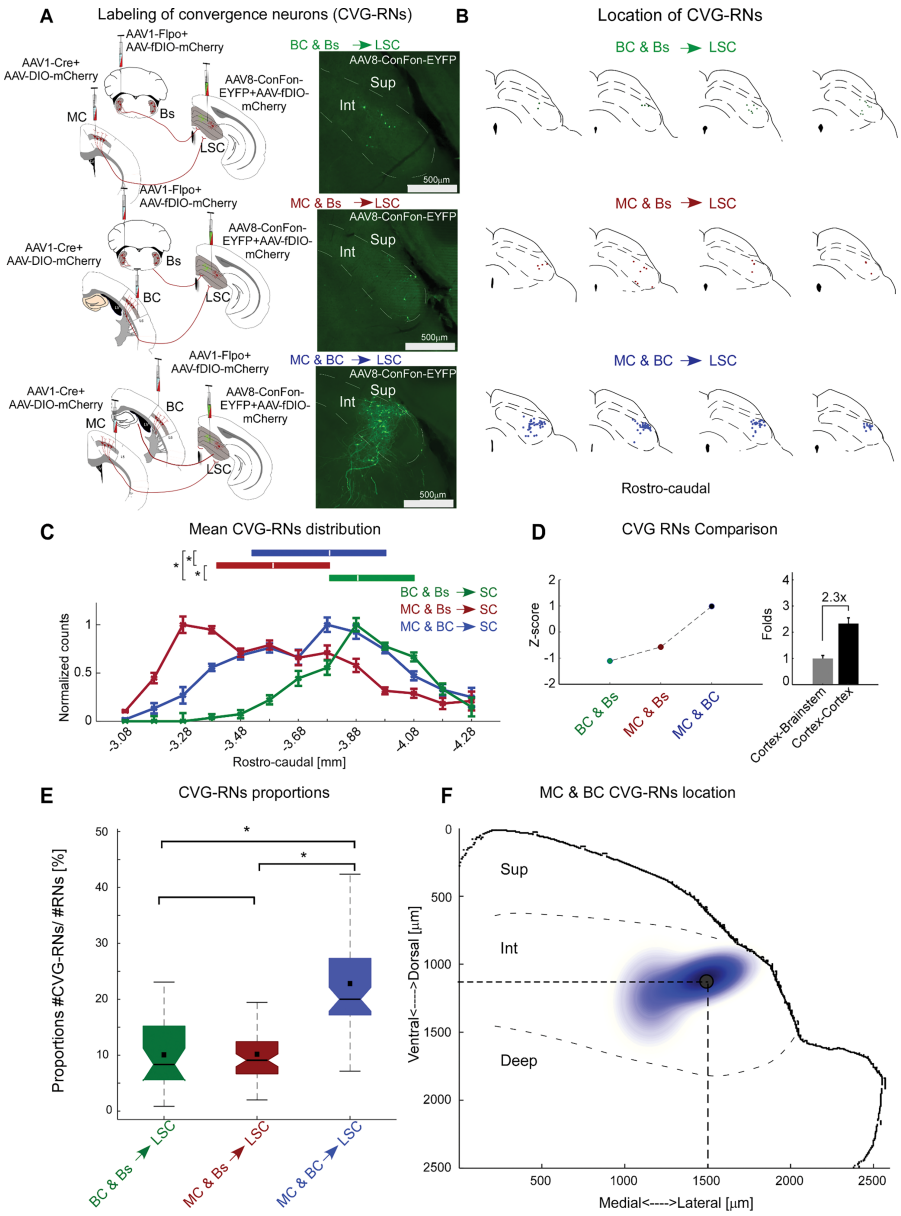

FIGURE 2.6 – *Caption on next page.*

In summary, the whisker SC receives direct input from the periphery, and convergent and non-convergent L5 of motor and barrel cortices into single neurons. A subpopulation of RNs ranging from 20 to 30 % have convergent input from at least two of the projecting areas shown anatomically (Figure 2.6) and functionally (Figure 2.7), suggesting a fast integration of motor commands with somatosensory information for collicular computations.

2.5.3 *Physiological putative triple convergence*

As presented at the beginning of this Chapter, three Rbp4-Cre mice were injected with AAV_4-DIO ChR2-mCherry in MC and BC, to test how MC- & BC-L5 activation and the ascending sensory inputs from Bs interact in SC. Compared with awake recordings from section 2.1, I observed a lower yield of whisker deflection responding units.

Although anecdotal, cortical L5 and Bs projections are integrated within SC modifying the somatosensory representation.

Figure 2.8A shows an example recording with around 15 % of significantly modulated units upon whisker deflection. From these units, only five respond to either MC- or BC-L5 stimulation. L5 stimulation shifts the second component of the whisker response with a latency similar to Figure 2.7. A more detailed PSTH in Figure 2.8B shows that when stimulating MC-L5 few of the second component spikes still occur in the example raster when compared with BC-L5 stimulation.

These results point to a possible convergence of multiple projecting regions into single recipient cells to perhaps adjust sensorimotor transformations. Anatomical experiments are needed to test the hypothesis of triple convergent RNs in SC. Either using the triple conditioning strategy proposed by Fenno et al. [16] with only viral injections or a colour intersectional approach using any anterograde labelling in one of the three projecting sites in addition to the established dual intersectional strategy, single cells receiving convergent inputs from the three whisker-relevant projecting sites would be labelled. Given the lower proportion of cortico-trigeminal convergence in SC, I expect that only a handful of neurons receiving monosynaptic input from MC, BC, and Bs to integrate peripheral inputs with processed somatosensory information and motor commands to update ongoing computations in the whisker system.

FIGURE 2.6 *(cont.)* – **A.** (left) Schematic showing the injection protocol to reveal "3 choose 2" (three combinations) by reusing the intersectional approach in wild-type mice. (right) Slice examples showing the expression degree for BC & Bs (green), MC & Bs (red), and MC & BC (blue) combinations. **B.** Schematic reconstruction of EYFP expression along the AP axis for the three combinations (colour code as in **A**). **C.** AP distribution of the three combinations showing a distinct location amongst these subpopulations (colour code as in **A**). **D.** (left) Z-score transformation of counted cells, (right) where cortico-cortical convergence is 2.33-fold higher deviation from cortico-trigeminal counts. **E.** Percentages of convergent to RNs for each combination showing the significantly greater proportion of cortico-cortical vs. cortico-trigeminal convergent cells. **F.** Two-component Gaussian mixture model showing a probability map of finding a cortico-cortical convergent cell with the highest value at ML: 1492 µm and DV: 1126 µm, in the dorsal part of the lateral intermediate layer of SC.
Figure take from Martín-Cortecero et al. [48].

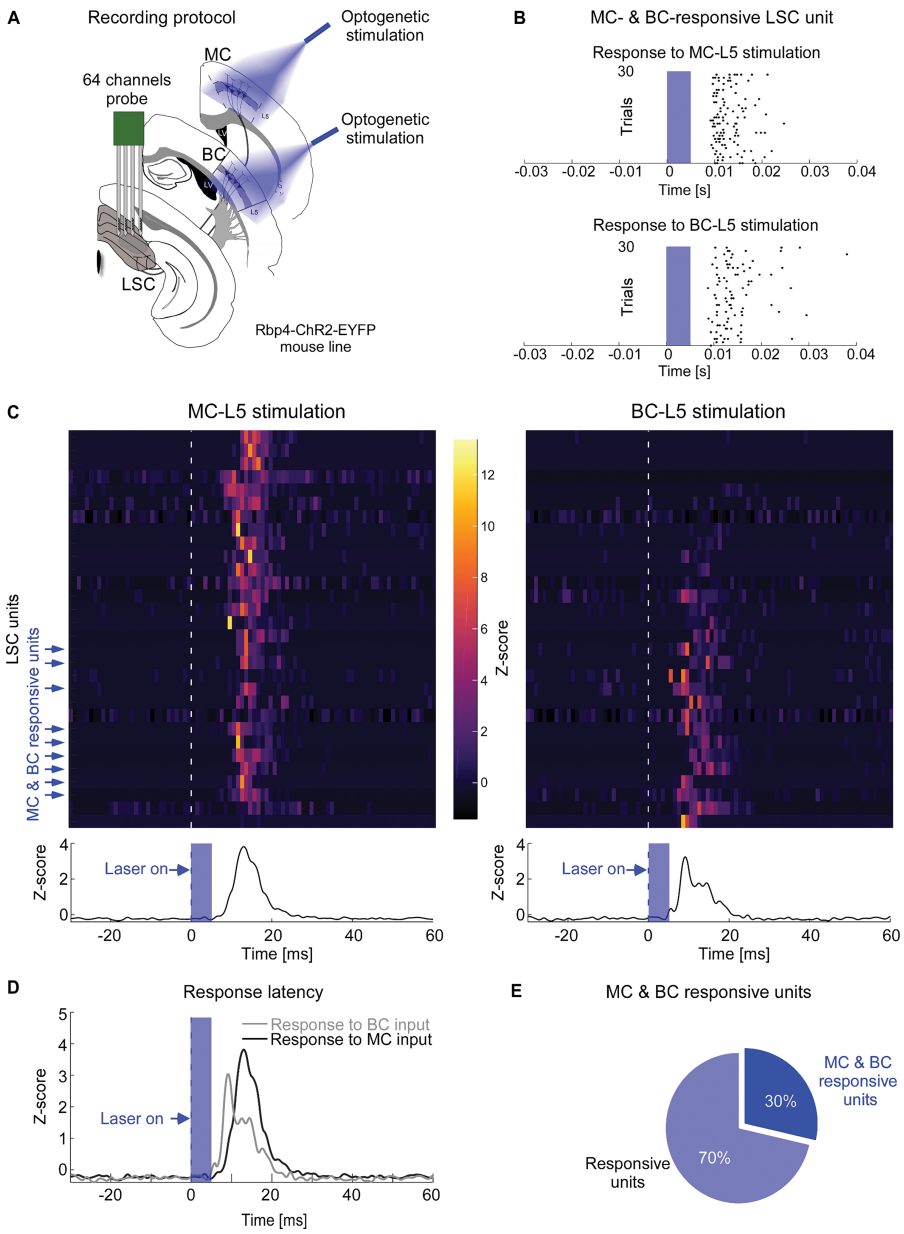

FIGURE 2.7 – **A.** Schematic of optogenetic stimulation of L5 of MC and BC, and electrophysiology recording in SC. **B.** Example rasters with 30 trials of a single unit responding to L5 stimulation of MC and BC. (**B-D**) Blue rectangles represent optogenetic stimulation. **C.** Normalised single unit and population PSTHs of 30 responsive units in z-scores ordered by ascending magnitude to BC-L5 stimulation. The blue arrows on the left indicate functionally convergent RNs that responded to both BC- and MC-L5 stimulation. **D.** Population PSTHs from **C.** in black for MC and grey for BC stimulation overlaid. **E.** Pie chart showing convergent unit proportion (30 % of laser responsive units).
Figure taken from Martín-Cortecero et al. [48].

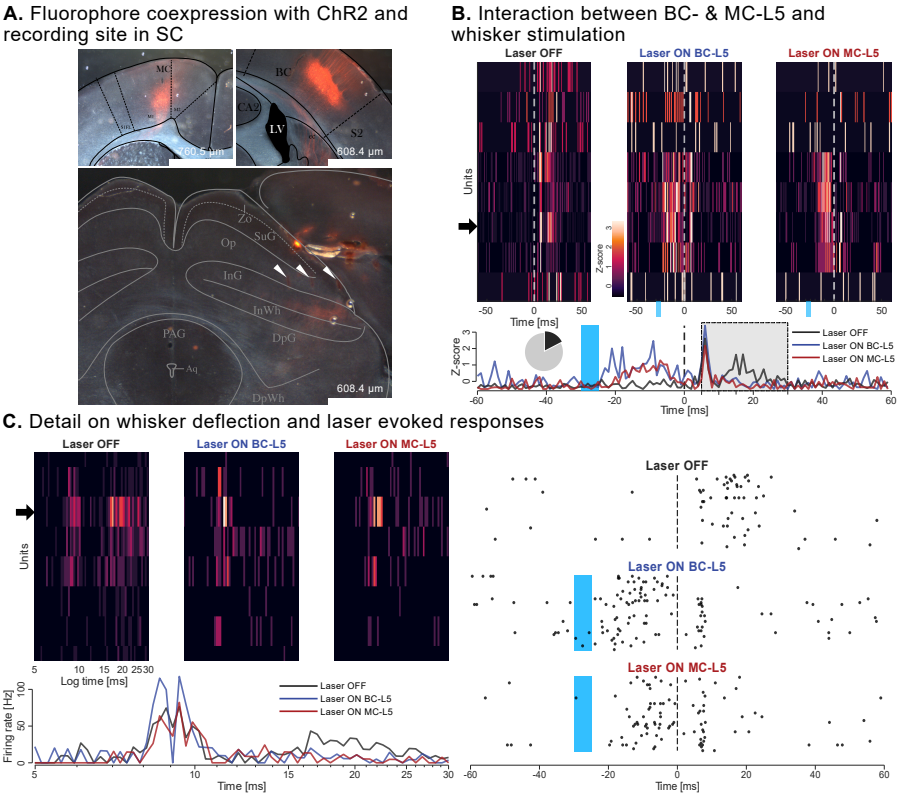

FIGURE 2.8 – **A.** Slices of MC, BC (top), and SC (bottom) showing expression of mCherry in L5 cells and their axons reaching SC. White arrowheads point at lesions from the four-shank probe marking the recording site in SC. **B.** Example single unit and population PSTHs showing eight out of 46 recorded units with a significant modulation ($p < 0.05$, paired two-sided Wilcoxon test, small pie chart). Blue rectangle indicates laser delivery in both Laser ON and Laser OFF conditions. Dashed white and black lines at 0 ms indicate the whisker deflection onset. **C.** Detailed single unit and population PSTHs showing 5 to 30 ms (left), and raster plot from a unit responding to all three stimulations (right) indicated by a black arrow by the edge of the single unit PSTHs. Unpublished data collected and analysed by me.

2.6 CORTICAL AND TRIGEMINAL TRANS-COLLICULAR PATHWAYS TO THE DIENCEPHALON AND BRAINSTEM

Single neurons in SC form functional synapses with axons originating from MC, BC, and Bs. While the SC, as a whole nucleus, has down- and upstream projections, it remains unclear whether RNs specifically have long-range projections. To answer this question, question #1, anterograde experiments from section 2.3 were repeated only this time slicing most of the brains to look for labelled axons from RNs.

All RNs populations send long projections to several contra- and mainly ipsilateral regions throughout the brain. Figure 2.9A shows a schematic reconstruction of the axons found in the diencephalon and brainstem from the three RNs types. To compare axons from RNs in different regions and across projecting areas, a qualitative axon

count was developed in which a richly innervated area would be attributed a value of one, whereas a region with low axon density would get a value of zero. Figure 2.9B shows RN-output maps for all projecting regions populating diencephalon and brainstem. Surprisingly, all trans-collicular pathways innervated similarly the upstream and downstream nuclei[1]. The lateral-posterior nucleus of the thalamus (LP) received significantly more innervation from Bs→RN than from any cortico-collicular RN population. Finally, MC trans-collicular pathway directly innervates the brainstem, indicating a strong candidate for a route transmitting motor commands.

If RNs send long-range projections, a question would be: Do iRNs also project up- and downstream or do they only inhibit local circuits? Experiments from section 2.4 were repeated and the brains examined looking for fluorescent signal from iRNs axons. Figure 2.9C shows example slices with labelled axons from iRNs. Inhibitory axons had the highest density in the zona incerta (ZI) as well as in POm and the parafascicular (PF) nucleus of the thalamus. This inhibitory connectivity suggests that iRNs follow an organised spatio-temporal activation that either inhibits the ZI – the main inhibition source for POm [73] – or POm directly. Something noteworthy is that no axons from iRNs were found in the brainstem, which suggests that Bs→iRNs do not directly suppress contra-lateral ascending sensory streams. Bs→iRNs has the lowest axon density compared against cortico-collicular pathways (Fig. 2.9C), but their relative distribution is equivalent (Fig. 2.9B).

This novel inhibitory trans-collicular pathway to the diencephalon could have a relevant contribution on cognition.

SUMMARY Whisker-relevant regions broadly innervate the whisker-sensitive SC and preferentially target iNs. Projections from Bs might carry direct sensory information to SC, however, top-down connections quickly inform SC about more processed sensorimotor computations, giving the whisker sensitivity to SC. The organisation of cortical projections vs. Bs differ in the DV axis, which could compartmentalise quick sensorimotor computations in the SC.

In the next chapter, I describe the effects of manipulating cortico-collicular pathways and their implications on mice behaviour.

1 See Martín-Cortecero et al. [48] for a complete list of innervated nuclei per projecting region.

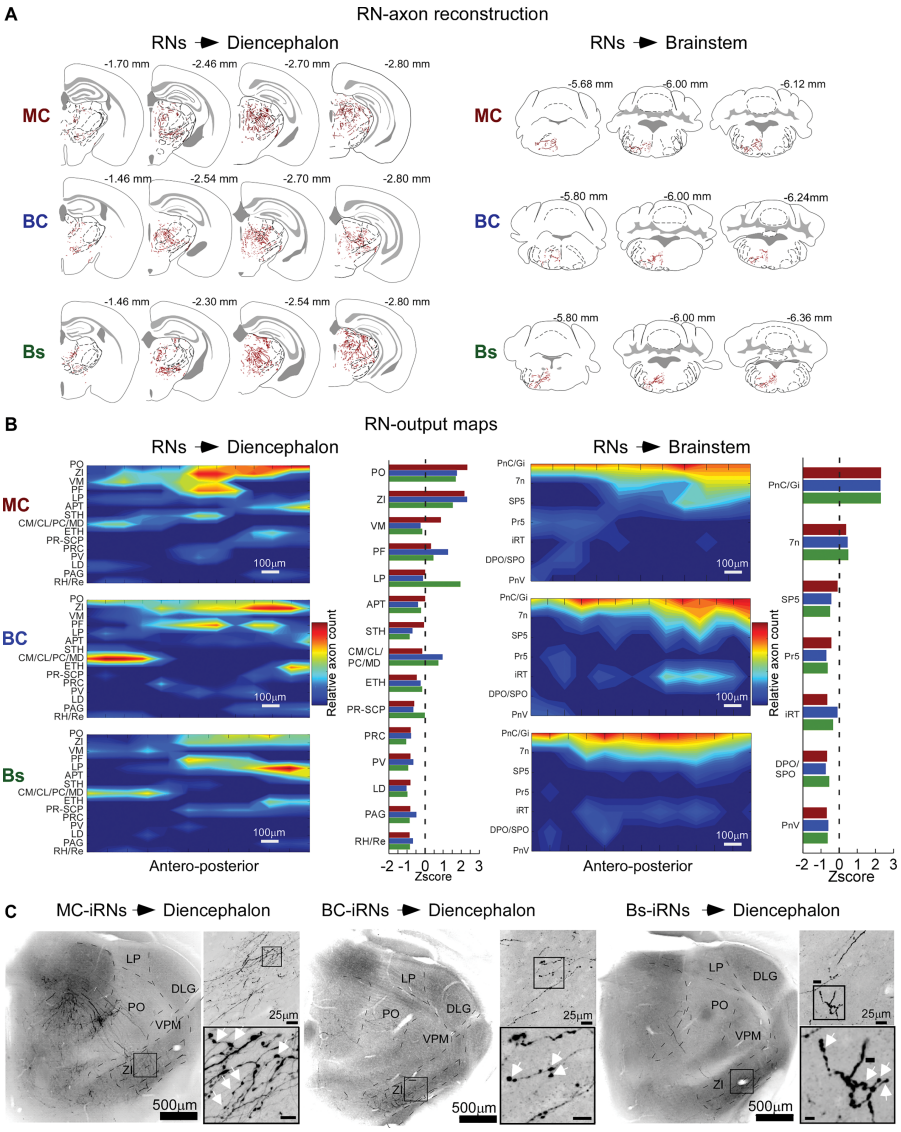

FIGURE 2.9 – **A.** Schematic reconstruction of the labelled axons in the diencephalon (left) and the brainstem (right) for all three RN populations: MC→RN in red, BC→RN in blue, and Bs→RN in green. **B.** RN-output (or axon density) maps showing a similar distribution for all three pathways (diencephalon left, brainstem right). Only the lateral-posterior nucleus of the thalamus (LP) has a significantly higher innervation from Bs→RNs than from cortico-collicular RNs. **C.** Example slices of inhibitory trans-collicular pathways in the diencephalon with a higher magnification on the ZI due to rich iRNs innervation.
Figure taken from Martín-Cortecero et al. [48].

3

BEHAVIOURAL RELEVANCE OF CORTICO- AND TRIGEMINO-COLLICULAR PATHWAYS

"All models are wrong."
. . . but some are useful.

— George E. P. Box, 1976 [7]

The second stage of my project consisted of establishing a behavioural paradigm with head-fixed, awake mice in which I could *a*. evoke a SC-associated behaviour; *b*. quantify the evoked behaviour; and *c*. measure the effect of manipulating different parts of cortico-collicular pathways described in chapter 2. More specifically, I used pharmacological and intersectional viral approaches to test different components of cortico-collicular pathways. The main method in this second stage was to express opsines in different RNs populations to manipulate them while the mouse was fixed on the roller. In this way, I assessed the effect of different neural groups and their interaction with ascending Bs→RNs somatosensory inputs.

In the following section, I describe the setup and measurements for evaluating mice startled behaviour.

3.1 SETUP AND BEHAVIOURAL MEASUREMENTS

I developed a behavioural setup for head-fixed awake mice in which I evoked a SC-associated behaviour, startled by an air puff to their whiskers. The setup was equipped with a high-speed camera, a rotary encoder, an air puff delivery tube, and a micro-manipulator, which enabled me to introduce a multichannel silicone probe or a micropipette for drug delivery (Figure 3.1A).

More details about the roller in subsection 5.3.3.

The high-speed camera primarily recorded the animals' face so I could track and analyse the position of different body parts frame by frame. I used the estimated positions from DeepLabCut (DLC) in every frame to draw auxiliary geometric shapes overlaid on the mouse's face to compute eight signals [39, 51, 56] (Figure 3.1B). From the tracked body parts and the encoder position eight measurements per frame were computed. The measurements were 1-4. the mean whisker position and fan arc of each side tracked whiskers, 5. the arc between both side's mean whisker positions, 6. a symmetry index, 7. the nose position, and 8. the roller speed. A symmetry index of zero would mean that the whiskers' position is perfectly symmetrical, whereas a value of -1 or 1 would mean that the whiskers are asymmetrical, toward the mouse's right or left side, respectively (Fig-

See subsection 5.6.2 for more information on the measured signals computation.

ure 3.1C, Figure 5.1). The rotary encoder recorded the roller's position throughout the experiment and, taking the roller speed as a proxy, I could associate mice's locomotion with the whisker puff. One trial consisted of a single whisker puff delivered with at least 1 s between each puff.

For every trial and signal, the maximum absolute difference within 25 to 350 ms post-puff (evoked) and −350 to −25 ms pre-puff (spontaneous) was extracted, and normalised by the maximum amplitude in the session. The mean values of the normalised amplitudes were used to build a polygon representing a mouse's behaviour per session. The area of this polygon, called amplitude index, would summarise the animal's overall reaction in a session, and comparing sessions of the same animal and across different animals was then straightforward (Figure 3.1D).

To assess whether the evoked behaviour was whisker dependent, a puff intensity test was performed by varying the air pressure from 0 to 3 Bar in steps of 0.5 or 0.6 Bar (Figure 3.1E). A proportional relationship was observed, which confirmed that the intensity of the puff evoked a proportional behaviour in mice.

Quantification of the elicited behaviour allowed me to measure the effect magnitude of manipulations of increasingly specific nodes in cortico-collicular pathways.

3.1.1 *Validation of the whisker-sensitive region in superior colliculus*

One of the first questions to answer was regarding the involvement of SC in the evoked behaviour. In order to test the participation of SC on the elicited behaviour, I recorded neural activity in the whisker-sensitive region of SC with a 64-channel silicone probe in awake, head-fixed mice in the roller set-up.

Consistent with findings in section 2.1, I observed a population of neurons exhibiting increased firing activity in response to whisker stimulation ((72 ± 23) % responsive units from 162 experiments, 13 612 units, 65.3 % were up-modulated and 2.3 % down-modulated, Figure 3.2) [5, 10, 48]. The evoked neural responses varied depending on the recording site. A multiple component response indicated that the silicone probe was placed in the whisker-sensitive region. The earliest component occurred around 22 ms after puff trigger onset, followed by a second peak, and around 100 ms a sustained elevated activity for some units. Since the neural response latency precedes the behaviour onset, a question that I sought to answer was what relationship does SC activity have with the amplitude index.

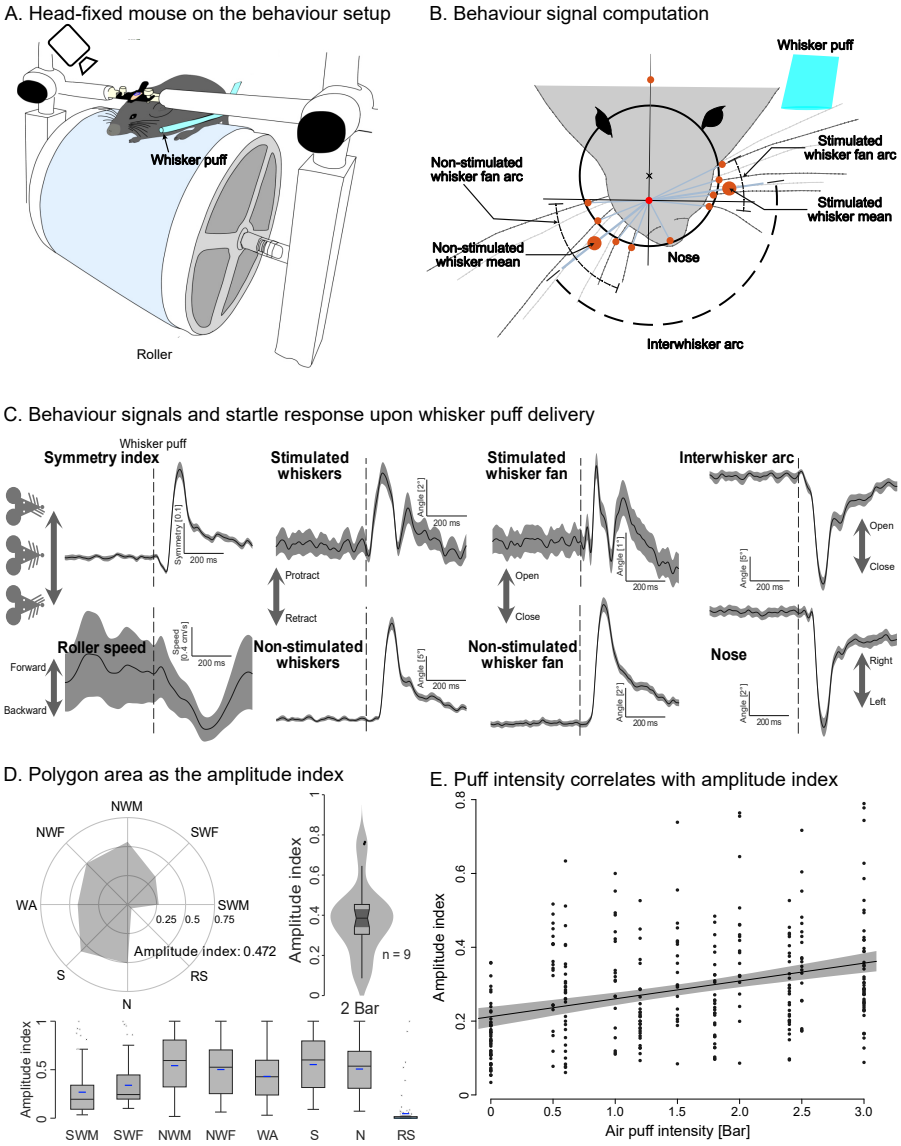

FIGURE 3.1 – Caption on next page.

3.2 AMPLITUDE INDEX AND NEURAL ACTIVITY IN SUPERIOR COLLICULUS CORRELATE

Before manipulating whisker-relevant collicular pathways, a first question regarding the relationship between SC neural activity and observed behaviour needed to be addressed. To do this, I averaged the spike counts per unit in a sliding window for all trials. For example, unit X underwent five trials and in the first iteration of the sliding window from -50 to -30 ms it had average spike counts $\vec{c}_\tau$. These average values were z-scored and used to regress the amplitude indices per trial (also a five element vector, $\vec{a}_\tau = m \cdot \vec{c}_\tau + a_0$). For every regression, a goodness-of-fit (R^2) was computed (in 1606 units from 15 experiments). After all units were individually processed, a time-

... amplitude indices $\vec{a}$ in trial τ and offset a_o.

FIGURE 3.1 *(cont.)* – **A.** Schematic of a head-fixed mouse on the roller setup with the whisker puff targetting the left whisker set and the high-speed camera pointing at the animal's face. **B.** Auxiliary geometric shapes and estimated body part positions as orange dots overlaid on a mouse face to compute stimulated and non-stimulated whisker fan arc, interwhisker arc, and nose angle. **C.** Example mean traces for all behaviour signals. S: symmetry index, RS: roller speed, SWM: stimulated whisker mean, NWM: non-stimulated whisker mean, SWF: stimulated whisker fan arc, NWF: non-stimulated whisker fan arc, WA: the arc between both sides' mean whisker positions, N: nose. Average across trials shown in solid dark grey line and standard error of the mean (SEM) in light grey. **D.** Polygon for an example session with an area – amplitude index – of 0.472. The session's variability is shown by the box plots at the bottom with the average indicated as a dash in blue, and population amplitude indices on the top right ($N = 9$, median $\pm$ interquartile range (IQR): 0.39 ± 0.15; IQR is used for all uncertainty unless otherwise stated). **E.** Air pressure vs. amplitude index per session for nine mice depicted as dark grey dots.
Behavioural experiments were performed by Ann-Kristin Kenkel and Dr. Martín-Cortecero, and data analysis by Ann-Kristin Kenkel and me.

resolved R^2 indicated which units were most related to the amplitude index and during which time window.

Ordering unit PSTHs from the highest to the lowest maximum R^2 revealed that 95.7 % of non-zero units (above the white line) were modulated by the whisker puff. Furthermore, the maximum spike count in the response window (20 to 200 ms) was higher in the non-zero R^2 units than zeroed-valued R^2 units. Notably, 65 % of the zeroed-valued units were also modulated by the whisker-puff. In other words, a unit's R^2 was not directly associated with its whisker puff response, but serves as an indicator that the response of such unit might have a higher spike count. Moreover, I observed that 75.7 % of all units increased their activity upon whisker-puff, while only 1.3 % decreased and 23.0 % were non-modulated. The distribution of the maximum

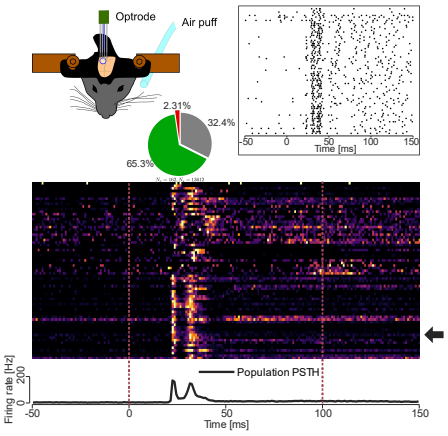

FIGURE 3.2 – Schematic drawing of the recording protocol with a 64-channel silicone probe (top left), and normalised single unit and population PSTH upon whisker puff (bottom). Example raster of a single unit with multi-component whisker response (top right); the unit is indicated in the PSTH image with a black arrow. Pie chart indicating the proportion of responsive units in every experiment (green for up-, red for down-, and grey for non-modulated, 162 experiments and 13 612 units; top middle)

R^2 per unit had its centre of mass close to zero (mean: 0.032, median: 0) and a shape similar to a Gamma distribution (shape $\kappa = 0.042$, and scale $\theta = 0.761$, Figure 3.3A). Latencies of the maximum R^2 per unit were distributed along the response window with most non-zero R^2 units clustering around 20 to 50 ms, and another group clustered between 50 and 200 ms (Figure 3.3D). Highest R^2 units were sparse and without a clear temporal organisation of the SC activity in regards to the amplitude index.

I repeated the regression on amplitude indices, but this time I progressively removed the units with the lowest R^2 values until the highest 10 % units remained. I did not observe any difference in the overall R^2 since removing non-participating units from the regression could be equivalent to subtracting a zero (Figure 3.3B). Unexpectedly, when progressively removing the highest R^2 units until keeping only the lowest 10 % R^2 units, the population median R^2 was still unaffected (Figure 3.3C). However, it is important to note that the maximum R^2 reduces after removing 30 % of highest R^2 units. If low-R^2 units are able to keep the population R^2 median unaffected, the sampled units build a population code where redundancy might play a crucial role in protecting SC functionality against neural damage. Since these results showed no difference in removing 'unrelated' units from the regression, I decided to keep the entire population for further regressions.

In addition, I searched for time windows that displayed a higher R^2 value compared to the activity preceding the puff-evoked response. As the latency of maximum R^2 indicated, the population R^2 increased post-puff in relation to pre-puff activity (Figure 3.3D). Specifically, two windows corresponding to 50 to 80 and 140 to 170 ms had higher population R^2 than windows prior to the whisker puff (Kruskal-Wallis test, Figure 3.3B, detailed pairwise comparison Table 3.6), which marks a period when SC activity is correlated with the produced trial-by-trial behaviour.

Results of single unit and population regressions suggest the presence of a SC population code, where computations that produce a motor command are distributed among collicular neurons, each contributing in a weighted fashion [3].

3.3 SUPERIOR COLLICULUS IS INVOLVED IN ELICITED BEHAVIOUR

Next, to investigate whether SC influences the elicited response to the puff, behavioural observations were conducted under a 15 min baseline condition, followed by the administration of 300 nL [10 mMol] of a fluorescent GABA agonist muscimol into the whisker-sensitive region of SC (Figure 3.4).

Muscimol is classically used to silence neural activity [36] effectively removing the influence of the affected population from the circuitry

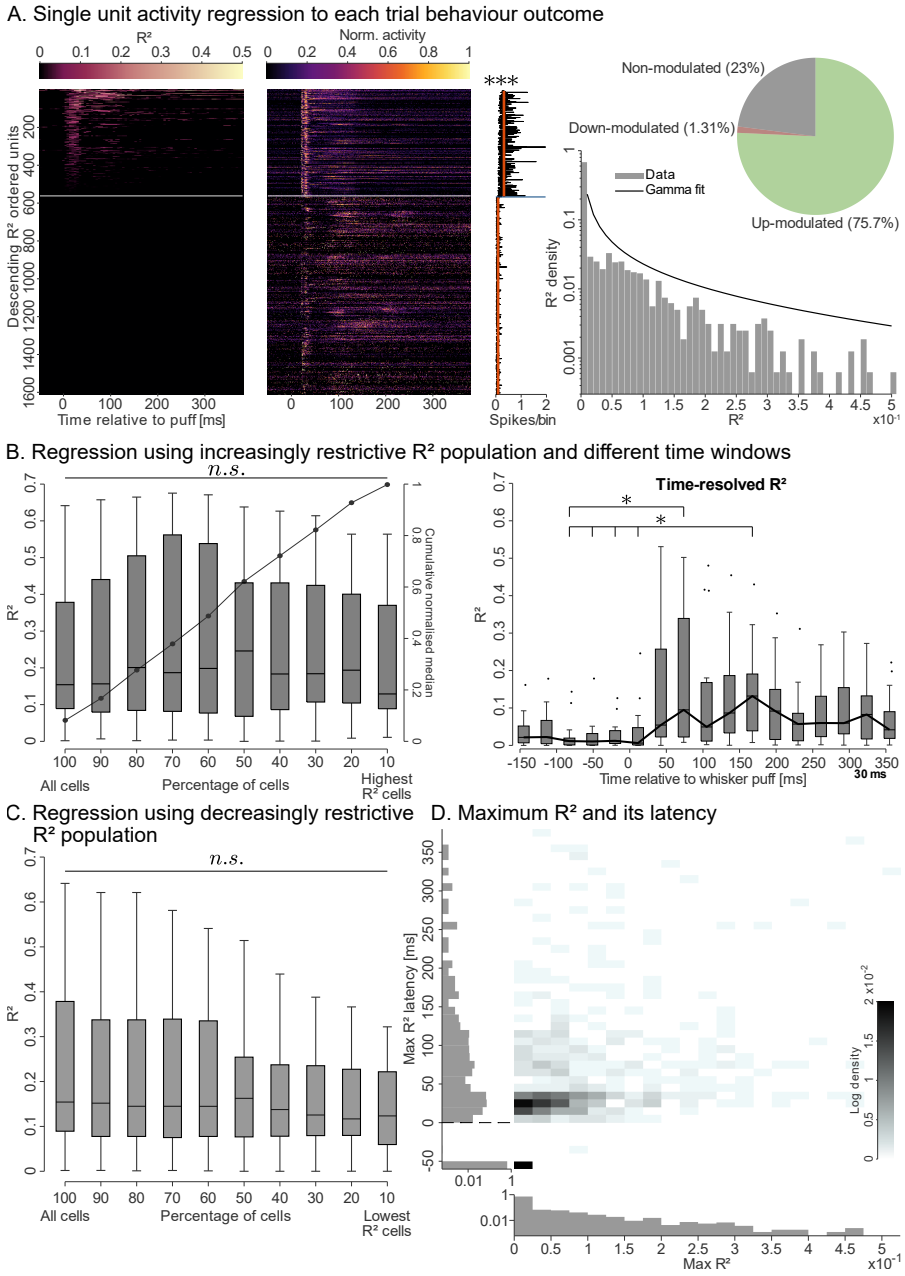

FIGURE 3.3 – Caption on the next page.

and, ultimately, from behaviour. Indeed, the increased GABAergic tone in SC removed collicular influence on the elicited behaviour and reduced the population amplitude index. The collicular response to a whisker puff, along with the stark reduction of the amplitude index by SC silencing, suggest that SC plays a crucial role in the evoked behaviour.

FIGURE 3.3 *(cont.)* – **A.** R^2 for single unit activity regression within a 20 ms sliding window to amplitude indices per trial organised in descending R^2 values (left), single unit PSTHs and the maximum mean spike per bin within 20 and 200 ms after the puff (1 ms width, right). A white line divides units in non-zero and zero R^2. Maximum spike count within the response window for all units with non-zero on the top and zeroed R^2 ($p = 9.55 \times 10^{-210}$, two-sided Wilcoxon test). R^2 distribution and pie chart showing the proportion of up-, down- and non-modulated units (N = 1606). **B.** Regression using an increasing R^2 threshold, which restricted the number of units used (left). Notice that using higher R^2 units, or removing zero- or low-valued units, does not improve regression. Whole population regression per experiment (N = 15) in 30 ms windows from −150 to 370 ms relative to the puff (right, $p = 4.55 \times 10^{-6}$, $\chi^2 = 54.34$, comparison details in Table 3.6). **C.** Regression using a decreasing threshold passing lower R^2 units without any significant difference between different subpopulations ($p = 0.87$, $\chi^2 = 4.6$, Kruskal-Wallis test). The maximum R^2 is, however, lower if only the low R^2 units are used. **D.** Bivariate histogram for the maximum R^2 and its latency.

3.4 SUPERIOR COLLICULUS REQUIRES MOTOR CORTEX INPUTS TO ACHIEVE THE ELICITED BEHAVIOUR

Having observed the strong behavioural effect of removing SC from the circuit, the next question was: is the motor cortico-collicular pathway involved in the elicited behaviour? To address this question, I silenced the communication from MC to SC by injecting a synaptic vesicle blocker AAV_5-SIO eOPN3-mScarlet [46] in Rbp4-Cre mice. MC-L5 neurons expressed eOPN3 in their terminals. One possibility is that SC is executing a sensorimotor transformation without influence from cortex and, thus, the elicited behaviour would not be modified. On the other hand, MC could keep certain tone in SC that keeps the circuit responsible for the elicited behaviour excitable.

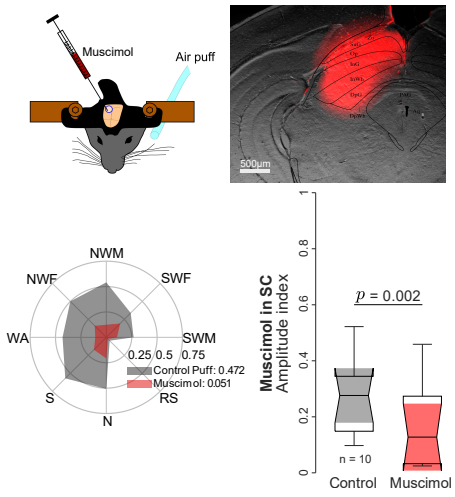

FIGURE 3.4 – Schematic drawing of 300 nL [10 mMol] of muscimol injection protocol after recording each mouse's baseline behaviour and example slice showing red fluorescence in SC from the muscimol injection (top). Example polygons showing an approximately ten-fold decrease in the amplitude index after SC silencing (bottom left). Population box plots indicate a significant amplitude index reduction with the drug delivery (bottom right, $p = 2 \times 10^{-3}$, paired, two-sided Wilcoxon test).
Dr. Martín-Cortecero and I performed the experiments, and I data analysis.

Using a blue laser from the RWD system for 600 ms before each puff onset, eOPN3 synaptic blockade was activated and sustained while recording neural activity and behaviour (Figure 3.5A). Removing MC inputs in SC is sufficient to significantly reduce the population amplitude index compared to baseline ($p = 0.031$, Wilcoxon test two-sided paired). Individually, seven out of eight behavioural measurements are significantly reduced (Figure 3.5B, Table 3.1).

Furthermore, I recorded collicular activity using a 64-channel electrode while providing optogenetic stimulation to MC axons. As expected, the whisker puff evoked a multi-component response in collicular neurons. eOPN3 activation did not influence the earlier components (from 20 to 50 ms) of the puff response but significantly reduced the activity from 50 to 200 ms ($p \ll 1 \times 10^{-3}$, Wilcoxon two-sided test, Figure 3.5C).

These results suggest that part of the collicular sensorimotor transformation is impeded within a specific time window between 50 and 200 ms, time in which inputs from MC might regulate SC-dependent behaviour in specific contexts.

AI	LASER OFF	LASER ON	p-VALUES
SWM	0.25 ± 0.15	0.19 ± 0.06	0.0313
SWF	0.37 ± 0.10	0.29 ± 0.07	0.0313
NWM	0.42 ± 0.15	0.27 ± 0.17	0.0313
NWF	0.37 ± 0.13	0.25 ± 0.14	0.0313
WA	0.32 ± 0.16	0.23 ± 0.12	0.0313
S	0.40 ± 0.18	0.26 ± 0.16	0.0313
N	0.41 ± 0.12	0.28 ± 0.15	0.0313
RS	0.08 ± 0.05	0.06 ± 0.03	0.0938

TABLE 3.1 – Amplitude index median $\pm$ IQR and p-values per signal in Laser OFF and Laser ON conditions for MC$\not\rightarrow$SC experiments; eOPN3 experiments (Figure 3.5B).

3.5 ACTIVATION OF MC$\rightarrow$IRNS REDUCES AMPLITUDE INDEX

Since silencing the whole SC and removing MC inputs into SC lead to a reduction in amplitude index, how does MC achieve, for example, a down-modulation of the evoked behaviour in physiological conditions? To answer this question, non-physiological excitation of MC$\rightarrow$iRNs could provide evidence for down-modulating puff-evoked behaviour. Taking advantage of the intersectional viral approach described in the previous chapter (chapter 2), and by Martín-Cortecero et al. [48], MC$\rightarrow$iRNs could be specifically targetted and activated to address this question. AAV_8-Con/Fon ChR2-EYFP and AAV_1-Flpo

To express a Con/Fon virus, cells need to express both Flpo and Cre.

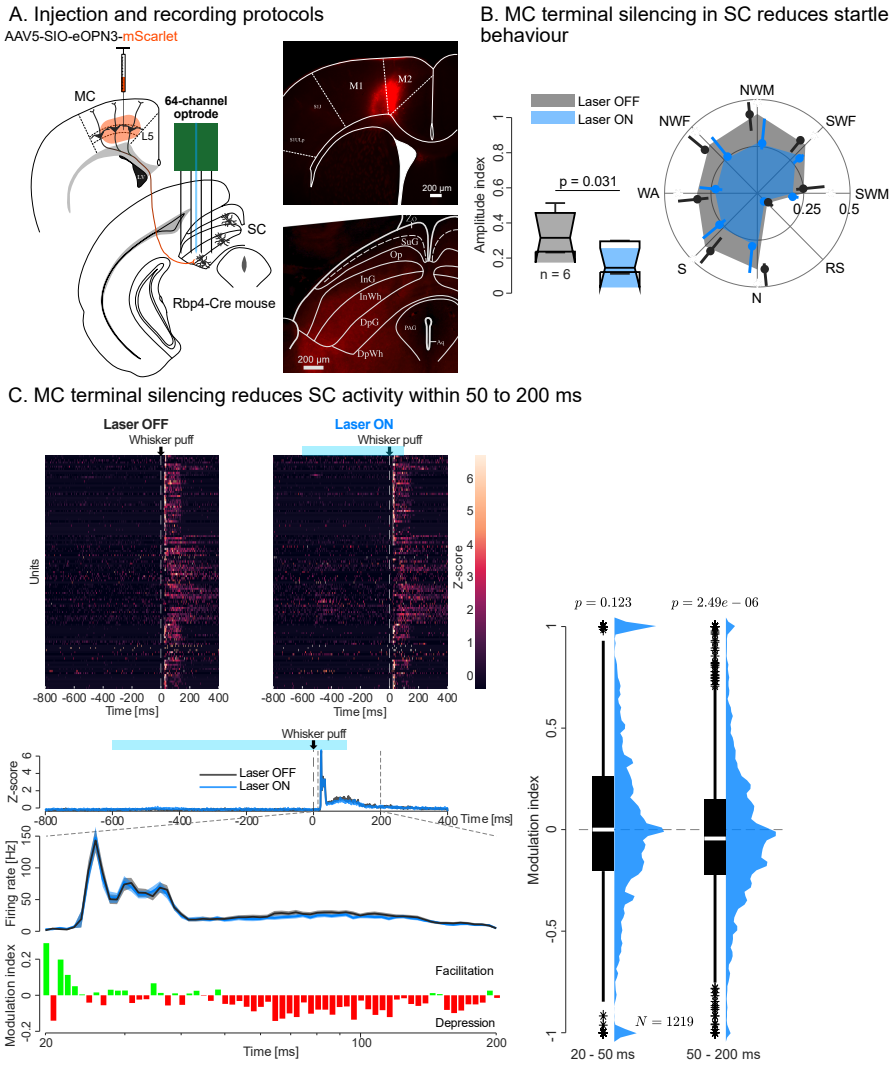

FIGURE 3.5 – Caption on next page.

were injected in SC and in MC of GAD-Cre mice, respectively, in order for MC→iRNs to express ChR2 (Figure 3.6A).

Mice were head-fixed on the roller and stimulated optogenetically to activate MC→iRNs expressing ChR2. Seven out of eight body parts were significantly reduced for the tested population. The population amplitude index was strongly reduced, which is specific to MC→iRN pathway given a lack of effect in other tested pathways (MC→excitatory recipient neurons (eRNs) [**MC!** (**MC!**)→eRNs] and BC→iRNs, Figure 3.6B, Table 3.2).

Furthermore, I recorded collicular activity upon whisker puff (Laser OFF) and whisker puff paired with optogenetic stimulation (Laser ON, Fig. 3.6A). In contrast to the continuous activation of eOPN3-expressing MC terminals, I stimulated MC→iRNs with a 300 ms-long train at 40 Hz with 5 ms pulses. In the Laser ON condition, the optogenetic stimulation started 100 ms before the onset of the whisker puff and lasted 100 ms after the offset. I observed a reduction of the puff

FIGURE 3.5 *(cont.)* – **A.** Schematic showing the injection protocol of AAV_5-SIO eOPN3-mScarlet in MC and the recording site in SCi & deep layers of SC (SCd). An example slice showing expression of mScarlet in MC. **B.** Population plots for the amplitude index (left) and individual body parts showing the effect of silencing MC axons in SC ($p = 0.031$, Wilcoxon test, right). Laser OFF condition is depicted in grey and Laser ON in light blue (median $\pm$ IQR and p-values reported in Table 3.1). **C.** Example PSTHs of single units in Laser OFF and Laser ON conditions with a white dashed line and a downward arrow indicating the whisker puff, and light blue rectangles the laser delivery (top). Population PSTHs in Laser OFF (dark grey) and Laser ON (light blue) conditions showing the whisker puff temporality of collicular activity (middle). Logarithmic binning within 20 to 200 ms to show a detailed image of the conditions activity. A bin-by-bin comparison using the modulation index shows the reduced activity upon MC terminal silencing (bottom). Population modulation index for responsive windows 20 to 50 and 50 to 200 ms showing activity decrease in the latter window (1219 units, $p = 0.12$ and $p = 2.49 \times 10^{-6}$, respectively, two-sided Wilcoxon test, bottom right).

response during the Laser ON condition within a 20 to 50 ms window compared to Laser OFF, in addition to the 50 to 200 ms (Figure 3.6C). Interestingly, MC→iRNs interfere with ascending sensory information, in contrast to eOPN3 activation in MC terminals (Fig. 3.5). Reduction of the earlier components of SC response suggests that MC→iRNs makes synaptic contact with Bs→RNs or BC→RNs, which offers a window into intra-collicular computation and the interplay between different circuits involved in whisker SC-dependent behaviours.

Activation of MC→iRNs reduces the maximum amplitude of the elicited behaviour, which could point to a negative feedback to, for example, control overshooting orientation behaviour and adjust the resulting end position.

AI	LASER OFF	LASER ON	p-VALUES
SWM	0.30 ± 0.09	0.22 ± 0.13	3.60×10^{-3}
SWF	0.33 ± 0.08	0.32 ± 0.14	0.0352
NWM	0.40 ± 0.12	0.33 ± 0.13	4.85×10^{-3}
NWF	0.39 ± 0.13	0.34 ± 0.12	4.85×10^{-3}
WA	0.35 ± 0.10	0.29 ± 0.13	5.62×10^{-3}
S	0.41 ± 0.13	0.38 ± 0.14	8.61×10^{-3}
N	0.41 ± 0.13	0.39 ± 0.13	9.88×10^{-3}
RS	0.07 ± 0.04	0.05 ± 0.05	0.136

TABLE 3.2 – Amplitude index median $\pm$ IQR and p-values per signal in Laser OFF and/vs. Laser ON conditions for MC→iRNs experiments (Table 3.2B).

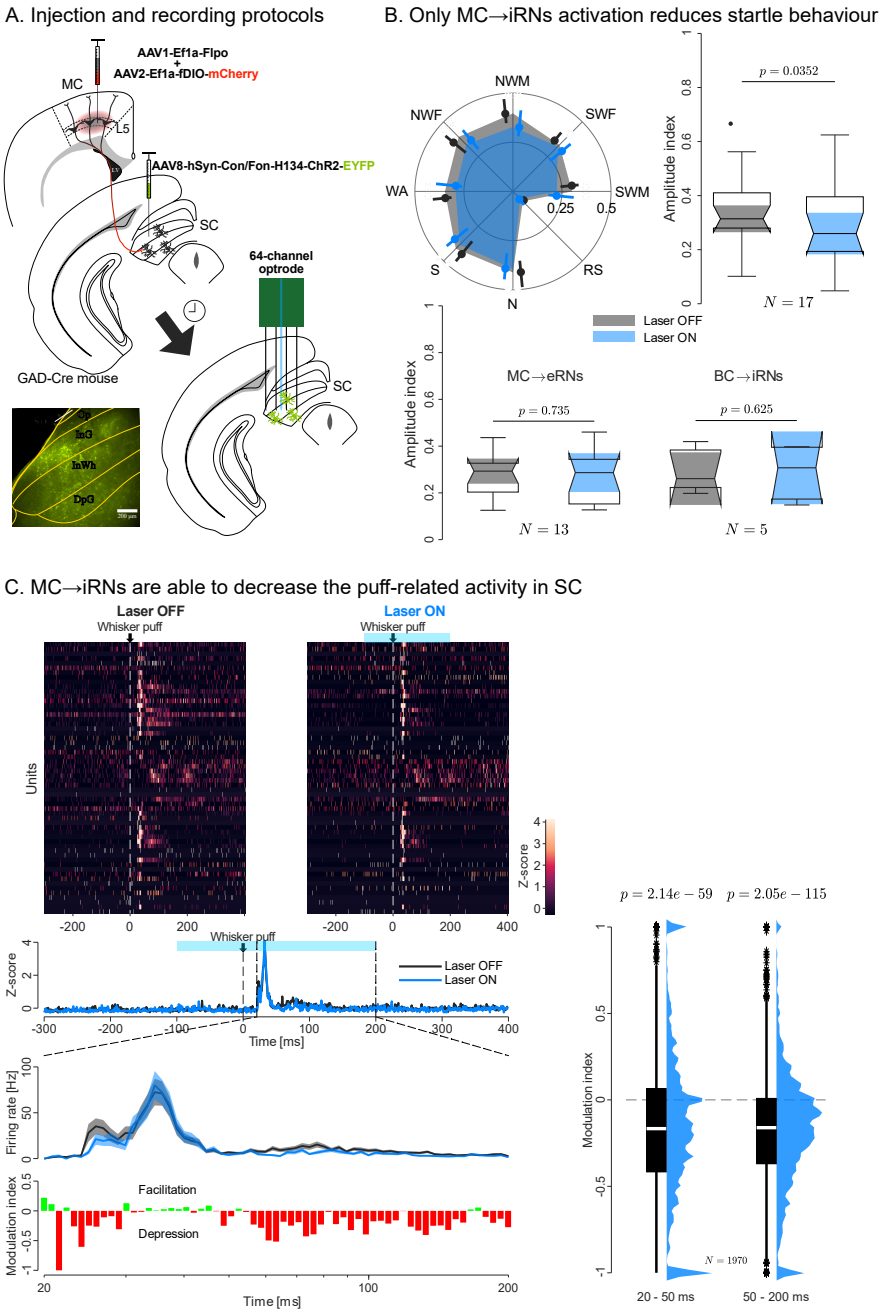

FIGURE 3.6 – Caption on next page.

3.6 BEHAVIOUR RECONSTRUCTION

Finally, I investigated whether neural activity in the SC encoded information about the behaviour over time and not only to the amplitude index (Fig. 3.3). To address this question, I performed a linear regression, specifically a Gaussian generalised linear model (Gaussian GLM), using the binned unit spike counts of the whole population in 5 ms bins as the predictor and the binned behaviour as the output variable. The Gaussian GLM was fitted to MC→iRNs experiments in Laser OFF

See subsubsection 5.6.3 for details on the implementation.

FIGURE 3.6 *(cont.)* – **A.** Schematic of the intersectional virus injection (AAV_1-Flpo + AAV_2-fDIO mCherry cocktail in MC, and AAV_8-Con/Fon ChR2-EYFP in SC), recording protocols in GAD-Cre mice ($N = 17$), and example slice of EYFP expression in MC→iRNs. **B.** Reduction in all body parts except for the roller speed (RS, top left, median ± IQR and p-values reported in Table 3.2) and in population amplitude index for Laser ON (light blue) vs. Laser OFF (light grey, top right, $p = 0.0352$, two-sided paired Wilcoxon test). Activation of MC→eRNs and BC→iRNs have no effect on mice's amplitude indices (bottom, $p = 0.735$ & $N = 13$, and $p = 0.625$ & $N = 5$, respectively; two-side paired Wilcoxon test). **C.** Examples of z-scored single unit and population PSTHs in Laser OFF (dark grey) and Laser ON (blue, top). A light blue rectangle indicates laser delivery in Laser ON condition. Logarithmic zoom in for a 20 to 200 ms window showing reduced activity in Laser ON compared with Laser OFF. Modulation index on a bin-by-bin basis to show the activity reduction within 20 to 50 and 50 to 200 ms. Population box plot of modulation indices for all recorded units ($N = 1970$) showing significant reduction in both 20 to 50 and 50 to 200 ms windows (right, $p = 2.14 \times 10^{-59}$ and $p = 2.05 \times 10^{-115}$, respectively; sign test).

condition trials [11, 18] (Figure 3.7A), and after k-fold cross-validation, a resulting matrix θ_c was used to reconstruct behavioural signals, which were then compared to the observed signals (Figure 3.7B). The analysis showed that the spiking activity in SC can explain approximately half of the behavioural signals' variance (R^2 range from 0.40 to 0.54), and could even accurately predict the amplitude index for NWF, NWM, S, and N (Figure 3.7C & D). To test whether SC activity was more related to the behaviour before or after the puff, I computed R^2 values in these time windows (pre- and post-puff, medians, IQR, and p-values in Table 3.3). NWF, S, and N were better reconstructed post-puff, whereas SWM and RS pre-puff. SWF, NWM, and WA had no difference, but SWF had a strong tendency to be better reconstructed pre-puff. This mixture of results did not point to either better or worse reconstruction in any of the considered windows. However, because the whisker puff protracts the stimulated whiskers, animals try to explore the origin of the stimulus by retracting their stimulated whiskers and protracting non-stimulated. This situation is unique to the head-fixed set-up where mice cannot orient their bodies to the puff tube and are forced to explore in an 'untrained' manner. Perhaps in a more naturalistic environment where mice can explore a presented object by protracting their whiskers, the reconstructed amplitude indices could match the observed and the pre- vs. post-puff reconstructions could yield no difference between pre- and post-puff.

To extract more information about the SC relationship to the observed behaviour from the model, I asked whether the number of recorded or the fraction of responding units were an indicator for a session R^2, and whether the estimated matrix θ_c can reconstruct the behaviour in Laser ON trials.

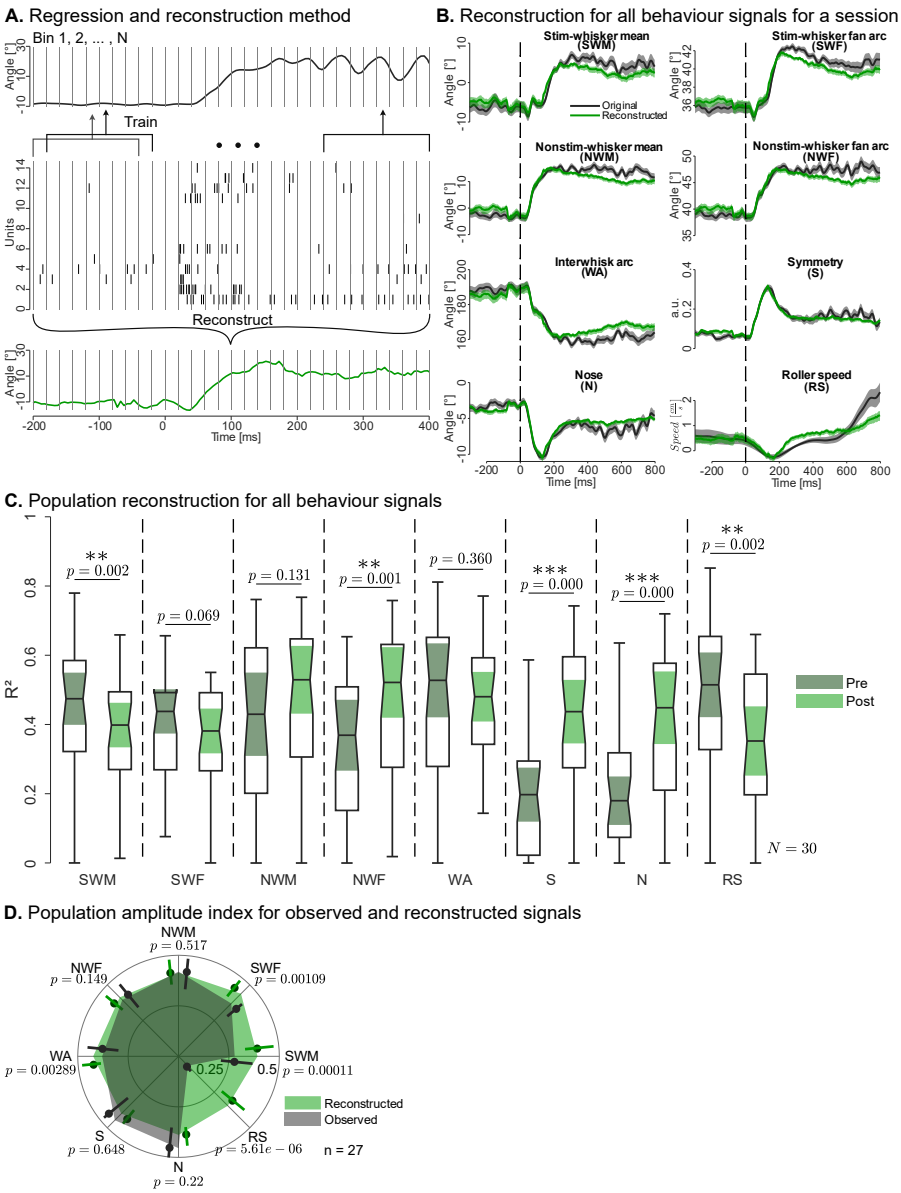

FIGURE 3.7 – **A.** Diagram showing the linear fitting between binned neural activity for all recorded units and observed behaviour (dark grey, top). In short, N bins are used for all units' spikes (raster, middle) as predictor variables of a single behaviour bin (top, black). After cross-validated training, the matrix $theta_c$ was used to reconstruct the behaviour (light green). **B.** Example mean behaviour signals with observed behaviour in dark grey and reconstructed in green.**C.** Population R^2 box plots for reconstructed pre- (dark green) and post-puff (light green) for all signals ($N = 30$, median $\pm$ IQR and p-values reported in Table 3.3). **D.** Population polygons of observed (light grey) and reconstructed (green) amplitude indices ($N = 27$, median $\pm$ IQR and p-values in Table 3.4).

3.6.1 *Number of recorded units and their responsive fraction*

Additionally, R^2 values from each experiment indicate that increasing the number of units recorded in SC improves prediction accuracy, similar to previous regression results. To analyse how different body parts were reconstructed, a principal component analysis (PCA) was performed on each signal R^2 and plotted the first two principal component (PC), since these explain 96.56 % of the R^2 variance, against one another and against the number of responsive units in 20 to 200 ms. The first PC (PC1) indicated that a signal's R^2, could be used to approximate others' R^2. This means that they varied around each other; within 1.96 σ. The second PC (PC2) showed an interesting grouping, where four signals SWM, SWF, RS, and WA (group A) were better reconstructed than the other four signals (group B) in some experiments, and vice versa; in a see-saw fashion. A high or low R^2 (PC1) was unrelated to how well either group of signals was reconstructed (PC2) Figure 3.8A.

To answer whether the number of recording units had an influence on the behaviour reconstruction, PC1 and 2 were plotted against the number of recorded units. As expected, the PC1 proportionally increased with the recorded units in an experiment (Figure 3.8B, R^2: 0.33, $p = 8.96 \times 10^{-4}$, *F*-test vs. constant model, `fitlm`). In contrast, PC2 had no relationship with how many units were recorded (Figure 3.8C, R^2: 0.05, $p = 0.24$). To identify whether the fraction of responsive units was predictive of how well an experiment behaviour would be reconstructed, PC1 and 2 were plotted (Fig. 3.8A, insets). Unexpectedly, I did not observe a linear relationship between the fraction of responsive units and PC1 (R^2: 0.09, $p = 0.11$, `fitlm`, *F*-test against a constant model), or with PC2 (R^2: 6.59×10^{-3}, $p = 0.67$). My expectations were to find at least a similar relationship to the one between

R^2	PRE-PUFF	POST-PUFF	p-VALUES
SWM	0.47 ± 0.26	0.40 ± 0.22	1.83×10^{-3}
SWF	0.44 ± 0.22	0.38 ± 0.23	0.0687
NWM	0.43 ± 0.42	0.53 ± 0.34	0.131
NWF	0.37 ± 0.36	0.52 ± 0.35	1.48×10^{-3}
WA	0.53 ± 0.37	0.48 ± 0.25	0.360
S	0.20 ± 0.27	0.44 ± 0.32	8.19×10^{-5}
N	0.18 ± 0.24	0.45 ± 0.37	1.15×10^{-4}
RS	0.51 ± 0.33	0.35 ± 0.35	2.11×10^{-3}

TABLE 3.3 – Reconstruction R^2 Median $\pm$ IQR and p-values ($N = 30$, paired two-sided Wilcoxon test) for pre- and post-puff R^2 in Laser OFF trials (Figure 3.7C).

AI	OBSERVED	RECONSTRUCTED	p-VALUES
SWM	0.39 ± 0.14	0.28 ± 0.16	1.10×10^{-4}
SWF	0.44 ± 0.10	0.37 ± 0.09	1.09×10^{-3}
NWM	0.41 ± 0.12	0.42 ± 0.15	0.517
NWF	0.41 ± 0.11	0.39 ± 0.15	0.149
WA	0.42 ± 0.09	0.38 ± 0.15	2.89×10^{-3}
S	0.40 ± 0.09	0.45 ± 0.15	0.648
N	0.39 ± 0.09	0.45 ± 0.15	0.220
RS	0.35 ± 0.15	0.07 ± 0.04	5.61×10^{-6}

TABLE 3.4 – Amplitude indices for observed and reconstructed polygons median $\pm$ IQR and p-values ($N = 27$, paired, two-sided Wilcoxon test, Figure 3.7D).

PC1 and the number of recorded units. However, since this was not the case, the idea that a population code in SC gained strength with improved reconstruction upon a bigger collicular sample, regardless on the whisker representation.

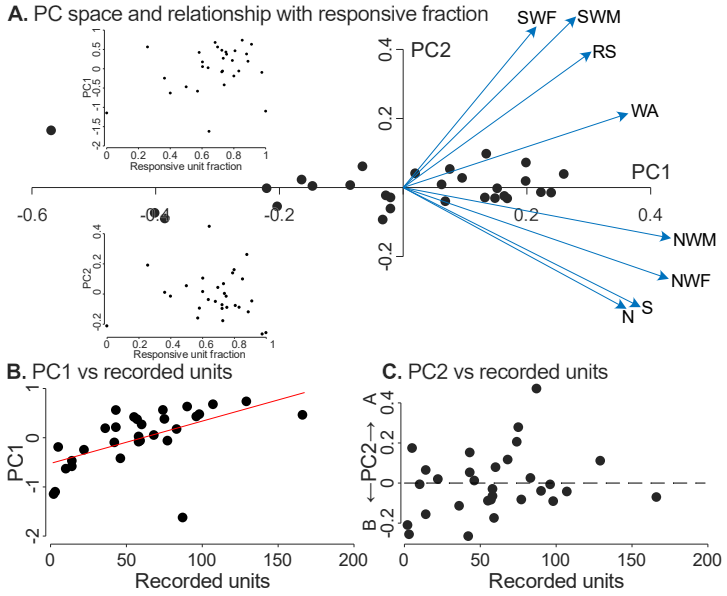

FIGURE 3.8 – **A.** PC1 vs. PC2 showing the distribution of all reconstructed experiments ($N = 30$). Blue arrows indicate the PC coefficients representing each signal. Fraction of responding units within 20 to 200 ms vs. PC1 (inset, top left), and vs. PC2 with no apparent relationship (inset, bottom left). **B.** Number of recorded units vs. PC1 indicating proportional improvement of R^2 with responding unit proportion. **C.** Number of recorded units vs. PC2 indicates no relationship between these variables. Negative values of the second PC indicate a higher R^2 for group A (SWM, SWF, RS, and WA) than group B (NWM, NWF, S, and N), and vice versa.

3.6.2 *Disrupted reconstruction of Laser ON trials*

Reconstructing behaviour in Laser ON trials could either yield similar results as Laser OFF, or MC→iRNs activation removed the spiking activity that was used to perform the reconstruction. In the first case, the effect observed in section 3.5 would probably be achieved through long-range inhibitory projections outside SC and place SC as a MC relay centre for motor adjustments. In the latter case, the model would be useful and validate SC as having a causal role in the evoked behaviour; an orientation behaviour.

Indeed, when reconstructing Laser ON trials using matrix θ_c, the reconstruction deviated from the observed signals, coinciding with the onset of the laser stimulation of MC→iRNs (Figure 3.9A). This deviation seems to persist even after the laser offset, which considerably decreases the R^2. Although the directionality of the signal for the puff evoked behaviour is kept in the Laser ON trials, the response shape was blurred.

Reconstructing Laser ON trials in the same experiments from the Laser OFF reconstructions showed that activation of MC→iRNs inhibits crucial spiking activity used by the model (Figure 3.9B, Table 3.5). Every signal's R^2 was strongly reduced by MC→iRNs activation, which shows the relative effect on *a*. the proportionally tiny population sampled with 64 channel probes, and *b*. the entire population responsible for the evoked behaviour. On one hand, the model capability to reconstruct the animal's behaviour with a handful of units, disrupted by MC→iRNs, evidences a strong effect on the sampled units. On the other hand, the increasing specificity of my manipulations shows the smallest effect of MC→iRNs on the amplitude index, which might be affecting a small portion of the whole population responsible for the observed behaviour.

R^2	LASER OFF	LASER ON	p-VALUE
SWM	0.45 ± 0.25	0.05 ± 0.31	4.29×10^{-6}
SWF	0.43 ± 0.21	-0.06 ± 0.29	1.73×10^{-6}
NWM	0.54 ± 0.30	0.06 ± 0.39	1.36×10^{-5}
NWF	0.51 ± 0.35	0.03 ± 0.32	1.24×10^{-5}
WS	0.53 ± 0.25	0.10 ± 0.43	1.02×10^{-5}
S	0.42 ± 0.30	-0.04 ± 0.20	2.60×10^{-6}
N	0.40 ± 0.37	-0.06 ± 0.32	2.88×10^{-6}
RS	0.48 ± 0.30	0.03 ± 0.75	1.73×10^{-6}

TABLE 3.5 – Reconstruction R^2 Median $\pm$ IQR and p-values per signal in Laser OFF and Laser ON conditions showing the strong disruption of SC activity by MC→iRNs stimulation (Figure 3.9B).

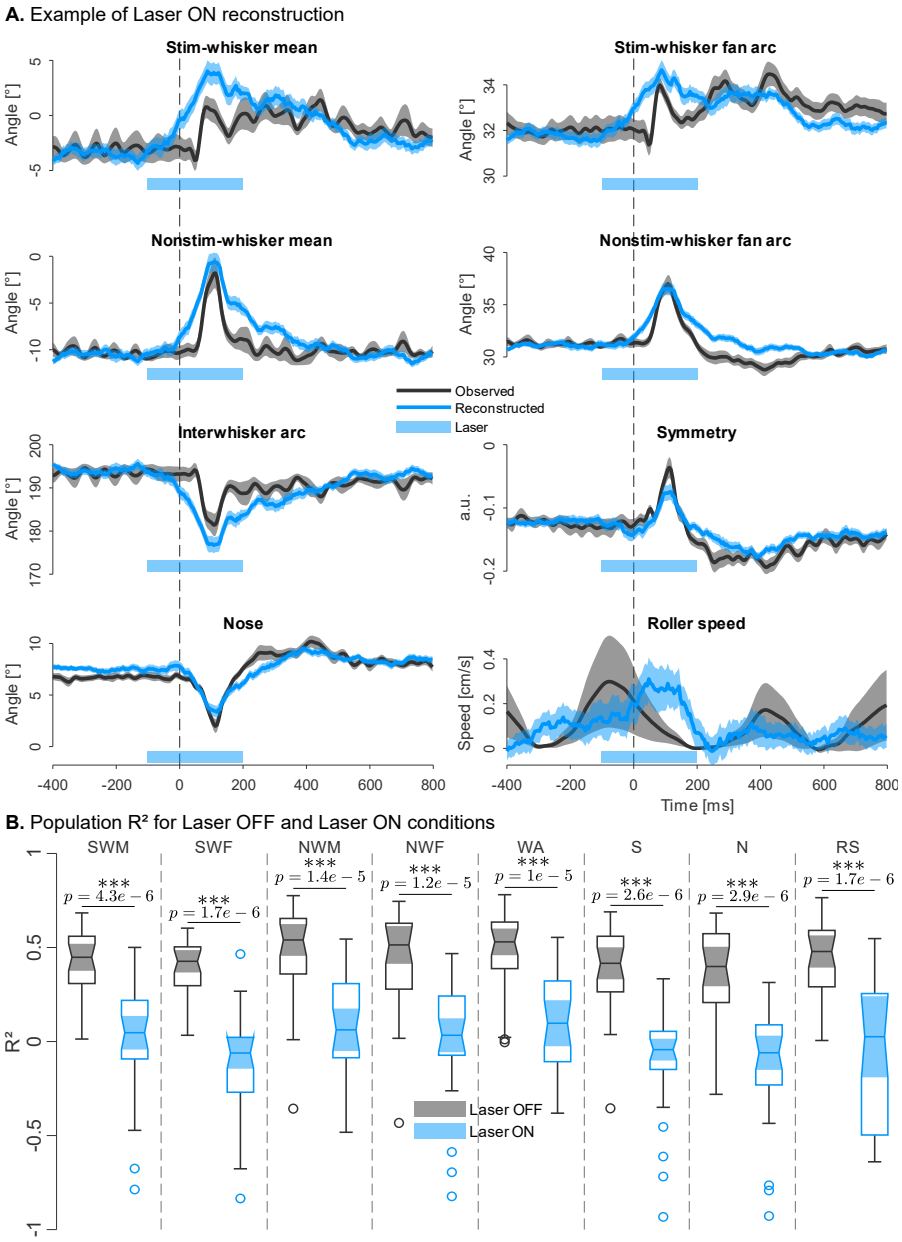

FIGURE 3.9 – **A.** Example for observed (dark grey) and reconstructed signals (blue) for Laser ON trials. Blue rectangles represent laser activation. Notice that the reconstructed signals deviate from observed after the laser onset. **B.** Population R^2 for Laser OFF (grey) and Laser ON (blue) reconstructions showing the activity disruption from physiological conditions upon MC→iRNs. Median, IQR, and p-values are reported in Table 3.5. Negative R^2 values indicate that the reconstruction was worse than a horizontal line through the observed signal mean.

SUMMARY In this second stage, I established a set-up in which I quantified the behavioural effect of an unexpected whisker puff, and how different manipulations in the whisker-relevant collicular pathways impact the whisker puff behavioural reaction. I first established a measurement which indicated the degree of elicited movement

with the amplitude index as a proxy. Next, I tested the relationship between the elicited behaviour and the whisker puff intensity and SC neural activity, independently. Starting with a gross manipulation by silencing the complete SC hemisphere, increasing the specificity by silencing MC inputs to SC (MC$\not\rightarrow$SC), and finally exciting MC$\rightarrow$iRNs, I disentangled part of a causative pathway in the orientation circuits that reduce the amplitude of movement. Finally, the Gaussian GLM confirmed that SC has a causative role in the orientation behaviour by achieving R^2 values of 0.5. The model and muscimol experiments showed that SC is not the sole actor in producing the orientation behaviour. In the next chapter (chapter 4), I will discuss some interpretations of the model results and how more informed manipulation could have an impact on the orientation behaviour and its ethological relevance.

TABLE 3.6 – Time window comparisons in ms for Figure 3.3B. One way ANOVA Tukey's honestly significant difference procedure was used for multiple comparisons. A − B reporting group difference at 95 % confidence intervals.

TIME-WINDOW A	B [ms]	AB DIFF	p-VALUE
−160	−126.88	−5.67 [−98.81, 87.48]	1.00
−160	−93.75	23.07 [−70.08, 116.21]	1.00
−160	−60.63	22.47 [−70.68, 115.61]	1.00
−160	−27.5	11 [−82.14, 104.14]	1.00
−160	5.63	12.67 [−80.48, 105.81]	1.00
−160	38.75	−62.07 [−155.21, 31.08]	0.651
−160	71.88	−70.13 [−163.28, 23.01]	0.423
−160	105	−46 [−139.14, 47.14]	0.956
−160	138.13	−63.2 [−156.34, 29.94]	0.620
−160	171.25	−83.73 [−176.88, 9.41]	0.139
−160	204.38	−52.93 [−146.08, 40.21]	0.867
−160	237.5	−33.67 [−126.81, 59.48]	0.998
−160	270.63	−50.8 [−143.94, 42.34]	0.901
−160	303.75	−57.47 [−150.61, 35.68]	0.771
−160	336.88	−51.87 [−145.01, 41.28]	0.885
−160	370	−42.47 [−135.61, 50.68]	0.979
−126.88	−93.75	28.73 [−64.41, 121.88]	1.00
−126.88	−60.63	28.13 [−65.01, 121.28]	1.00
−126.88	−27.5	16.67 [−76.48, 109.81]	1.00
−126.88	5.63	18.33 [−74.81, 111.48]	1.00
−126.88	38.75	−56.4 [−149.54, 36.74]	0.796
−126.88	71.88	−64.47 [−157.61, 28.68]	0.583
−126.88	105	−40.33 [−133.48, 52.81]	0.988
−126.88	138.13	−57.53 [−150.68, 35.61]	0.770
−126.88	171.25	−78.07 [−171.21, 15.08]	0.234
−126.88	204.38	−47.27 [−140.41, 45.88]	0.945
−126.88	237.5	−28 [−121.14, 65.14]	1.00
−126.88	270.63	−45.13 [−138.28, 48.01]	0.963
−126.88	303.75	−51.8 [−144.94, 41.34]	0.886
−126.88	336.88	−46.2 [−139.34, 46.94]	0.955
−126.88	370	−36.8 [−129.94, 56.34]	0.995
−93.75	−60.63	−0.6 [−93.74, 92.54]	1.00
−93.75	−27.5	−12.07 [−105.21, 81.08]	1.00

TIME-WINDOW A	B [ms]	AB DIFF	p-VALUE
−93.75	5.63	−10.4 [−103.54, 82.74]	1.00
−93.75	38.75	−85.13 [−178.28, 8.01]	0.121
−93.75	71.88	−93.2 [−186.34, −0.06]	0.0497
−93.75	105	−69.07 [−162.21, 24.08]	0.453
−93.75	138.13	−86.27 [−179.41, 6.88]	0.108
−93.75	171.25	−106.8 [−199.94, −13.66]	8.18×10^{-3}
−93.75	204.38	−76 [−169.14, 17.14]	0.278
−93.75	237.5	−56.73 [−149.88, 36.41]	0.789
−93.75	270.63	−73.87 [−167.01, 19.28]	0.327
−93.75	303.75	−80.53 [−173.68, 12.61]	0.189
−93.75	336.88	−74.93 [−168.08, 18.21]	0.302
−93.75	370	−65.53 [−158.68, 27.61]	0.553
−60.63	−27.5	−11.47 [−104.61, 81.68]	1.00
−60.63	5.63	−9.8 [−102.94, 83.34]	1.00
−60.63	38.75	−84.53 [−177.68, 8.61]	0.129
−60.63	71.88	−92.6 [−185.74, 0.54]	0.0533
−60.63	105	−68.47 [−161.61, 24.68]	0.469
−60.63	138.13	−85.67 [−178.81, 7.48]	0.115
−60.63	171.25	−106.2 [−199.34, −13.06]	8.92×10^{-3}
−60.63	204.38	−75.4 [−168.54, 17.74]	0.291
−60.63	237.5	−56.13 [−149.28, 37.01]	0.802
−60.63	270.63	−73.27 [−166.41, 19.88]	0.342
−60.63	303.75	−79.93 [−173.08, 13.21]	0.199
−60.63	336.88	−74.33 [−167.48, 18.81]	0.316
−60.63	370	−64.93 [−158.08, 28.21]	0.570
−27.5	5.63	1.67 [−91.48, 94.81]	1.00
−27.5	38.75	−73.07 [−166.21, 20.08]	0.347
−27.5	71.88	−81.13 [−174.28, 12.01]	0.179
−27.5	105	−57 [−150.14, 36.14]	0.782
−27.5	138.13	−74.2 [−167.34, 18.94]	0.319
−27.5	171.25	−94.73 [−187.88, −1.59]	0.0413
−27.5	204.38	−63.93 [−157.08, 29.21]	0.599
−27.5	237.5	−44.67 [−137.81, 48.48]	0.967
−27.5	270.63	−61.8 [−154.94, 31.34]	0.659
−27.5	303.75	−68.47 [−161.61, 24.68]	0.469
−27.5	336.88	−62.87 [−156.01, 30.28]	0.629
−27.5	370	−53.47 [−146.61, 39.68]	0.857

TIME-WINDOW A	B [ms]	AB DIFF	p-VALUE
5.63	38.75	−74.73 [−167.88, 18.41]	0.306
5.63	71.88	−82.8 [−175.94, 10.34]	0.153
5.63	105	−58.67 [−151.81, 34.48]	0.742
5.63	138.13	−75.87 [−169.01, 17.28]	0.281
5.63	171.25	−96.4 [−189.54, −3.26]	0.0336
5.63	204.38	−65.6 [−158.74, 27.54]	0.551
5.63	237.5	−46.33 [−139.48, 46.81]	0.954
5.63	270.63	−63.47 [−156.61, 29.68]	0.612
5.63	303.75	−70.13 [−163.28, 23.01]	0.423
5.63	336.88	−64.53 [−157.68, 28.61]	0.582
5.63	370	−55.13 [−148.28, 38.01]	0.824
38.75	71.88	−8.07 [−101.21, 85.08]	1.00
38.75	105	16.07 [−77.08, 109.21]	1.00
38.75	138.13	−1.13 [−94.28, 92.01]	1.00
38.75	171.25	−21.67 [−114.81, 71.48]	1.00
38.75	204.38	9.13 [−84.01, 102.28]	1.00
38.75	237.5	28.4 [−64.74, 121.54]	1.00
38.75	270.63	11.27 [−81.88, 104.41]	1.00
38.75	303.75	4.6 [−88.54, 97.74]	1.00
38.75	336.88	10.2 [−82.94, 103.34]	1.00
38.75	370	19.6 [−73.54, 112.74]	1.00
71.88	105	24.13 [−69.01, 117.28]	1.00
71.88	138.13	6.93 [−86.21, 100.08]	1.00
71.88	171.25	−13.6 [−106.74, 79.54]	1.00
71.88	204.38	17.2 [−75.94, 110.34]	1.00
71.88	237.5	36.47 [−56.68, 129.61]	0.996
71.88	270.63	19.33 [−73.81, 112.48]	1.00
71.88	303.75	12.67 [−80.48, 105.81]	1.00
71.88	336.88	18.27 [−74.88, 111.41]	1.00
71.88	370	27.67 [−65.48, 120.81]	1.00
105	138.13	−17.2 [−110.34, 75.94]	1.00
105	171.25	−37.73 [−130.88, 55.41]	0.994
105	204.38	−6.93 [−100.08, 86.21]	1.00
105	237.5	12.33 [−80.81, 105.48]	1.00
105	270.63	−4.8 [−97.94, 88.34]	1.00
105	303.75	−11.47 [−104.61, 81.68]	1.00
105	336.88	−5.87 [−99.01, 87.28]	1.00

TIME-WINDOW A	B [ms]	AB DIFF	p-VALUE
105	370	3.53 [−89.61, 96.68]	1.00
138.13	171.25	−20.53 [−113.68, 72.61]	1.00
138.13	204.38	10.27 [−82.88, 103.41]	1.00
138.13	237.5	29.53 [−63.61, 122.68]	1.00
138.13	270.63	12.4 [−80.74, 105.54]	1.00
138.13	303.75	5.73 [−87.41, 98.88]	1.00
138.13	336.88	11.33 [−81.81, 104.48]	1.00
138.13	370	20.73 [−72.41, 113.88]	1.00
171.25	204.38	30.8 [−62.34, 123.94]	0.999
171.25	237.5	50.07 [−43.08, 143.21]	0.912
171.25	270.63	32.93 [−60.21, 126.08]	0.999
171.25	303.75	26.27 [−66.88, 119.41]	1.00
171.25	336.88	31.87 [−61.28, 125.01]	0.999
171.25	370	41.27 [−51.88, 134.41]	0.984
204.38	237.5	19.27 [−73.88, 112.41]	1.00
204.38	270.63	2.13 [−91.01, 95.28]	1.00
204.38	303.75	−4.53 [−97.68, 88.61]	1.00
204.38	336.88	1.07 [−92.08, 94.21]	1.00
204.38	370	10.47 [−82.68, 103.61]	1.00
237.5	270.63	−17.13 [−110.28, 76.01]	1.00
237.5	303.75	−23.8 [−116.94, 69.34]	1.00
237.5	336.88	−18.2 [−111.34, 74.94]	1.00
237.5	370	−8.8 [−101.94, 84.34]	1.00
270.63	303.75	−6.67 [−99.81, 86.48]	1.00
270.63	336.88	−1.07 [−94.21, 92.08]	1.00
270.63	370	8.33 [−84.81, 101.48]	1.00
303.75	336.88	5.6 [−87.54, 98.74]	1.00
303.75	370	15 [−78.14, 108.14]	1.00
336.88	370	9.4 [−83.74, 102.54]	1.00

Part III

DISCUSSION

4

DISCUSSION

Putting together both stages of my thesis, my colleagues and I revealed the whisker-relevant cortico- and trigemino-collicular pathways and showed the capabilities of the motor cortico-collicular pathway on ascending somatosensory inputs. In this project, my colleagues and I investigated the causality of motor cortico- and trigemino-collicular pathways on the orientation behaviour through different manipulations. Many questions, however, remain open and are relevant for the continuation of the project (Figure 4.1).

4.1 INTRA- AND EXTRA-COLLICULAR INTERACTIONS

Imagining a mouse exiting its burrow to grab something to eat after sunset, it tries to catch an appetising smell by rising its snout high in the air. When the mouse returns to the ground with all its limbs, its whiskers touch an unfortunate and so far silent grasshopper that evokes a dangerous orientation behaviour, making the grasshopper a crispy meal.

4.1.1 *Inter- and intra-RNs interactions*

First, Bs→RNs are activated in parallel to the lemniscal whisker pathway which evokes a response in BC. Before BC→RNs are activated through BC, Bs→RNs might already have elevated BC→RNs membrane potential such that when aps from BC reach their collicular target cells, these unequivocally fire. Perhaps, depending on the context, MC could have risen MC→iRNs excitability to avoid energy-wasting movements, or lowered it to achieve greater orientation behaviour. Question *a.* proposes to investigate the interactions between different RNs that could impact the resulting orientation movement, e. g. through the described MC→iRNs. Systematic blockage and activation of these different RNs types could reveal their behavioural function and interactions through electrophysiology recordings. A hypothesis is that ascending sensory activated inhibition (Bs→iRNs) could function similar to 'lateral inhibition' in the lemniscal pathway [40], where barreloid-specific VPM neurons activate surrounding barreloid inhibition in the reticular nucleus of the thalamus (TRN).

a. *Interactions between RNs from two projecting sites?*

Similarly, to answer questions *b.* and *g.*, dual recordings in SC and a projecting site could reveal spatio-temporal patterns activating eRNs and/or iRNs. The lack of effect from other RNs, i. e. MC→eRNs and BC→iRNs, was under the specific experimental conditions that mice

b. *Interactions between e- and iRNs from a single projecting site?*

g. *What do other RNs do?*

were submitted. Therefore, I suggest that less constraining contexts in which mice could move freely should be investigated. For example, to reveal BC→iRNs functionality, two sets of experiments could be enough to achieve this goal by independently expressing excitatory and inhibitory DREADDs in BC→iRNs in the roller set-up and a freely-moving context (while hunting in low-light conditions).

c. *Are any RNs Pitx2⁺?*

Linking the specificity of RNs with results from the Tripodi Lab [22, 50, 75], question *c.* could reveal further specific neural populations

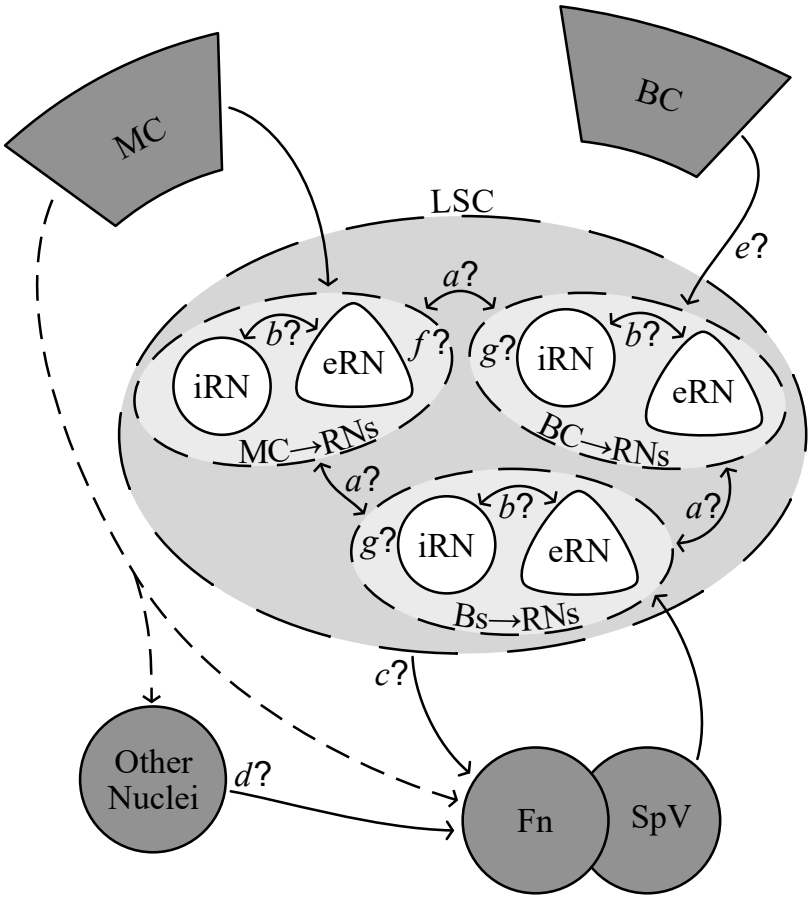

FIGURE 4.1 – Circuit model for cortico- and trigemino-collicular pathways in lateral SC (LSC). Paths with a question mark indicate uncertainty and future investigation: *a*. The question mark over the arrows connecting pairs of RNs from two projecting sites indicates the uncertainty of the interaction between these neural populations: beside convergence, do RNs from, e. g. MC and BC interact and, if so, to what degree? *b*. Do iRNs and eRNs from a projecting site interact? *c*. The arrow from SC to facial nucleus (7N) indicate uncertainty on the RNs→Bs neural types. Since Pitx2⁺neurons are responsible for head and neck movements [22, 50, 75], how many RNs from any projecting site are also Pitx2⁺? *d*. What other nuclei are involved in the whisker-driven orientation behaviour? *e*. What happens to the amplitude index when BC→SC is silenced (BC↛SC)? *f*. What function do MC→iRNs play in 'natural' behaviour? And, *g*. what function do other RNs have? E. g. what is the function of Bs→iRNs?

that control head and neck movements and that receive input from whisker-relevant regions.

4.2 ORIENTING CIRCUIT

As shown in section 2.6, all three RNs populations innervate a myriad of nuclei that could participate in orienting behaviour. Particularly, question *d.* proposes that SC connections to motor and pre-motor nuclei such as striatum, cerebellum, or parafascicular nucleus in the thalamus; ZI for appetitive behaviour; POm for ascending sensory processing; or directly 7N could uncover the full circuitry for orienting behaviour. Usseglio et al. [69] showed evidence on "genetically distinct glutamatergic neurons of the brainstem reticular formation (RTf)" (V2a RTf) that receive motor commands from SC, cerebellum, and periacueductal grey (PAG). The region of the contra-lateral SC that projects to V2a RTf neurons coincides with results from section 2.3, where whisker-relevant RNs localise in LSC. In addition, Usseglio and colleagues report that V2a RTf neurons are anatomically organised, projecting to different sections of the spinal cord that produce orientation or locomotion changes, making them direct targets of SC orienting commands. Isa et al. [31] deepens the knowledge of crossed and uncrossed descending SC pathways participating in orienting and defence-like behaviours, respectively. Isa and colleagues, retrogradely labelled RTf projecting SC neurons and found that the crossed descending pathway responsible for orienting behaviour originates where RNs from the whisker-relevant neurons are organised. These two independent studies confirm that the investigated cortico- and trigemino-collicular pathways are part of the complete orienting circuits of the brain: Bs provides ascending somatosensory input to SC; SC provides input to 7N, which is, in turn, responsible for activating facial muscles [21, 42, 48]. Depending on the population of Bs→RNs activated, the crossed or uncrossed pathway could evoke a resulting orienting or defence-like behaviour. Cervical-projecting V2a RTf neurons are strong recipient candidates from the three investigated whisker-relevant pathways.

d. *What other nuclei could participate in the orienting behaviour?*

Ascending axons from RNs shown in section 2.6 and in [4, 31, 48, 69] could change the individual's brain state. Gharaei et al. [21] reported that SC modulates BC activity through a loop BC → SC → POm → BC. Notably, no axons from iRNs were found in the brainstem, highlighting that inhibitory trans-collicular pathways are only ascending.

Finally, although MC modulate whisker movements, MC does not connect monosynaptically to 7N, but achieves whisker movements by innervating surrounding nuclei: "... cells in M1 do not project directly to the facial nucleus, which innervates the whisker musculature, but reach the facial nucleus through disynaptic pathways. A principal pathway consists of a projection from M1 L5 cells to an ensemble of

cells distributed around the facial nucleus, which are thought to form a 'central pattern generator' for whisking movements ... " Brecht et al. [8].

4.3 REMOVING PROCESSED WHISKER INFORMATION FROM BARREL CORTEX TO SUPERIOR COLLICULUS

Since silencing the MC terminals did not affect the early temporal components of the puff response, an experiment would be to block BC terminals in SC with eOPN3. After Cohen, Hirata and Castro-Alamancos [12], and later Castro-Alamancos and Favero [10] showed anatomical and electrophysiological evidence for BC→SC in vitro, processed whisker information conveyed to SC could (and I believe should have) an impact on the amplitude index and overall behaviour. As shown in Figure 3.2, the whisker puff evokes a multi-component response in SC. The earliest component is attributed to Bs→SC, while the following component could be associated with BC→SC. If BC→SC is silenced (BC↛SC, question *e.*), I expect to see a reduction of the second component of the neural puff response, which could disrupt computations for orienting commands and, hence, reduce the behaviour amplitude.

e. *What is the effect of silencing BC inputs to SC?*

Alternatively, expressing eOPN3 in Bs terminals in SC (Bs↛SC) would remove the ascending sensory information to SC and maybe even prevent mice from reacting to the whisker puff at all. The experiment would be an intermediate step after the muscimol (section 3.3) and before MC terminal silencing in SC section 3.4 experiments. I expect to see a reduced amplitude index almost as strong in muscimol experiments after silencing Bs terminals in SC. This injection, however, has a high risk of damaging brainstem nuclei performing autonomous functions. My colleagues Dr. Martín-Cortecero and Berin E. Boztepe had to sacrifice a third or fourth of all mice injected in brainstem to reveal Bs→RNs before the required time for viral expression due to severe pain symptoms. Autopsy of the sacrificed animals revealed that the digestive track showed signs of necrosis, which pointed to damage during injection surgery to brainstem nuclei responsible for peristaltic bowel movements.

4.3.1 *Motor cortex terminals activation in superior colliculus*

Is the amplitude index reduction due to inhibition of intra-collicular circuits or trans-collicular targets?

In section 3.4, I showed that MC↛SC suffices to reduce the amplitude index of the orientation behaviour. However, experimentation with Rbp4-Cre and wild-type mice injected to express ChR2 in MC to stimulate their axon terminals in SC was performed but did not show a clear effect under the Laser ON condition vs. Laser OFF. From the possible explanations, a technical issue with both virus or mouse lines could be the culprit. The fact that I did not observe any clear spiking

activity or optotagged units upon terminal optogenetic stimulation supports the hypothesis that the problem was technical.

A biological possibility is that when ChR2 is activated in MC terminals, both excitatory and inhibitory neurons are activated. Synchronous activation of e- and iRNs might have a null to minimal effect. Alternatively, if the excitatory and inhibitory activity does not cancel each other, collicular network dynamics would need to be addressed by introducing MC terminals activation at different time points around the whisker puff, e. g. 400, 100 and 30 before and 20 ms after the puff trigger onset.

A solution for activating MC terminals in SC might be to add further control of the collicular network by reducing inhibition with a chemogenetic approach. An injection of a ChR2-expressing virus in MC and DIO DREADD Gi in SC of GAD-Cre mice would achieve a combined manipulation of chemo- and optogenetic approach. The experiment would constitute the following stages: *1*. a baseline measurement of whisker puff, and pairing MC terminals activation with the whisker puff at different time points; *2*. activation of the inhibitory DREADDs in SC iNs by injecting CNO or J60; and *3*. repetition of the first stage without inhibitory influence in SC. Without iNs activity in SC, I expect to see an increase in mice's behaviour amplitude. Luckily, I am indirectly supervising James A. Auwn as he performs these proposed experiments. Preliminary results show single unit activation or inhibition upon optogenetic stimulation. One step further would be to express DREADD Gi in MC→iRNs and ChR2 in MC using the intersectional approach to pinpoint the behavioural function of MC→eRNs. A more complicated but direct alternative would be to use GAD-Cre mice to express Con/Fon DREADD Gi in MC→iRNs, and Coff/Fon ChR2 in MC→eRNs. Finally, the same injections and experiments could be performed in vGlut2-Cre mice to replicate MC→iRN results.

4.4 ETHOLOGICAL RELEVANCE OF THE WHISKER-SENSITIVE REGION

Mice are in the middle of the food chain, making them prey and predators [34]. Medial SC conducts predator avoidance (predators) as evidenced by Ito and Feldheim, while lateral SC performs orientation towards a stimulus (prey) [31, 76]. Because the lower visual field in the ventral part of the retina maps to the lateral SC, where the whiskers, forelimbs, and face are represented in the SCi, my findings could have a direct impact on hunting efficiency and success. Hunting under low light conditions or even in darkness makes whisker sensation vital for a successful attack. I propose freely-moving experiments in which opto-, chemogenetic manipulations, or both are preformed in specific components of the cortico- and trigemino-collicular pathways to measure the effects on hunting (question *f.*). Geng et al. [20] provide

f. *What is the function of MC→iRNs in a 'natural' environment?*

a window into SC in during hunting context, where they report that cholecystokinin positive neurons (CCK^+) in the Sp5 pars interpolaris (Sp5I) are needed to evoke predatory behaviours in mice upon whisker touch. Geng and colleagues provide direct evidence that Sp5I Bs→RNs are needed for initiating hunting.

Cholecystokinin is a digestive hormone secreted by the duodenum.

Given the innervation of ZI from every type of RNs reported in section 2.6, I expect to observe a modulation of hunting behaviours even in food-restricted mice. Based on results in section 3.5, my hypothesis is the following. If MC→iRNs are activated with excitatory DREADDs during hunting, I expect that mice would loose appetite to hunt through the iRNs→ZI innervation, hence reducing ZI activity [2, 65].For example, first-attack latency could be a good measurement for this purpose. I expect mice with hyper-excitable MC→iRNs to have increased first-attack latency but perhaps overshooting when orienting to their prey.

Ultimately, freely-moving experiments testing manipulation effects on mice behaviour in a hunting arena could confirm the hypothesis that the whisker-relevant pathways are crucial for hunting.

4.5 EXPERIMENTAL IMPROVEMENTS

An additional camera to record mice's pupil diameter as a proxy for their arousal state might serve as *a*. a predictor for reaction amplitude, *b*. another measurement for assessing puff-related not directly observable behavioural changes. To further explore or build on behavioural findings, future experiments could incorporate an additional camera to measure pupil diameter as a proxy for arousal state. This would enable one to investigate the impact on the differential brain-wide arousal level pre- and post-puff [71]. In turn, the whisker puff would change the arousal state of mice and affect the next trial.

4.6 GAUSSIAN GLM IMPLICATIONS

The behavioural experiments were arranged with decreasing inhibition magnitude. After presenting the set-up and the relationship between the amplitude index and SC activity, I reported the muscimol experiments in which the whole SC was removed from the circuit and observed a strong first piece of evidence for SC causality in whisker-driven orientation behaviour. The manipulation that followed was to silence MC inputs to SC, which reduced population spiking activity specifically in the 50 to 200 ms post-puff window and the population amplitude index. One more step towards finer inhibition was with MC→iRNs activation. Inhibiting post-synaptic intra- and extracollicular neurons from MC→iRNs also reduced the amplitude index. However, BC→iRNs activation served as an important control to support the specificity of MC→iRNs. In addition, MC→eRNs activation

did not increase the population amplitude index, which could have similar network dynamics to exciting MC terminals with ChR2 in SC. Thus, mere inhibition of SC does not translate into a reduction of the amplitude index as seen with BC→iRNs, but rather the source of such inhibition as with MC→iRNs.

Because the only input to the model was SC activity of MC→iRNs experiments in Laser OFF condition, an important assumption was that the SC is the only actor causing the orienting behaviour (OB):

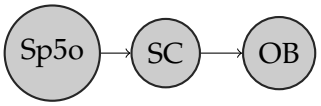

FIGURE 4.2 – Tested model having SC as the only cause of OB upon Sp5o activation.

Given the circuit model (Fig. 4.1), this model is wrong, but turns out to be useful. Hypothetically, if the sampled population in SC was the sole contributor to OB, the model would be able to keep the R^2 in Laser ON similar to Laser OFF trials since SC activity would be the only cause (and predictor) of the OB. In addition, muscimol experiments from section 3.3 would have completely depleted the evoked behaviour, and, although strongly reduced, an evoked behaviour could still be measured.

The effect of MC→iRNs on the amplitude index vs. the reduction of R^2 in Laser ON reconstruction could be due to relative population sizes. On the experimental part, inhibiting post-synaptic neurons from MC→iRNs seems to have a smaller effect in the whole population responsible for the OB than the sampled population on the Laser ON reconstruction R^2. The assumption of the tested model in Figure 4.2 was bold and proved wrong when the OB in muscimol experiments was not absent, discarding SC as the sole contributor. In addition, if the tested model turned out to be true, then MC→eRNs activation should have increased the OB. As discussed in subsection 4.3.1, network dynamics could have prevented a linear effect on SC manipulations. An increase of the amplitude index upon a manipulation of the collicular network would provide valuable input to approximate the complete circuitry of orienting behaviour.

The model had the following implications: Firstly, the time-resolved variability explained by the model only with SC activity is rather high, which confirms that the sampled population in SC contains information needed for OB in close temporal relation (−100 to 100 ms). Secondly, disrupted SC activity in Laser ON trials lessens collicular participation in OB and hence, dampens the reconstruction in Laser ON condition. Low R^2 for Laser ON reconstruction suggests that other nuclei and/or non-sampled collicular populations produce the observed OB. Systematic silencing of N1 and N2 through experimental manipulations could increase the relative contribution of SC and, therefore, the reconstruction R^2, correctly pondering SC as one of the

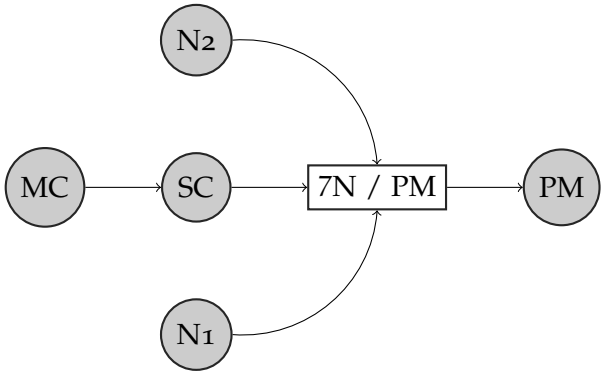

FIGURE 4.3 – A simple approximation to the circuitry responsible for orienting behaviour. In a next model, internal circuitry of SC, e. g. Pitx2^{+} MC→, or BC→eRNs, should be represented as interconnected nodes. Omitting Sp5 inputs to SC for simplicity.

main contributors to OB. Similarly, if increasing SC activity increases OB, then regression in this condition could potentially improve with respect to baseline.

A more detailed analysis, as Chinta and Pluta [11] did for their modelling, could be to look at the weights per unit in the estimated matrix θ_c to pick out the individual contributions within the analysed time window. Results from single unit and amplitude index regression per trial yielded no difference (section 3.2). However, looking at a time window and not at a particular point in time, such as the maximum amplitude differential, could yield a better resolution for which unit participates at what specific time. For example, the predicting, reflecting and simultaneous units for locomotion and whisking [11]. One could also look at the redundancy of the recorded population and measure how widespread is the theorised population code. Unfortunately, due to time constraints, I did not train the Gaussian GLM in MC↛SC experiments. If I did, I would expect a smaller difference between eOPN3 Laser ON vs. Laser OFF than in MC→iRNs Laser ON vs. Laser OFF R^2 values because MC→iRNs activation reduces SC activity in the whole response window, while eOPN3 only in 50 to 200 ms post-puff.

The proposed model in Figure 4.3 has two more nodes, N1 and N2, connected to 7N, proposing other nuclei contributing to the OB. Nodes/nuclei participating in the OB could be those projecting directly and even indirectly to 7N. To test this model, a first step could be to record in SC and systematically manipulate N1 and N2 and measure the physiological contributions of each node. Achieving a baseline measurement, further recordings in N1, N2, and SC could be fed into Gaussian GLM or another model with interactions to accurately describe and predict orienting behaviour using spiking activity in these regions.

4.6.1 *Principal components of R^2*

The PCA of the R^2 in Laser OFF trials yielded two main results. PC1 means that R^2 values from all measurements covary: if one measurement had R^2 of 0.5, one could expect the rest R^2 to vary around that value. I hypothesized about how well a given experiment would be reconstructed, based on rich sampling of the whisker-sensitive region. Since no relationship was found between the number of responding units and PC1 (Fig. 3.8), some other contributing neurons that are not necessarily whisker sensitive could be identified by analysing matrix θ_c.

Secondly, two clusters of measurements indicated that the members of one group were higher than the other, and vice versa. When $PC2 = 0$, then both groups had similar R^2. The switch between these two groups of measurements could indicate that SC is compartmentalised into contra- and ipsi-lateral motor maps within a single hemisphere, and was randomly sampled during electrode insertion in the whisker-sensitive region. However, considering that the recordings were conducted in the hemisphere responsive to stimulated whiskers, I expected to observe reconstruction results for the represented side always outperforming the non-represented side. This might go in line with the crossed and uncrossed descending pathways, where recordings mainly in the crossing pathway could result in higher R^2 values for SWM, for example.

Another possible cause for group A and B reconstruction difference could be that, since the stimulation protracts whiskers, head-fixed mice are forced to explore the origin of the stimulus by retracting their stimulated whiskers and protracting the non-stimulated whiskers. This situation is not present in natural nor in their home-cage environments. Mice explore objects by facing an object of interest and protract their whiskers to touch the object repeatedly in an oscillating movement (whisking). This phenomenon could be reflected in both reconstruction analyses, i. e. the PC2 and the difference in amplitude indices per behavioural signal. The constraining condition of mice in the roller set-up could be relaxed for the following experiments.

4.7 INTERESTING TAKES IN SUPERIOR COLLICULUS

In this final section, I present two quotes that are not directly related to my project but interested me when I found them. The first one is that the multi-modal nature of SC is not hard-wired since birth, but is rather a plastic process, 'shaped by experience': "In the colliculus, where visual, somatosensory, and auditory stimuli are combined, dividing the region into distinct sensorimotor pathways provides an elegant way to consolidate the triggering of distinct behaviors and minimize response times ... Alignment of different senses in SC is

shaped by experience and, therefore, plastic during development . . . " – Hoy and Farrow [30].

The second quote is about bats' SC. Many bats do not rely on vision to navigate space, but on echolocation. Since SCs in visually guided animals is densely innervated by retinal input, bat SC is instead innervated by an auditory organisation that is yet to be revealed: "... electrophysiological recordings in the SC of the same insectivorous bat corroborate the lack of auditory spatial topography compared to other species and other modalities. ... Auditory responses depend on combinatorial effects of frequency, intensity, and timing rather than the inherently topographic nature of visual input on the retina." – Allen et al. [1]. One possibility is that bats have a Fourier space representation in their SC, having 'intensity and timing' as amplitude and phase, respectively. Similar to magnetic resonance imaging, where a high-frequency, high-intensity magnetic field is deployed so that antennas receive resonant radio signals to reconstruct the desired tissue through an inverse Fourier transformation (spatial representation). I hypothesise that bats have such a spatial perception through a Fourier space.

Part IV

MATERIALS & METHODS

5

MATERIALS AND METHODS

In this chapter, I describe all surgical procedures in section 5.2, which include viral injections in subsection 5.2.2, head plate implantation in subsection 5.2.3, and preparatory work for experiments in subsection 5.2.4. I describe the equipment used in section 5.3, for electrophysiology (subsection 5.3.1), optogenetic manipulations (subsection 5.3.2), and for the awake setup and mice habituation to the roller (subsection 5.3.3). Section 5.4 describes the procedure for awake experiments. The stimulation protocol used is described in subsection 5.4.1, together with the behaviour recording in subsection 5.4.2. Analysis pipelines are described in section 5.6 for electrophysiology 5.6.1 and behavioural data 5.6.2 independently. Finally, in subsection 5.6.3 I describe the linear models I deployed to find and validate a causal relationship between neural activity and observed behavioural signals.

Before diving into the procedural and equipment details, I provide a few statements regarding ethical approvals and the living organisms used in my thesis. I used adult mice as my animal model for all my experiments. Table 5.2 shows mouse lines and virus combinations to answer specific questions.

5.1 ANIMALS

Mice aged between 8 and 12 weeks at the time of intervention were housed in individual cages in a ventilated Scantainer (Scantainer Classic, SCANBUR A/S, Karlslunde, Denmark) with ad libitum access to food and water. Relative humidity and temperature oscillated between 45 to 65 % and 20 to 22 °C, respectively. Since mice are nocturnal, their circadian rhythm was inverted, matching mine to perform behavioural experiments during the day; ideally before lunch. Otherwise, mice or I would have fallen asleep, which would be a suboptimal situation. Males were preferred over females for awake, head-fixed experiments on the roller to avoid female pheromones on the set-up. I cleaned the roller set-up thoroughly whenever females were used before fixing any males, and vice versa. After every session, however, I cleaned the setup by removing any excretion left behind. I had no gender nor circadian limitations or preferences for anaesthetised experiments.

ETHICS STATEMENT The ethical approval for all experimental procedures was granted by the Regierungspräsidium Karlsruhe, Germany, with the following approval numbers: 35-9185.81/G-216/19, 35-9185.81/G-289/21, T-39-20, and 35–9185.82/A-8/20.

5.2 ANAESTHETISED PROCEDURES

I ensured that every surgery I performed was as painless and comfortable as possible by administering analgesic and anaesthetic drugs. To this end, all mice were unconscious and reflex-free before applying any pressure on their heads with the ear bars or injecting any substance under their scalps.

5.2.1 *Stereotactic surgery, general procedure*

Mice were head-fixed on a stereotactic frame (Kopf, USA) under 1.2 to 2 vol% gaseous anaesthesia (Isofluoran Baxter, Baxter, Germany) mixed with medical-degree 98 % oxygen at 0.6 to 0.8 L/min flow rate. To reduce pain and discomfort during surgery, subcutaneous Lidocaine (Lidocainhydrochlorid 2 %, bela-pharm, Germany) was administered subcutaneous (sc), and a humidifying ointment (Bepanthen, Bayer, Germany) kept the animal's eyes lubricated. Whilst the Lidocaine was being absorbed, the scalp fur was trimmed around the head: above the neck, ears, and forehead.

After trimming the fur, the Lidocaine should have been absorbed and, depending on the surgical aim, a portion of the scalp was removed to fit the head plate and perform acute electrophysiological recordings, or a small incision was made on the scalp to reveal the skull around regions of interest.

The administered analgesic (Carprofen, 5 mg/kg, CP-Pharma Handelsgesellschaft mbH, Burgdorf, Germany) effect started about 30 min after the application. Therefore, a sc dose was applied at this point if the surgery was only for viral injection or anaesthetised electrophysiology experiment preparation. Otherwise, the analgesic was applied before implanting the headplate.

Next, the head position was adjusted to the stereotax coordinate system. Bregma and lambda were used as landmarks for DV, AP, and ML axes, and for angular corrections, i. e. roll, pitch and yaw. All desired coordinates were marked with either an extra-fine marker or a fine-tip drill (RWD, China). These markings were verified and, if necessary, corrected with the stereotax monoscope. Craniotomies were performed with the smallest drill tip (310 104 001 001 007, Hager & Meisinger GmbH, Neuß, Germany) to limit tissue damage. When the brain was exposed, Ringer's solution was applied for around 10 min to keep the tissue moist and to allow haemorrhages, if any, to stop.

5.2.2 *Viral injections*

Meanwhile, a 100 nL hand-tapered glass-pipette (Blaubrand, IntraMARK, Germany) with a P-97 micropipette puller (Sutter Instrument Co., California, USA) was 'cooked' and filled with 200 or 300 nL of

INJECTION SITE	VOLUME [nL]	AP	ML	DV [mm]
MC	200	1.00	1.00	−0.6; −0.8
BC	200	−1.00	2.95	−0.6; −0.8
Bs	200	−5.90	1.70	−4; −4.2
SC	300	−3.60	1.30	−2; −1.8; −1.6
SC (rAAV)	200	−3.60	1.30	−2

TABLE 5.1 – Coordinates for viral injections. The number of DV coordinates indicate 100 nL (or 200 nL for rAAV) deposited in the injection site. Bs injections corresponded to the Sp5 pars oralis (Sp5o).

viral particle solution for cortex or SC, respectively. The filling process was as follows: 1. a syringe was connected with the glass pipette through a silicon tube and attached to a custom-built holder to handle it with the stereotax knobs; 2. a squared piece of sterile paraffin film (Parafilm "M" Laboratory Film, Pechiney Plastic Packaging, USA) was placed on the mouse's skull; 3. a 2 µL droplet of the viral particle solution was placed on the paraffin; 4. the tip of the glass pipette was cut, carefully moved to the droplet's centre and the necessary volume was suctioned. Once the desired/required volume was loaded, the leftover droplet was recovered and the paraffin was discarded.

The stereotax coordinate system for the glass pipette was corrected using bregma. The glass pipette was positioned above target's ML and AP coordinates, and DV coordinates were referenced to pia $(Z = 0)$. The pipette was carefully inserted into the brain and as soon as the deepest DV coordinate was reached, the viral injection could start by carefully increasing the pressure in the syringe. The flow rate was about 2 nL/s. Once 100 nL were injected, the pressure in the syringe was released. Between viral deposits, a pause of 5 to 10 min allowed the solution to diffuse into the tissue.

When the desired volume was injected, the glass pipette was slowly removed (approximately 30 µm/s) to avoid pulling the viral solution upward. Finally, the craniotomy was sealed with sterile bone wax (Ethicon, Johnson & Johnson, USA) and either the skin was closed with either 3 to 5 absorbable stitches (Coated Vicryl V734D polyglactin, Ethicon) and the mouse was taken to its preheated home cage, or proceeded as in section 5.2.3 or section 5.2.4.

Depending on which component of the cortico-collicular pathway was targeted, a combination of mouse line and virus injections was used. Table 5.2 contains specific combinations for mouse lines and virus used, and Table 5.3 all viruses used in both stages of my project. For example, if I wanted to manipulate MC→iRNs in SC, two injections in a GAD-Cre mouse would suffice: AAV_1-flpo in MC and AAV_8-Con/Fon ChR2 in SC. The AAV_1-Flpo would infect the cells in MC and move anterogradely through the axon to infect post-synaptic

neurons. Hence, GAD^+ cells in SC which receive input from MC would express both Cre and Flpo, completing the requirements for expressing ChR2.

MOUSE LINE	PURPOSE	VIRUS
Rbp4-Cre×ChR2	MC- & BC-L5→SC experiments	—
GAD-Cre	Labelling or manipulating iRNs or eRNs	Con/Fon-ChR2 or Coff/Fon-ChR2
GAD-Cre×GFP	iRNs labelling & validation	DIO-mCherry
vGlut2-Cre	eRNs manipulation	Con/Fon-ChR2
Rbp4-Cre	Terminal expression of opsines	DIO-ChR2 or SIO-eOPN3
Ntsr1-Cre×EYFP	Cortico-collicular pathway origin	AAVr mCherry

TABLE 5.2 – Mouse lines and virus combinations used to manipulate or label specific parts of the cortico-collicular pathway.

5.2.3 *Head plate implantation*

Following stereotactic surgery in subsection 5.2.1, a sc analgesic was administered on the animal's back.

If the experimental aim was an electrophysiology recording, a well to hold Ringer's solution was implanted on the skull with two-component dental cement (Paladur, Kulzer, Germany) and covered as described in subsection 5.2.4. Once the well was fixed, the contact area of the skull was increased by gently scratching the skull in a lattice for a three-component dental cement (Super-bond, Sun Medical, Japan). The headplate was placed on the mouse's skull using a custom-built holder. The average distance between the headplate and skull was subjectively minimised by adjusting the head's pitch between 5 to 10°. With the headplate in place, ice-cooled Super-bond was applied from the inside out, filling all gaps between the headplate and the skull. Any residual gaps were filled with Paladur or with more Super-bond if the gaps were too big for the surgeon's consideration. Finally, mice recovered from surgery in their preheated home cage at 39 °C with a rewarding portion of oatmeal.

5.2.4 *Electrophysiology recording preparations*

Anaesthetised experiment surgery preparation

For anaesthetised recordings, mice were administered injected and vaporised anaesthetics. Firstly, a solution of 5 % urethane (Sigma, Germany) was administered to awake mice (1.2 g/kg) with an intraperitoneal

VIRUS	TITER [vg/mL]	SUPPLIER	ID	EXPRESSION
PENN AAV hSyn Cre WPRE hGH	1.80×10^{13}	Addgene	#105553-AAV1	Cre
AAV_2-hSyn-DIO-EGFP	3.00×10^{12}	Addgene	#50457-AAV2	Cre-dependent EGFP
AAV_2-hSyn-DIO-mCherry	4.00×10^{12}	Addgene	#50459-AAV2	Cre-dependent mCherry
AAV_8-hSyn Con/Fon EYFP	1.00×10^{13}	Addgene	#55650-AAV8	Cre and Flpo dependent EYFP
AAV_2-Ef1a-fDIO mCherry	1.10×10^{13}	Addgene	#114471-AAV2	Flpo dependent mCherry
AAV_1-EF1a-Flpo	7.00×10^{12}	Addgene	#55637-AAV1	Flpo
AAV_1-Ef1a-fDIO EYFP	2.10×10^{13}	Addgene	#55641-AAV1	Flpo dependent
AAVrg-CAG-hChR2-tdTomato	7.00×10^{12}	Addgene	#28017-AAVrg	tdTomato
$AAV_{1/2}$-CAG-SyPhy-EGFP	NaN	T. Kuner Lab	-	EGFP
$AAV_{1/2}$-CBA-SyPhy-mOrange	NaN	T. Kuner Lab	-	mOrange
AAV_8-hSyn Con/Fon hChR2 (H134R)-EYFP	2.30×10^{13}	Addgene	#55645-AAV8	Cre and Flpo dependent ChR2-EYFP
AAV_5-hSyn1-SIO-eOPN3-mScarlet-WPRE	1.00×10^{13}	Addgene	#125713-AAV5	Cre dependent inhibitory eOPN3

TABLE 5.3 – Virus list for pathway labelling and opsine expression in specific neural populations. Titer unit indicates viral genomes per millilitre (vg/mL). NaN indicates that the titer was not determined.

NUCLEUS	AP	ML	DV [MM]
SC	−3.60	1.25	−2.10 to −2.50
MC	1.00	1.00	−1.00 to 1.20
BC	−3.00	2.00	−1.00 to −1.20

TABLE 5.4 – Coordinates for neural recordings.

(ip) injection, and immediately returned to their home cage under constant supervision. Unconscious mice were head-fixed to the custom electrophysiology set-up with a low concentration (0.2 to 0.8 %) of isofluorane through a self made silicon mask. The craniotomies were carved with a lower accuracy than the Kopf stereotactic frame. To increase the likelihood of hitting the target with multi-channel silicone probes, craniotomies were about 80 to 150 % bigger than for viral injections, which allowed for correction of inaccuracies. With the craniotomies ready, a small plastic well (around 3 to 4 mm of diameter) was fixed around the centre of the recording site with Paladur to create a well of Ringer's solution for the reference electrode. The well was cemented to both the skull and a metallic rod that secured the animal's head position. Once the cement hardened, the earbars were removed to relieve pressure from the mouse's head. A heat control system kept the animal at 38 °C acting through a heating pad and a rectal thermostat.

The targeted regions were SC, MC, and BC (Table 5.4). To identify the whisker-sensitive region in SC, I used a mesh attached to the piezoelectric device to stimulate as many whiskers as possible. Additionally, I used a 4-shank, multi-electrode silicone probe (64 channels, ASSY-77 E-1, Cambridge NeuroTech, Cambridge, UK) to increase spatial sampling across the ML axis and record aps in SC upon whiskers stimulation.

To achieve independent optogenetic stimulation of MC- and BC-L5 in Rbp4-Cre×EYFP-ChR2 mice, a movable optical fibre and a glass-electrode were sequentially placed barely touching pia mater over MC and BC. Local-field potentials (LFPs) were recorded in MC and BC, but these data were not presented. The stimulation protocol consisted of three conditions: 1. a 5 ms laser pulse stimulating sequentially MC- or BC-L5 (based on [54]); 2. a 50 ms whisker deflection, and; 3. a paired stimulation in which the 5 ms laser pulse onset started 30 ms before the whisker stimulation onset. The experiment lasted approximately 40 min, spending 20 min exploring, e. g. MC-L5 effects before moving the glass-electrode and optical fibre to BC.

Awake head-fixed experiment preparation

For awake recordings, mice were prepared 15 to 18 h before the experiment. All animals that underwent awake recordings had a headplate implanted as described in subsection 5.2.3 and needed either a new or larger craniotomy. The craniotomy was small enough to reduce tissue damage but large enough to loosely fit the E-1 probe; usually around 1.2 to 1.5 mm. A two-component bio-compatible silicone sealant (Kwik-Cast, Microprobes for Life Science, USA) filled the Ringer's solution well and covered the exposed tissue. Finally, the mouse was returned to its pre-heated home cage with a small hill of oatmeal as a reward.

5.3 EQUIPMENT

5.3.1 *Electrophysiology recording system*

The electrophysiology recording system consisted of the following equipment: *a*. a 64-channel silicone probe(s); *b*. a 64-channel mini-amplifier and digital-to-analogue converter (DAC) chip(s) (RHD-2164, Intan Technologies, USA); *c*. a USB-2 interface board (RHD-EVAL); *d*. and only for anaesthetised experiments, a USB-2 interface (Micro 1401 mkII, Cambridge Electronic Design Limited [CED], Cambridge, UK).

Only anaesthetised experiments could have two recording sites: A glass-electrode or an H-3 probe was used in cortex, and either a H-5 or an E-1 for SC. Additionally, the protocol within anaesthetised experiments was controlled by Spike2 (CED) through the CED interface. The CED interface also recorded the amplified LFP from MC and BC glass-electrode, which consisted of a silver plated electrode inside a 1 µm-tip pulled glass pipette, which had a resistance between 4 and 6 MΩ. In contrast, all awake experiments were targeted only at SC and are described in subsection 5.6.1.

5.3.2 *Optogenetic stimulation systems*

In this section, I describe two laser systems used for optogenetic manipulations. The control signal given to either laser generator was created by the CED interface for anaesthetised experiments or by a microcontroller (Arduino Uno, Arduino, Italy) for awake experiments.

CUSTOM-BUILT LASER I used a custom-built laser system consisting of the following components: 1. a 488 nm solid-state laser (• Sapphire, Coherent, Germany, maximum output power 22 mW); 2. an ultrafast shutter (Uniblitz, USA); 3. a collimator; and 4. an optical fibre (inner diameter 400 µm, NA 0.48, ThorLabs, USA). The custom-built

system was used for all anaesthetised and for few experiments on the roller.

RWD LASER SYSTEM An IOS-465 module 465 nm (• 100 mW maximum output power, RWD Life Science Co., Ltd., Guangdong, China) . was used to optogenetically activate different opsines in the roller set-up.

The roller set-up was described in subsection 5.3.3

5.3.3 *Behavioural setup*

The setup consisted of *a*. a Pilates foam cylinder (roller) mounted on a low-friction metallic frame built by the Feinmechanik workshop of Heidelberg University[1]; *b*. a magnetic incremental ring (MR 100 N 71 B 152 A 0, RLS, Slovenia) mounted on the side of the roller; *c*. a rotary encoder (RLC2IC, RLS); and *d*. a tube to deliver the air puff to the mouse's whiskers. The roller frame had two screws to fix the implanted head plate. The air puff was placed such that no other part of the face would be stimulated but the whiskers as shown in Figure 3.1A.

ROLLER HABITUATION Mice were habituated to both the roller and experimenter for 3 consecutive days with increasing session duration, i. e. 10, 20 and 30 min, respectively. Mice were rewarded with a few droplets of condensed milk approximately once every 5 to 10 min, and with oatmeal when returned to their home cage. During the first habituation session, most animals were walking backward or sideways. In the second session, animals were walking forward and even grooming, and in their last session, some mice were eager to lick their reward. Because the air puff delivery system was noisy (around 68 dB) a white noise was played throughout the habituation. The noise volume was increased every session to approximately 70 dB. Although unpleasant, mice seem to get used to the noise and are able to ignore it.

Mice love condensed milk and oats!

5.4 AWAKE RECORDINGS

The following day after craniotomy renewal, mice were recovered and fixed in the roller set-up. The room was as dark as possible for experimenters to continue preparing animals for acute electrophysiology experiments. However, a light source was placed to illuminate the craniotomy while preparing for the probe insertion. The white noise from the habituation sessions was played from the moment mice were head-fixed until the experiment was finished.

Animals were immediately rewarded with a drop of condensed milk after being fixed and before removing the silicone cap from the

1 Big thanks to Nico Schmutz and his team!

implanted well. The tube for delivering the whisker puff was adjusted to match the mice's whisker fan centre to deflect as many whiskers as possible without stimulating any other part of their bodies. The silicone seal was removed, exposing the brain tissue. The craniotomy was washed with Ringer's solution to remove debris, if any. When the silicone seal was removed, the well was filled with Ringer's solution to keep the tissue moist and reduce its mechanical resistance for the insertion of the silicon probe. If necessary, the silver reference cable was prepared by stripping off the coating, sanding the exposed section, and immersing it for 3 to 5 s in ferric chloride ($FeCl_3$). The reference cable was then connected to the RHD amplifier and placed inside the well, immersed in Ringer's solution.

Section 5.2.4 describes prior preparation for the recording session.

Before lowering the optrode, I removed enough Ringer's solution from the well to reduce light refraction without drying the tissue surface. As soon as the probe touched the surface of the brain, I zeroed the DV axis and inserted the optrode at around 10 µm/s into the recording site (Table 5.4). If the tissue offered high resistance and the silicone probe started to bend, the probe was retracted and the pia was pierced to allow the probe to penetrate the tissue. Once the probe was in position, a 10 min pause with the light source turned off allowed the tissue surrounding the probe to settle, hoping for a low unit drift during the recording. Neural data were recorded at 30 kHz, with an anti-aliasing bandpass filter with cut-frequencies of 0.5 Hz and 15 kHz.

5.4.1 *Stimulation protocol*

The stimulation protocol was programmed in Bonsai-Rx [44], which consisted of a state machine iterating through the following stages:

A. an initial and non-repeatable stage with a 10 s timer allowed every hardware component to initialise;

B. a sample was drawn from a normal distribution[2] at 1 Hz;

C. if the normal sample was greater than 1.70 ($p = 0.0444$), a continuous uniform distribution u from 0 to 3 was sampled to deliver a stimulation condition:

if $u < 2$ a microcontroller (Arduino Uno, Arduino, Italy) waited 100 ms to generate a 100 ms squared pulse that fed into an air valve regulator module from Modular Electronics for Cell Physiology (Max-Planck-Institute for Medical Research, manufactured by Sigmann Elektronik, Germany);

if $u > 1$ a 300 ms pulse was generated to deliver optogenetic stimulation.

2 $\mathcal{N}(\mu = 0, \sigma = 1)$, which yielded around 40 trials in 15 min

Therefore, if $1 < u < 2$, both stimuli were delivered. This paired condition was called Laser ON. Note that because of the introduced delay for generating the puff command, the laser stimulation started and finished 100 ms before and after puff onset and offset. When $u < 1$, only the whisker puff was delivered, a condition called Laser OFF. This protocol was applied to RNs, eRNs, and iRNs experiments. For eOPN3 experiments (MC$\not\rightarrow$SC), the Laser ON condition consisted of a 800 ms pulse that started 600 ms before the whisker puff onset.

5.4.2 *Behaviour recording*

The position of the roller and the mice's face were recorded with a rotary encoder (RLC-2-IC-A-D-20-D-0-A-0 & magnetic wheel MR100S, RLS) and with a high-speed camera (BFS-U3-4S2M-C, Sony IMX287, Mono Blackfly 3, Flir, USA), respectively. The magnetic ring has an accuracy of 0.1 deg/step. The encoder detected each step and fed the position into the serial port of a microcontroller through an interruption protocol (Arduino Mega) together with the recorded trigger onsets. The microcontroller appended time stamps per interruption in µs and fed them to Bonsai. Finally, Bonsai created two comma-separated value (CSV) files. One with each interruption and another with the recording computer's timestamp and the command to the microcontroller.

The video was sampled at 654 frames per second (FPS), the maximum rate allowed by Windows 10 (Microsoft, USA) and stored in AVI video format files for processing with DLC.

5.5 EUTHANASIA AND HISTOLOGY

After the last experiment or reporter expression, mice were deeply anaesthetised with an ip injection of Ketamine (120 mg/kg) and Xylazine (20 mg/kg, both CP-Pharma) to quickly access their heart for transcardiac perfusion with a 4 % paraformaldehyde (PFA) solution in phosphate buffered saline (PBS, gibco, Life Technologies Limited, UK) to carefully extract their brains. Extracted brains were immersed in an identical PFA solution for 16 to 18 h to ensure a high degree of stiffness. The tissue was sliced with a vibratome (HM650V, Thermo Scientific Microm GmBH, Walldorf, Germany) with 50 to 100 µm thickness for microscopy and histology. Brain slices were mounted on glass slides with Mowiol (4-88, Sigma-Aldrich, Darmstadt, Germany) for viral expression validation with a stereo microscope (M80, Leica Microsystems, Germany). Berin E. Boztepe, Dr. Martín-Cortecero, and Katharina Ziegler performed perfusions, histology, cell counting, and microscopy.

5.6 DATA ANALYSIS

I used MATLAB (R2024b, MathWorks, USA) to synchronise electrophysiological and behavioural data using the laser signal recorded with Intan and captured by the high-speed camera. Then I performed a trigger analysis of both data sets.

The following subsection (5.6.1) describes the trigger-based processing pipeline for electrophysiology data. Subsection 5.6.2 describes the extraction and computation of behavioural signals for the analysis of behaviour. Finally, subsection 5.6.3 describes the approach for computing a linear relationship between the spikes of recorded putative single neurons and the animal's behaviour.

5.6.1 *Electrophysiology*

Neural data were recorded as unsigned 16-bit binary files (`uint16`) directly from Bonsai-Rx. I delivered optogenetic stimulation as a continuous pulse and as a frequency train in separate runs of the protocol. This characteristic led to more than one recording file per experiment. The resulting recording files were concatenated into a single binary file to allow the spike-sorting algorithm to find units along all parts of the experiment.

Kilosort 2.0.2 [57, 58, 64], a MATLAB-based, graphics-processing unit (GPU) accelerated, spike-sorting algorithm, processed the concatenated session file. The spike membership estimation was manually inspected and curated using Phy2 [38], a Python-based graphical interface to merge, split, and label spike clusters. All clusters, hereafter units, were manually labelled as either *good*, *multi-unit activity (MUA)*, or *noise*. A custom script in MATLAB stacked spikes of all non-noise units in a logical $N_u \times N_s \times N_\tau$ matrix, where N_u is the number of units, N_s the samples in trial τ from a total of N_τ. A user-defined window (usually -350 to 400 ms) relative to the onset of a considered stimulus condition, e. g. all whisker puffs in an experiment. In this way, one could easily count spikes per trial, unit, condition, and a specific time window.

For whisker puff trials, a 20 to 200 ms responsive period was considered. Only units with more than 3 % of spikes falling under a 1.5 ms inter-spike interval (ISI) threshold were considered for further analysis.

PUFF RESPONSIVENESS Units were classified as puff-responsive if median spike counts across trials were significantly different (`ranksum` MATLAB function, $\alpha = 0.05$, paired, two-sided Wilcoxon test) in spontaneous (usually from -330 to -150 ms depending on the laser onset relative to the puff onset) vs. responsive windows.

LASER-RESPONSIVENESS Although determined, these data were not used for the conclusions of my thesis. Briefly, responsiveness to the laser was determined depending on the expressed opsine and the cells' molecular identity. If ChR2 was expressed in iRNs, units with $p < 0.05$ in the median test from the puff responsiveness but between 5 to 15 ms and -15 to -5 ms was considered as responsive. A 8 ms window starting at 4 ms after the laser onset and a mirrored spontaneous window, i. e. -12 to -4 ms were considered for the spike median test for eRNs and RNs. Units with standard deviation < 4 ms and mean < 6 ms were considered optotagged. Since SC is multisensory, any activity evoked beyond the response window was not considered.

SPIKING ACTIVITY HISTOGRAMS Once unit responsiveness was assigned, I built population PSTHs per considered condition that could be ordered e. g. by the magnitude of response or by the estimated DV position on the probe. PSTHs could also be built using a subset of units, e. g. laser or puff responsive. I compared each unit's response and spontaneous median spike count amongst different conditions as in the stimulus-responsiveness test to identify units that were significantly modulated by e. g. the laser in a paired condition. I also compared PSTHs among conditions as a whole or a subset of the population using the modulation index. The modulation index was calculated as $M = (B - A) / (A + B)$, where A and B are conditions to be compared, and M the resulting modulation index.

5.6.2 *Behaviour*

Videos were processed by DLC, a Python-based, GPU-accelerated, pre-trained deep-learning toolbox for tracking objects and animals without markers [39, 51, 56]. A total of 40 frames from 25 different videos were used to train DLC for tracking mice's nose, four whiskers from each side, the centre point of the headplate, and the recording site in the roller set-up. DLC median filter was used on the output files to smooth the tracking to avoid estimation artefacts. Most of the videos were processed in the high performance cluster (bwForCluster Helix, sd19B001).

BEHAVIOURAL MEASUREMENTS Since every whisker was tracked using a point, a reference line was needed to calculate their angle in each frame. The reference line should divide the mouse's face into two symmetrical halves, orthogonal to the ML axis. I chose to fit a circle using DLC whisker and nose points because, after visual inspection, the centre point of the circle was approximately on the reference line in frames with different and asymmetric whiskers and nose positions. Hence, the circle centre served as an anchor point to create the reference line. I selected the headplate position as the

second point to draw the reference line. DLC likelihood was used to calculate a weighted mean headplate position as $\overline{p}_{hp} = \mathbf{P}_{hp} \cdot \vec{\rho}$, where $\vec{\rho}$ is DLC's L2 normalised likelihood, $\mathbf{P}_{hp}$ is the DLC estimation of the headplate position in $(\vec{x}_f, \vec{y}_f)$ coordinates for each frame f, and $\overline{p}_{hp}$ the resulting weighted mean. The angle for each whisker was calculated using an auxiliary line, a 'whisker' line, which intersected DLC whiskers points and the reference line at a pivotal point. The pivotal point was the golden ratio of the distance from the nose to the centre of the circle. Each whisker angle was calculated with the normal vectors of the reference $\vec{r}$ and whisker $\vec{w}$ lines as follows:

The golden ratio is defined as $\left(1+\sqrt{5}\right) \div 2$ and its presence in nature continues to be the object of several mathematical and artistic studies [62].

$$\theta_w = \cos^{-1}\left(\frac{\vec{r}\cdot\vec{w}}{|\vec{r}|\,|\vec{w}|}\right),$$

where θ_w is the angle of whisker w. The nose angle calculation was identical but using an orthogonal vector to the reference normal vector ($\perp \vec{r}$) and the normal vector $\vec{n}$ of the line crossing the DLC nose and pivotal points.

Additionally, I measured the arc in between both sets of whiskers on each side and computed a symmetry index as

$$S = \cos\left(\overline{\theta}_{w,s}\right) - \cos\left(\overline{\theta}_{w,n}\right),$$

where S is the symmetry index, $\overline{\theta}_{w,s}$ is the stimulated whiskers mean angle, and $\overline{\theta}_{w,n}$ non-stimulated. Positive values of S indicate asymmetry towards the puff, while $S = 0$ indicates perfect symmetry (Figure 5.1). Fig. 3.1b shows the auxiliary geometric shapes overlaid on the mouse's face to measure behavioural signals. Theoretically, S can take values between -2 to 2. However, the only case where this could happen is if $\overline{\theta}_{w,s}$ and $\overline{\theta}_{w,n}$ had values beyond the borders marked in Fig. 5.1 with a -1 or 1.

ROLLER SPEED COMPUTATION When the magnetic ring on the side of the roller turned enough to detect a step, an interrupt protocol in the Arduino Mega sent the position of the magnetic ring through the serial communication port to Bonsai-Rx. The roller position CSV file contained the encoder position followed by a time-stamp in µs from the Arduino Mega every time the current position changed. Additionally, the CSV file contained trigger identities 'P' or 'L' for puff and laser, respectively, followed by the µs time stamp. Rarely did interruptions overlap and disrupt the file writing process. For example, whilst a roller position was being written (75,5 436 436\n) when a puff trigger interrupted (P,5 436 687\n) leaving the file messed up (75,5436P, 5 436 687\n436\n). When these errors occurred, I used the trigger identifiers to fix the strings. Corrected:

```
75,5436436\n
P,5436687\n
```

Another source of errors in the roller position file was environmental noise. Big enough interference caused interruptions that resulted in non-existent trigger timestamps. Luckily, having redundant signal recording made my life easier to correctly identify and eliminate errors.

Without errors in the roller position and trigger times CSV file, the roller speed was calculated by *a*. unwrapping the roller positions, since the encoder started from the opposite edge when surpassed its `int16` range; *b*. resampling the signal using a time-axis matching the video frame rate; *c*. differentiated to get the speed; *d*. and 18 Hz low-pass zero-phase filtered to correct for jittery position values. Figure 3.1B shows example traces for all measured behavioural parameters and the auxiliary geometric shapes for their computation.

Electrophysiological and behavioural signals differed in duration due to hardware and sampling frequency differences. Therefore, video-extracted behaviour signals were enough mirror-padded samples to match electrophysiology duration and trigger times. These two last steps were achieved by correlating the intensity values around the optic fibre from videos with recorded laser trigger signals. Once both behaviour and electrophysiology were matched, the signals of the same session were concatenated along the time axis.

PUFF-EVOKED MOVEMENT ANALYSIS To study the behavioural relevance of SC manipulations, body part movements were sliced around the puff onset and stacked as electrophysiological data in sub-

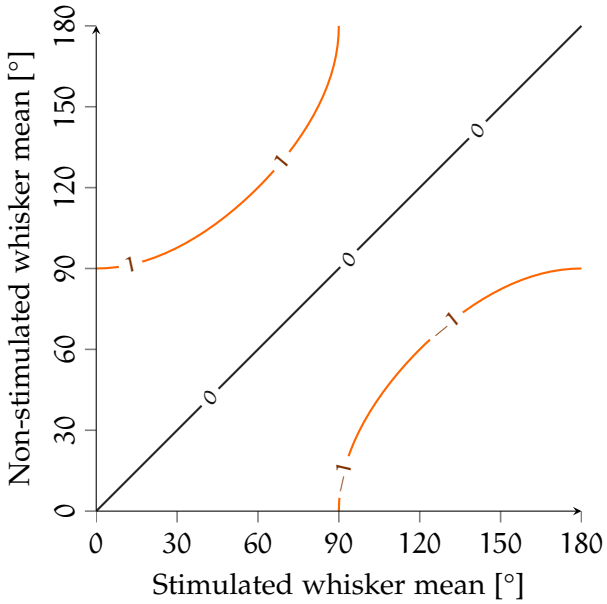

FIGURE 5.1 – Contour plot of the symmetry index. Perfect symmetry indicated by diagonal black line where $S = 0$, and theoretical whisker range where $|S| \geqslant 1$ is indicated by red curved lines.

section 5.6.1. Intan trigger times were used to cut all signals extracted from videos, whilst Arduino trigger times cut the roller speed. The resulting 3-D matrix was size $N_b \times s \times \tau$, where N_b was the number of behaviour signals, and s and τ are samples relative to the trigger onset and trials, respectively. The relationship between samples and time is $t = s/\omega_s$.

E. g. the sample number 30 000 *corresponds to* 1 s *if using a* 30 kHz *sampling frequency.*

The orientation amplitude for a behavioural signal b in a session was the absolute maximum difference between the median in −350 to −25 ms pre-puff and signal values in 25 to 350 ms post-puff:

$$\mathbf{A} = \left|\max\left(b_e - \tilde{b}_s\right)\right|,$$

where $\mathbf{A}$ represents the resulting amplitudes, b_e the values of signal b in the post-puff window e, and $\tilde{b}_s$ the median value in the pre-puff window s. A small adjustment was made for stimulated whiskers due to passive deflections of the whisker puff, in which a 125 to 450 ms post-puff window was considered.

$\mathbf{A}$ was a $\tau \times 8$ matrix: $\mathbf{A} = \left[\,\vec{a}_1, \cdots, \vec{a}_b\,\right]$, with $\vec{a}_b = [\,a_1, \cdots, a_\tau\,]$. Each column of the matrix $\mathbf{A}$ was normalised by their maximum value $(\vec{a}_b / \max(\vec{a}_b))$. The average amplitude index per measurement was used to construct an octagon, whose area was a proxy for the overall orientation behaviour amplitude in an experiment. For example, if a mouse moved all body parts in average half of the maximum amplitude during a session, an equilateral polygon would be constructed as shown in Figure 5.2a.

In case of including or removing behaviour signals, the axes would be adjusted accordingly. Figure 5.2b shows a hypothetical case with five behaviour signals, making a pentagon.

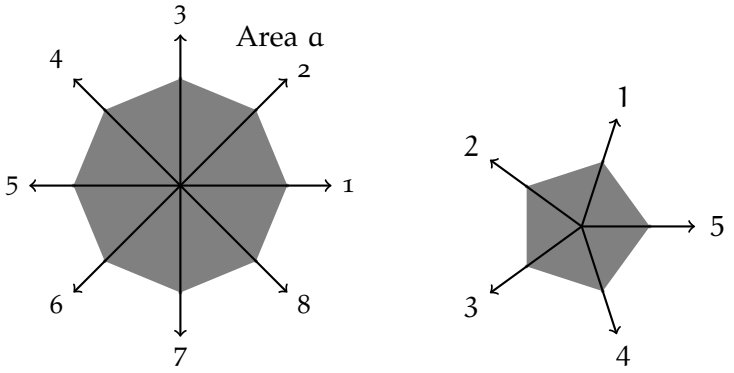

(A) Octagon (B) Pentagon

FIGURE 5.2 – Example polygons for (**a**) eight and (**b**) five behaviour signals.

5.6.3 *Electrophysiology & behaviour relationship*

Neural activity and amplitude index regression

The averaged and normalised activity of single units in a 20 ms sliding window in all trials, starting from −50 ms pre-puff until reaching 400 ms post-puff, was used to compute R^2 per regression. For example, a unit X had N trials and its normalised average spike counts in the first window per trial is a vector of N elements $\vec{s}$ that corresponds with the amplitude index vector $\vec{a}$. The regression is performed using MATLAB's function `fitlm`, which returns a R^2 before the sliding window advances 5 ms to repeat the same procedure until reaching 400 ms post-puff.

The R^2-dependent population regression was done by dividing the R^2 range (from 0 to the maximum R^2 $\left(R^2_e\right)$) per experiment into ten equal parts and using the response window (20 to 200 ms). The first threshold allowed all units of the experiment to participate in the regression. All following thresholds were compared with each unit R^2 to decide whether allowing units in the regression until reaching $0.9 \cdot R^2_e$ that allows the highest 10 % of the population. Averaged spiking activity of the supra-threshold units were used for regression with the amplitude index vector $\vec{a}$. Similarly and in opposite direction, another population regression to remove R^2 high-valued units first was performed. The main difference is that the average spiking activity of sub-threshold units were used and that the first threshold allowing all units was R^2_e. The threshold was then reduced consecutively until reaching only the lowest 10 % of the population, i. e. $0.1 \cdot R^2_e$.

For the whole population regression by time-windows, the procedure was similar to the first iteration of the R^2-dependent regression. The only difference was that the considered time windows varied from −160 to 380 ms in non-overlapping sliding windows of 30 ms. The collected R^2 per experiment were pair-wise compared using the Kruskal-Wallis test and post-hoc with Tukey's honestly significant difference procedure [29] (Tukey-Kramer multi-comparison correction, optimal for balanced one-way ANOVA).

Finally, the Gamma distribution fit was performed on the maximum R^2 per unit using MATLAB's function `fitdist`.

Behaviour reconstruction

A Gaussian GLM was implemented between neural activity and each behaviour signal to validate SC involvement in the orienting behaviour. I based the Gaussian GLM on the work of Chinta and Pluta [11], where they deployed a "self-motion decoder" to reconstruct "slow and fast whisker features" from the recorded SC activity.

Spikes for each unit and the behaviour signals were arranged in 5 ms bins from −800 to 800 ms around the whisker puff. For each binned

behaviour value, the spike count data was collected in a window relative to the considered bin from -100 to 100 ms to construct the design matrix $\mathbf{X}$. Every bin in behaviour was related to the spike count of all units within -100 to 100 ms. $\mathbf{X}$ was a $(N_b \cdot N_\tau) \times (N_u \cdot N_{rb})$ matrix composed by a collection of vectors

$$\mathbf{X} = \left[\vec{x}_{1,1}, \vec{x}_{2,1}, \cdots, \vec{x}_{1,2}, \vec{x}_{2,2}, \cdots, \vec{x}_{b,\tau} \right]^T,$$

where b is the considered behaviour bin belonging to trial τ. In turn, each vector $\vec{x}_{b,\tau}$ is composed by the consecutive spiking activity of each unit: $N_u \cdot N_{rb}$, where N_u is the number of units and N_{rb} the number of relative bins around the behaviour bin b:

$$\vec{x}_{b,\tau} = \left[x_{1,1}, x_{1,2}, \cdots, x_{1,rb}, x_{2,1}, x_{2,2}, \cdots, x_{2,rb}, \cdots, x_{u,rb} \right].$$

In this way, a considered behaviour bin b of trial τ had the binned activity in rb (relative) bins of unit u between -100 to 100 ms relative to bin b.

The model using behaviour and neural data of Laser OFF condition trials was trained using the analytical form $\theta_c = \mathbf{X}^T y \left(\mathbf{X}^T \mathbf{X}\right)^{-1}$ to compute the coefficient matrix θ_c with the binned behaviour signal y. A 20-fold cross-validation technique was used on trials of the experiment to compute the reconstruction error of the model and avoid over-fitting. I reconstructed and compared the behaviour signals vs. the observed signals to measure the model performance. Laser ON trials were reconstructed using a design matrix $\mathbf{X}_l$ and the coefficient matrix θ_c. Finally, the population polygons were constructed by measuring the amplitude of observed and reconstructed signals, exactly as in subsection 5.6.2.

BIBLIOGRAPHY

Allen, Kathryne M., Jennifer Lawlor, Angeles Salles and Cynthia F. Moss (Dec. 2021). 'Orienting our view of the superior colliculus: specializations and general functions'. In: *Current Opinion in Neurobiology* 71, pp. 119–126. ISSN: 09594388. DOI: 10.1016/j.conb.2021.10.005. URL: https://linkinghub.elsevier.com/retrieve/pii/S0959438821001161.

Arena, Giulia, Fabrizio Londei, Francesco Ceccarelli, Lorenzo Ferrucci, Elena Borra and Aldo Genovesio (Jan. 2024). 'Disentangling the identity of the zona incerta: a review of the known connections and latest implications'. In: *Ageing Research Reviews* 93, p. 102140. ISSN: 15681637. DOI: 10.1016/j.arr.2023.102140. URL: https://linkinghub.elsevier.com/retrieve/pii/S1568163723002994.

Basso, Michele A. and Paul J. May (Sept. 2017). 'Circuits for Action and Cognition: A View from the Superior Colliculus'. In: *Annual Review of Vision Science* 3.1, pp. 197–226. ISSN: 2374-4642. DOI: 10.1146/annurev-vision-102016-061234. URL: https://www.annualreviews.org/doi/10.1146/annurev-vision-102016-061234.

Benavidez, Nora L. et al. (June 2021). 'Organization of the inputs and outputs of the mouse superior colliculus'. In: *Nature Communications* 12.1, p. 4004. ISSN: 2041-1723. DOI: 10.1038/s41467-021-24241-2. URL: https://www.nature.com/articles/s41467-021-24241-2.

Bezdudnaya, Tatiana and Manuel A. Castro-Alamancos (July 2011). 'Superior colliculus cells sensitive to active touch and texture during whisking'. In: *Journal of Neurophysiology* 106.1, pp. 332–346. ISSN: 00223077. DOI: 10.1152/jn.00072.2011. URL: www.jn.org%20http://www.physiology.org/doi/10.1152/jn.00072.2011%20https://www.physiology.org/doi/10.1152/jn.00072.2011.

Bezdudnaya, Tatiana and Manuel A. Castro-Alamancos (May 2014). 'Neuromodulation of Whisking Related Neural Activity in Superior Colliculus'. In: *The Journal of Neuroscience* 34.22, pp. 7683–7695. ISSN: 0270-6474. DOI: 10.1523/JNEUROSCI.0444-14.2014. URL: https://www.jneurosci.org/lookup/doi/10.1523/JNEUROSCI.0444-14.2014.

Box, George E. P. (Dec. 1976). 'Science and Statistics'. In: *Journal of the American Statistical Association* 71.356, pp. 791–799. ISSN: 0162-1459. DOI: 10.1080/01621459.1976.10480949. URL: http://www.tandfonline.com/doi/abs/10.1080/01621459.1976.10480949.

Brecht, Michael, Miriam Schneider, Bert Sakmann and Troy W. Margrie (Feb. 2004). 'Whisker movements evoked by stimulation of single pyramidal cells in rat motor cortex'. In: *Nature* 427 (6976), pp. 704–

710. ISSN: 0028-0836. DOI: 10.1038/nature02266. URL: https://www.nature.com/articles/nature02266.

Budd, Graham E. (Dec. 2015). *Early animal evolution and the origins of nervous systems*. DOI: 10.1098/rstb.2015.0037.

Castro-Alamancos, Manuel A. and Morgana Favero (May 2016). 'Whisker-related afferents in superior colliculus'. In: *Journal of Neurophysiology* 115.5, pp. 2265–2279. ISSN: 0022-3077. DOI: 10.1152/jn.00028.2016. URL: https://www.physiology.org/doi/10.1152/jn.00028.2016.

Chinta, Suma and Scott R. Pluta (Apr. 2025). 'Whisking and locomotion are jointly represented in superior colliculus neurons'. In: *PLoS Biology* 23 (4). ISSN: 15457885. DOI: 10.1371/journal.pbio.3003087.

Cohen, Jeremy D., Akio Hirata and Manuel A. Castro-Alamancos (2008). 'Vibrissa sensation in superior colliculus: Wide-field sensitivity and state-dependent cortical feedback'. In: *Journal of Neuroscience* 28.44, pp. 11205–11220. ISSN: 02706474. DOI: 10.1523/JNEUROSCI.2999-08.2008. URL: http://www.jneurosci.org/content/jneuro/28/44/11205.full.pdf%20http://www.jneurosci.org/cgi/doi/10.1523/JNEUROSCI.2999-08.2008.

Corneil, Brian D. and Douglas P. Munoz (June 2014). 'Overt Responses during Covert Orienting'. In: *Neuron* 82.6, pp. 1230–1243. ISSN: 08966273. DOI: 10.1016/j.neuron.2014.05.040. URL: https://linkinghub.elsevier.com/retrieve/pii/S089662731400484X.

Ding, Yu, Na Xu, Yayue Gao, Zhemeng Wu and Liang Li (May 2019). 'The role of the deeper layers of the superior colliculus in attentional modulations of prepulse inhibition'. In: *Behavioural Brain Research* 364, pp. 106–113. ISSN: 18727549. DOI: 10.1016/j.bbr.2019.01.052.

Dräger, U. C. and D. H. Hubel (Jan. 1976). 'Topography of visual and somatosensory projections to mouse superior colliculus'. In: *Journal of Neurophysiology* 39.1, pp. 91–101. ISSN: 0022-3077. DOI: 10.1152/jn.1976.39.1.91. URL: https://www.physiology.org/doi/10.1152/jn.1976.39.1.91.

Fenno, Lief E. et al. (Sept. 2020). 'Comprehensive Dual- and Triple-Feature Intersectional Single-Vector Delivery of Diverse Functional Payloads to Cells of Behaving Mammals'. In: *Neuron* 107.5, pp. 836–853. ISSN: 10974199. DOI: 10.1016/j.neuron.2020.06.003.

Gandhi, Neeraj J. and Husam A. Katnani (July 2011). 'Motor Functions of the Superior Colliculus'. In: *Annual Review of Neuroscience* 34.1, pp. 205–231. ISSN: 0147-006X. DOI: 10.1146/annurev-neuro-061010-113728. URL: https://www.annualreviews.org/doi/10.1146/annurev-neuro-061010-113728.

García-Escudero, L. A., A. Gordaliza and A. Mayo-Iscar (June 2010). 'Discussion: The forward search: Theory and data analysis'. In: *Journal of the Korean Statistical Society* 39.2, pp. 135–136. ISSN: 12263192. DOI: 10.1016/j.jkss.2010.01.005. URL: https://link.springer.com/article/10.1016/j.jkss.2010.02.007.

Gehr, Carolin, Jérémie Sibille and Jens Kremkow (Apr. 2023). 'Retinal input integration in excitatory and inhibitory neurons in the mouse superior colliculus in vivo'. In: *eLife* 12, p. 2023.04.07.536092. ISSN: 2050084X. DOI: 10.7554/eLife.88289.1. URL: https://www.biorxiv.org/content/10.1101/2023.04.07.536092v1.abstract.

Geng, Dandan et al. (Mar. 2025). 'Cholecystokinin neurons in the spinal trigeminal nucleus interpolaris regulate mechanically evoked predatory hunting in male mice'. In: *Nature Communications* 16.1, p. 2544. ISSN: 2041-1723. DOI: 10.1038/s41467-025-57771-0. URL: https://www.nature.com/articles/s41467-025-57771-0.

Gharaei, Saba, Suraj Honnuraiah, Ehsan Arabzadeh and Greg J. Stuart (Apr. 2020). 'Superior colliculus modulates cortical coding of somatosensory information'. In: *Nature Communications* 11.1, p. 1693. ISSN: 2041-1723. DOI: 10.1038/s41467-020-15443-1. URL: https://www.nature.com/articles/s41467-020-15443-1.

González-Rueda, Ana et al. (July 2024). 'Kinetic features dictate sensorimotor alignment in the superior colliculus'. In: *Nature* 631.8020, pp. 378–385. ISSN: 14764687. DOI: 10.1038/s41586-024-07619-2. URL: https://www.nature.com/articles/s41586-024-07619-2.

Grillner, Sten (Dec. 2021). 'Evolution of the vertebrate motor system — from forebrain to spinal cord'. In: *Current Opinion in Neurobiology* 71, pp. 11–18. ISSN: 09594388. DOI: 10.1016/j.conb.2021.07.016. URL: https://linkinghub.elsevier.com/retrieve/pii/S095943882100091X.

Groh, Alexander, Christiaan P.J. De Kock, Verena C. Wimmer, Bert Sakmann and Thomas Kuner (2008). 'Driver or coincidence detector: Modal switch of a corticothalamic giant synapse controlled by spontaneous activity and short-term depression'. In: *Journal of Neuroscience* 28.39, pp. 9652–9663. ISSN: 02706474. DOI: 10.1523/JNEUROSCI.1554-08.2008. URL: http://www.jneurosci.org/cgi/doi/10.1523/JNEUROSCI.1554-08.2008.

Groh, Alexander and Patrik Krieger (2015). *Sensorimotor integration in the whisker system*. Ed. by Patrik Krieger and Alexander Groh. New York, NY: Springer New York, pp. 1–276. ISBN: 9781493929757. DOI: 10.1007/978-1-4939-2975-7. URL: http://link.springer.com/10.1007/978-1-4939-2975-7.

Groh, Alexander et al. (2014). 'Convergence of cortical and sensory driver inputs on single thalamocortical cells'. In: *Cerebral Cortex* 24.12, pp. 3167–3179. ISSN: 14602199. DOI: 10.1093/cercor/bht173.

Güntürkün, Onur, Roland Pusch and Jonas Rose (Mar. 2024). *Why birds are smart*. DOI: 10.1016/j.tics.2023.11.002.

Heimburg, Filippo et al. (Aug. 2024). *A tactile discrimination task to study neuronal dynamics in freely-moving mice*. DOI: 10.1101/2024.08.24.609326. URL: http://biorxiv.org/lookup/doi/10.1101/2024.08.24.609326.

Hochberg, Y. and A. C. Tamhane (1987). *Multiple comparison procedures*. USA: John Wiley & Sons, Inc. ISBN: 0471822221.

Hoy, Jennifer L. and Karl Farrow (Mar. 2025). 'The superior colliculus'. In: *Current Biology* 35.5, R164–R168. ISSN: 09609822. DOI: 10.1016/j.cub.2025.01.022. URL: https://linkinghub.elsevier.com/retrieve/pii/S0960982225000521.

Isa, Kaoru, Thongchai Sooksawate, Kenta Kobayashi, Kazuto Kobayashi, Peter Redgrave and Tadashi Isa (Sept. 2020). 'Dissecting the Tectal Output Channels for Orienting and Defense Responses'. In: *eneuro* 7.5, pp. 0271–20. ISSN: 2373-2822. DOI: 10.1523/ENEURO.0271-20.2020. URL: https://www.eneuro.org/lookup/doi/10.1523/ENEURO.0271-20.2020.

Isa, Tadashi, Emmanuel Marquez-Legorreta, Sten Grillner and Ethan K. Scott (June 2021). 'The tectum/superior colliculus as the vertebrate solution for spatial sensory integration and action'. In: *Current Biology* 31.11, R741–R762. ISSN: 18790445. DOI: 10.1016/j.cub.2021.04.001. URL: https://linkinghub.elsevier.com/retrieve/pii/S0960982221004796.

Isaías-Camacho, Emilio U.*, Jesús M. Martín-Cortecero*, James A. Auwn, Katharina Ziegler, Ann-Kristin Kenkel and Alexander Groh (2025). 'A motor cortico-collicular pathway shapes superior colliculus generated tactile orienting behaviour'. Manuscript in preparation.

Ito, Shinya and David A. Feldheim (Feb. 2018). 'The mouse superior colliculus: An emerging model for studying circuit formation and function'. In: *Frontiers in Neural Circuits* 12, p. 10. ISSN: 16625110. DOI: 10.3389/fncir.2018.00010. URL: http://journal.frontiersin.org/article/10.3389/fncir.2018.00010/full.

Jiang, Wan, Huai Jiang and Barry E Stein (2009). 'Orientation Behavior'. In: *Encyclopedia of Neuroscience*. Berlin, Heidelberg: Springer Berlin Heidelberg, pp. 3046–3046. DOI: 10.1007/978-3-540-29678-2{_}4281. URL: https://link.springer.com/10.1007/978-3-540-29678-2_4281.

Johnston, Graham A.R. (Sept. 2014). *Muscimol as an Ionotropic GABA Receptor Agonist*. DOI: 10.1007/s11064-014-1245-y.

Krauzlis, Richard J. (Apr. 2014). *Attentional Functions of the Superior Colliculus*. Ed. by Anna C. (Kia) Nobre and Sabine Kastner. Vol. 1. Oxford University Press. DOI: 10.1093/oxfordhb/9780199675111.013.014.

Laboratory, International Brain, Cortex Lab, Kenneth Harris and Matteo Carandini (2019). *phy*. URL: https://github.com/cortex-lab/phy.

Lauer, Jessy et al. (2022). 'Multi-animal pose estimation, identification and tracking with DeepLabCut'. In: *Nature Methods* 19, pp. 496–504.

Lavallée, Philippe and Martin Deschênes (July 2004). 'Dendroarchitecture and lateral inhibition in thalamic barreloids'. In: *Journal of*

Neuroscience 24.27, pp. 6098–6105. ISSN: 02706474. DOI: 10.1523/JNEUROSCI.0973-04.2004.

Liang, Feixue, Xiaorui R. Xiong, Brian Zingg, Xu ying Ji, Li I. Zhang and Huizhong W. Tao (May 2015). 'Sensory Cortical Control of a Visually Induced Arrest Behavior via Corticotectal Projections'. In: *Neuron* 86.3, pp. 755–767. ISSN: 10974199. DOI: 10.1016/j.neuron.2015.03.048. URL: http://www.ncbi.nlm.nih.gov/pubmed/25913860%0Ahttp://www.pubmedcentral.nih.gov/articlerender.fcgi?artid=PMC4452020.

Liu, Xue, Hongren Huang, Terrance P. Snutch, Peng Cao, Liping Wang and Feng Wang (Dec. 2022a). 'The Superior Colliculus: Cell Types, Connectivity, and Behavior'. In: *Neuroscience Bulletin* 38.12, pp. 1519–1540. ISSN: 19958218. DOI: 10.1007/s12264-022-00858-1. URL: https://link.springer.com/article/10.1007/s12264-022-00858-1%20https://link.springer.com/10.1007/s12264-022-00858-1.

Liu, Xue, Hongren Huang, Terrance P. Snutch, Peng Cao, Liping Wang and Feng Wang (Dec. 2022b). 'The Superior Colliculus: Cell Types, Connectivity, and Behavior'. In: *Neuroscience Bulletin* 38 (12), pp. 1519–1540. ISSN: 1673-7067. DOI: 10.1007/s12264-022-00858-1. URL: https://link.springer.com/article/10.1007/s12264-022-00858-1%20https://link.springer.com/10.1007/s12264-022-00858-1.

Lopes, Gonçalo et al. (2015). 'Bonsai: an event-based framework for processing and controlling data streams'. In: *Frontiers in Neuroinformatics* 9. ISSN: 1662-5196. DOI: 10.3389/fninf.2015.00007.

Lovejoy, Lee P. and Richard J. Krauzlis (Dec. 2010). 'Inactivation of primate superior colliculus impairs covert selection of signals for perceptual judgments'. In: *Nature Neuroscience* 13.2, pp. 261–266. ISSN: 10976256. DOI: 10.1038/nn.2470. URL: https://www.nature.com/articles/nn.2470.

Mahn, Mathias et al. (May 2021). 'Efficient optogenetic silencing of neurotransmitter release with a mosquito rhodopsin'. In: *Neuron* 109.10, pp. 1621–1635. ISSN: 10974199. DOI: 10.1016/j.neuron.2021.03.013.

Martin, Donna M et al. (Mar. 2004). 'PITX2 is required for normal development of neurons in the mouse subthalamic nucleus and midbrain'. In: *Developmental Biology* 267.1, pp. 93–108. ISSN: 00121606. DOI: 10.1016/j.ydbio.2003.10.035. URL: https://linkinghub.elsevier.com/retrieve/pii/S0012160603006870.

Martín-Cortecero, Jesús, Emilio Ulises Isaías-Camacho, Berin Boztepe, Katharina Ziegler, Rebecca Audrey Mease and Alexander Groh (Aug. 2023). *Monosynaptic trans-collicular pathways link mouse whisker circuits to integrate somatosensory and motor cortical signals*. DOI: 10.1371/journal.pbio.3002126. URL: http://biorxiv.org/lookup/doi/10.1101/2022.08.30.505868.

Martín-Cortecero*, Jesús M., **Emilio U. Isaías-Camacho***, Berin E. Boztepe*, Katharina Ziegler, Rebecca A. Mease and Alexander Groh (2023). 'Monosynaptic trans-collicular pathways link mouse whisker circuits to integrate somatosensory and motor cortical signals'. In: *PLoS Biology* 21 (5). ISSN: 15457885. DOI: 10.1371/journal.pbio.3002126.

Masullo, Laura, Letizia Mariotti, Nicolas Alexandre, Paula Freire-Pritchett, Jerome Boulanger and Marco Tripodi (Sept. 2019). 'Genetically Defined Functional Modules for Spatial Orienting in the Mouse Superior Colliculus'. In: *Current Biology* 29.17, pp. 2892–2904. ISSN: 09609822. DOI: 10.1016/j.cub.2019.07.083. URL: https://linkinghub.elsevier.com/retrieve/pii/S0960982219310073.

Mathis, Alexander et al. (2018). 'DeepLabCut: markerless pose estimation of user-defined body parts with deep learning'. In: *Nature Neuroscience*. URL: https://www.nature.com/articles/s41593-018-0209-y.

McHaffie, John G. and Barry E. Stein (Sept. 1982). 'Eye movements evoked by electrical stimulation in the superior colliculus of rats and hamsters'. In: *Brain Research* 247.2, pp. 243–253. ISSN: 00068993. DOI: 10.1016/0006-8993(82)91249-5.

Mease, Rebecca A., Patrik Krieger and Alexander Groh (May 2014). 'Cortical control of adaptation and sensory relay mode in the thalamus'. In: *Proceedings of the National Academy of Sciences of the United States of America* 111.18, pp. 6798–6803. ISSN: 10916490. DOI: 10.1073/pnas.1318665111.

Mease, Rebecca A., Anton Sumser, Bert Sakmann and Alexander Groh (2016). 'Corticothalamic Spike Transfer via the L5B-POm Pathway in vivo'. In: *Cerebral Cortex* 26.8, pp. 3461–3475. ISSN: 14602199. DOI: 10.1093/cercor/bhw123.

Mederos, Sara, Patty Blakely, Nicole Vissers, Claudia Clopath and Sonja B. Hofer (Feb. 2025). 'Overwriting an instinct: Visual cortex instructs learning to suppress fear responses'. In: *Science* 387.6734, pp. 682–688. ISSN: 0036-8075. DOI: 10.1126/science.adr2247. URL: https://www.science.org/doi/10.1126/science.adr2247.

Nath*, Tanmay, Alexander Mathis*, An Chi Chen, Amir Patel, Matthias Bethge and Mackenzie W Mathis (2019). 'Using DeepLabCut for 3D markerless pose estimation across species and behaviors'. In: *Nature Protocols*. URL: https://doi.org/10.1038/s41596-019-0176-0.

Pachitariu, Marius, Shashwat Sridhar and Carsen Stringer (2023). 'Solving the spike sorting problem with Kilosort'. In: *bioRxiv*. DOI: 10.1101/2023.01.07.523036. URL: https://www.biorxiv.org/content/early/2023/01/07/2023.01.07.523036.

Pachitariu, Marius, Nicholas Steinmetz, Shabnam Kadir, Matteo Carandini and Harris Kenneth D. (2016). 'Kilosort: realtime spike-sorting for extracellular electrophysiology with hundreds of channels'. In: *bioRxiv*.

DOI: 10.1101/061481. URL: https://www.biorxiv.org/content/early/2016/06/30/061481.

Paulin, Michael G. and Joseph Cahill-Lane (Jan. 2021). 'Events in Early Nervous System Evolution'. In: *Topics in Cognitive Science* 13.1, pp. 25–44. ISSN: 17568765. DOI: 10.1111/tops.12461.

Paxinos, George, Keith B.Franklin and Keith BJ.Frankin (2001). *The mouse brain steriotaxic coordinates*. elsevier science & technology books, p. 296. ISBN: 9780125476379.

Pessoa, Luiz (Feb. 2024). *Noncortical cognition: integration of information for close-proximity behavioral problem-solving*. DOI: 10.1016/j.cobeha.2023.101329.

Planat, Michel, Juan Alberto Rodriguez Velazquez, Callum Robert Marples and Philip Michael Williams (Oct. 2022). 'The Golden Ratio in Nature: A Tour across Length Scales'. In: *Symmetry 2022, Vol. 14, Page 2059* 14 (10), p. 2059. ISSN: 2073-8994. DOI: 10.3390/SYM14102059.

Redgrave, Peter et al. (Sept. 2010). 'Interactions between the midbrain superior colliculus and the basal ganglia'. In: *Frontiers in Neuroanatomy* 4.SEP, p. 6956. ISSN: 16625129. DOI: 10.3389/fnana.2010.00132. URL: www.frontiersin.org.

Roy, Aurko and Sebastian Pokutta (2016). 'Hierarchical Clustering via Spreading Metrics'. In: *Advances in Neural Information Processing Systems*. Ed. by D. Lee, M. Sugiyama, U. Luxburg, I. Guyon and R. Garnett. Vol. 29. Curran Associates, Inc. URL: https://proceedings.neurips.cc/paper_files/paper/2016/file/4d2e7bd33c475784381a64e43e50922f-Paper.pdf.

Shang, Congping et al. (June 2019). 'A subcortical excitatory circuit for sensory-triggered predatory hunting in mice'. In: *Nature Neuroscience* 22.6, pp. 909–920. ISSN: 15461726. DOI: 10.1038/s41593-019-0405-4. URL: http://www.nature.com/articles/s41593-019-0405-4.

Stein, Barry E., Braulio Magalhães-Castro and Lawrence Kruger (1975). 'Superior colliculus: Visuotopic-somatotopic overlap'. In: *Science* 189.4198, pp. 224–226. ISSN: 00368075. DOI: 10.1126/science.1094540.

Sumser, Anton, **Emilio Ulises Isaías-Camacho**, Rebecca Audrey Mease and Alexander Groh (Apr. 2025). 'Active and passive touch are differentially represented in the mouse somatosensory thalamus'. In: *PLOS Biology* 23 (4). Ed. by Alberto Bacci, e3003108. ISSN: 1545-7885. DOI: 10.1371/journal.pbio.3003108. URL: https://dx.plos.org/10.1371/journal.pbio.3003108.

Sumser, Anton, Rebecca A. Mease, Bert Sakmann and Alexander Groh (2017). 'Organization and somatotopy of corticothalamic projections from L5B in mouse barrel cortex'. In: *Proceedings of the National Academy of Sciences of the United States of America* 114.33, pp. 8853–8858. ISSN: 10916490. DOI: 10.1073/pnas.1704302114. URL: http://www.pnas.org/lookup/doi/10.1073/pnas.1704302114.

Usseglio, Giovanni, Edwin Gatier, Aurélie Heuzé, Coralie Hérent and Julien Bouvier (Dec. 2020). 'Control of Orienting Movements and Locomotion by Projection-Defined Subsets of Brainstem V2a Neurons'. In: *Current Biology* 30.23, pp. 4665–4681. ISSN: 09609822. DOI: 10.1016/j.cub.2020.09.014. URL: https://linkinghub.elsevier.com/retrieve/pii/S0960982220313452.

Valentine, Doreen E., Shiva R. Sinha and Cynthia F. Moss (Mar. 2002). 'Orienting responses and vocalizations produced by microstimulation in the superior colliculus of the echolocating bat, Eptesicus fuscus'. In: *Journal of Comparative Physiology A* 188.2, pp. 89–108. ISSN: 0340-7594. DOI: 10.1007/s00359-001-0275-5. URL: http://link.springer.com/10.1007/s00359-001-0275-5.

Wang, Chin-An and Douglas P. Munoz (2024). 'Linking the Superior Colliculus to Pupil Modulation'. In: *Modern Pupillometry*. Cham: Springer International Publishing, pp. 77–98. ISBN: 9783031548963. DOI: 10.1007/978-3-031-54896-3{_}2. URL: https://link.springer.com/10.1007/978-3-031-54896-3_2.

Wang, Lupeng, James P. Herman and Richard J. Krauzlis (Dec. 2022). 'Neuronal modulation in the mouse superior colliculus during covert visual selective attention'. In: *Scientific Reports* 12.1. ISSN: 20452322. DOI: 10.1038/s41598-022-06410-5.

Wang, Xiyue, Xiao lin Chou, Li I. Zhang and Huizhong Whit Tao (Feb. 2020). 'Zona Incerta: An Integrative Node for Global Behavioral Modulation'. In: *Trends in Neurosciences* 43.2, pp. 82–87. ISSN: 1878108X. DOI: 10.1016/j.tins.2019.11.007. URL: https://doi.org/10.1016/j.tins.2019.11.007%20https://linkinghub.elsevier.com/retrieve/pii/S0166223619302206.

White, Brian J. and Douglas P. Munoz (Aug. 2011). *The superior colliculus*. Oxford University Press. DOI: 10.1093/oxfordhb/9780199539789.013.0011. URL: https://academic.oup.com/edited-volume/41257/chapter/350823798.

Wilson, Jonathan J., Nicolas Alexandre, Caterina Trentin and Marco Tripodi (June 2018). 'Three-Dimensional Representation of Motor Space in the Mouse Superior Colliculus'. In: *Current Biology* 28.11, pp. 1744–1755. ISSN: 09609822. DOI: 10.1016/j.cub.2018.04.021.

Zhao, Zheng Dong et al. (Jan. 2023). 'Neurocircuitry of Predatory Hunting'. In: *Neuroscience Bulletin* 39.5, pp. 817–831. ISSN: 19958218. DOI: 10.1007/s12264-022-01018-1. URL: https://link.springer.com/article/10.1007/s12264-022-01018-1%20https://link.springer.com/10.1007/s12264-022-01018-1.

Ziegler, Katharina et al. (2023). 'Primary somatosensory cortex bidirectionally modulates sensory gain and nociceptive behavior in a layer-specific manner'. In: *Nature Communications* 14 (1). ISSN: 20411723. DOI: 10.1038/s41467-023-38798-7.

Zingg, Brian et al. (Jan. 2017). 'AAV-Mediated Anterograde Transsynaptic Tagging: Mapping Corticocollicular Input-Defined Neural

Pathways for Defense Behaviors'. In: *Neuron* 93.1, pp. 33–47. ISSN: 08966273. DOI: 10.1016/j.neuron.2016.11.045. URL: https://linkinghub.elsevier.com/retrieve/pii/S0896627316309138.

Zurita, Hector, Crystal Rock, Jessica Perkins and Alfonso Junior Apicella (Aug. 2018). 'A Layer-specific Corticofugal Input to the Mouse Superior Colliculus'. In: *Cerebral cortex (New York, N.Y. : 1991)* 28.8, pp. 2817–2833. ISSN: 14602199. DOI: 10.1093/cercor/bhx161.

DECLARATION

I hereby declare that I have written the submitted dissertation *Whisker somatosensation in the mouse superior colliculus: pathways and behaviour* myself and in this process, have used no other sources or materials than those explicitly indicated. This work was performed from April 2019 to June 2025 under the supervision of Prof. Dr. Alexander Groh in the Medical Biophysics Department at the University of Heidelberg, Germany.

Heidelberg, Germany, June 2025

Emilio Ulises Isaías Camacho

COLOPHON

This document was typeset using the typographical look-and-feel `classicthesis` developed by André Miede and Ivo Pletikosić. The style was inspired by Robert Bringhurst's seminal book on typography *"The Elements of Typographic Style"*. `classicthesis` is available for both LaTeX and LyX:

`https://bitbucket.org/amiede/classicthesis/`

Happy users of `classicthesis` usually send a real postcard to the author, a collection of postcards received so far is featured here:

`http://postcards.miede.de/`

Thank you very much for your feedback and contribution.

Final Version as of 13th June 2025 (4).